CUBIC SPLINE ELEMENTS

FOR

BOUNDARY INTEGRAL EQUATIONS

A THESIS
SUBMITTED TO THE
FACULTY OF GRADUATE STUDIES
IN PARTIAL FULFILLMENT
OF THE REQUIREMENTS FOR THE
DOCTOR OF PHILOSOPHY
DEGREE

BY

SEMIH BILGEN

DEPARTMENT OF ELECTRICAL ENGINEERING
UNIVERSITY OF MANITOBA
WINNIPEG, CANADA
MARCH 1982

CUBIC SPLINE ELEMENTS

FOR

BOUNDARY INTEGRAL EQUATIONS

BY

SEMIH BILGEN

A thesis submitted to the Faculty of Graduate Studies of
the University of Manitoba in partial fulfillment of the requirements
of the degree of

DOCTOR OF PHILOSOPHY

CORRECTIONS

p.21, eq'n. (2.15)

$$B_i(x) = \begin{cases} 0, & x \leq x_{i-2} \\ \xi^3, & x_{i-2} \leq x \leq x_{i-1} \\ -3\xi^3 + 3\xi^2 + 3\xi + 1, & x_{i-1} \leq x \leq x_i \\ 3\xi^3 - 6\xi^2 + 4, & x_i \leq x \leq x_{i+1} \\ -\xi^3 + 3\xi^2 - 3\xi + 1, & x_{i+1} \leq x \leq x_{i+2} \\ 0, & x_{i+2} \leq x, \end{cases}$$

in which ξ is defined on each nonzero interval as:

$(x-x_{i-2})/(x_{i-1}-x_{i-2})$, $(x-x_{i-1})/(x_i-x_{i-1})$, $(x-x_i)/(x_{i+1}-x_i)$,

$(x-x_{i+1})/(x_{i+2}-x_{i+1})$, respectively...

p.39, eq'n. (3.4)

$$\alpha_1(\xi) = -\xi^3 + 3\xi^2 - 3\xi + 1$$

p.44, eq'n. (3.15)

$$\frac{\partial^2 P_2}{\partial \eta^2}\Big|_{\substack{\xi=\xi \\ \eta=0}} = F2''(\eta=0)\beta 0(\xi) + F3''(\eta=0)\beta 1(\xi)$$

p.45, eq'n. (3.18)

$$\frac{\partial^2 P_2}{\partial \eta \partial \xi}\Big|_{\substack{\xi=\xi \\ \eta=0}} = F2'(\eta=0)\beta 0'(\xi) + F3'(\eta=0)\beta 1'(\xi)$$

p.48, eq'n. (3.23)

$$A_7(\xi,\eta) = \alpha_1(\eta)\beta 1(\xi) - \frac{4}{15}\alpha_2(\eta)\beta 1(\xi) + \frac{1}{15}\alpha_3(\eta)\beta 1(\xi),$$

in A_9 through A_{12}, the β-only terms should have a coefficient of 6 (six).

p.50, eq'n. (3.24)

$$\beta 0(\xi) = 1/6(-27\xi^3+6) \qquad 0 \leq \xi \leq 1/3$$

$$\beta 1(\xi) = 1/6(27\xi^3) \qquad 0 \leq \xi \leq 1/3 .$$

ABSTRACT

Boundary elements based on cubic spline functions are developed for use in the solution of boundary value problems formulated as integral equations. Two-dimensional (uni-variate) and three-dimensional (bi-variate) element configurations are defined. The three-dimensional element is an extension of the Coons patch technique of surface modelling. Implementation of Galerkin's method of integral equation solution using the developed spline elements is discussed. Green's function singularity arising on the double surface integral is rigorously treated. A technique of incorporating the singularities of source density due to geometrical features into the solution by utilizing modified spline expansion functions is presented. Cases of electrostatic and time-harmonic problems that involve homogeneous and inhomogeneous media are considered with alternative approaches to problem formulation. Comparisons are made with the classical pulse expansion - point matching method and with previous implementations of the Boundary Element Method using Lagrangian elements.

ACKNOWLEDGEMENTS

Writing this section unavoidably reduces a complex structure of support to a linear ordering of words of gratitude. A work of any significance in any area relies on prior accumulation. The individual, supported materially, academically, and emotionally, only adds his drop to the stream of efforts. The following few people are mentioned because their help was perceived as crucial in this particular instance.

Professor A. Wexler is deeply thanked for his guidance and support over the course of this work.

Süheylâ Bilgen's love and endurance made many things worth while. To his dear sister, Üstün Reinart, the author owes very much, including the existence of this dissertation. The author's daughter Bahar is thanked for her patience; she, together with the author's son, Deniz, provided very valuable encouragement without being aware of it.

Dr.Bruce H. McDonald is thanked for many helpful suggestions. Stimulating discussions with colleagues at the University of Manitoba, especially with Dr. M.H. Lean were appreciated. Bülent Yıldır's mesh generation package was used for data preparation in many three-dimensional applications.

A large portion of this work was financially supported by the Xerox corporation.

TABLE OF CONTENTS

LIST OF FIGURES

LIST OF TABLES

LIST OF SYMBOLS

a, $\bar{a}$	Real constants.
$\hat{a}$	Unit vector in an arbitrary direction.
a_s	Arbitrary coefficients of PDE solution.
A	Cross product determinant for differential surface.
$A(r\|r')$	Regular part of a singular kernel.
A_i	Weights of quadrature integration formula.
$A_j(\xi,\eta)$	Bi-variate B-spline shape function.
α	Wedge angle.
$\alpha_j(\xi)$	Uni-variate shape function.
b, $\bar{b}$	Real constants.
$\underline{b}$	Right-hand-side vector in the linear equation system resulting from the application of Galerkin's method to a boundary integral equation.
b_s	Arbitrary coefficients of a PDE solution.
$\underline{\underline{B}}$	Square matrix of B-spline basis entries.
$B_i(x)$	B-spline basis function.
$\beta 0$, $\beta 1$	Blending functions for surface patch.
c, $\bar{c}$	Real constants.
C	(i) Two-dimensional contour of a region. (ii) Capacitance.
$C(\xi,\eta)$	Interpolation function used in the surface patch.
$C_j(x)$	Arbitrary cubic spline function.
γ	Position-dependent coefficient used in the Green's theorem formulation.
$\Gamma\{\cdot\}$	General integral operator.

D	Set of Dirichlet boundaries.
$D_j(x)$	Arbitrary cubic spline function.
$\overline{dl}$, $\overline{dl'}$	Differential length vector in field and source coordinates.
$\overline{dr}_1$, $\overline{dr}_2$	Differential surface tangent vectors.
$\overline{ds}$	Differential surface vector.
E	Electrostatic energy.
$\overline{E}$	Maxwellian electric field.
E_o	Amplitude of a time-harmonic electric field.
E^i, E^s	Incident and scattered fields.
E_z	Magnitude of the axial component of the electric field.
$E(\xi,\eta)$	Interpolation function used in the surface patch.
ε_o, ε	Permittivity of free-space and of a medium.
$\underline{f}$	(i) Vector of unknowns in the linear equation system resulting from the application of Galerkin's method to a boundary integral equation. (ii) Vector of discrete values of a dependent variable of interpolation.
f_i	Discrete values of a dependent variable of interpolation.
$f(.)$	Arbitrary function.
$F(.,.)$	Arbitrary bi-variate function.
$F0(.)$, $F1(.)$	Edge curves of a surface patch.
Φ_i	Discrete values of $\Phi(i,\xi)$
$\Phi(i,\xi)$	General variable to be interpolated via a finite-element scheme.
$\Phi(x,y), \Phi(r,\theta)$	Scalar electrostatic potential.
$g(.)$	Boundary condition function.
$g(x)$	Interpolating function.
$G(.,.)$	Green's function.

G_e, G_i	Green's functions valid in the exterior and interior of a region.
h	Interpolation mesh size.
$h(s)$	Neumann boundary condition function.
$h_i(x)$	Hermite basis functions.
$\overline{H}$	Maxwellian magnetic field.
H^i, H^s	Incident and scattered magnetic fields.
$H_j^{(k)}$	Hankel function of the k'th kind and j'th order.
θ	Angular component of cylindrical coordinates.
i	Arbitrary integer.
I	(i) Value of a definite integral. (ii) Set of interface boundaries.
η	(i) Simplex variable. (ii) Characteristic impedance.
η^*	Transformed simplex variable.
j	Arbitrary integer.
J	(i) Jacobian of a transformation. (ii) Magnitude of a current density vector.
$J_s(.)$	Bessel function of order s.
J_z	Axial component of the current density in cylindrical coordinates.
k	(i) Arbitary integer. (ii) Propagation constant for a travelling wave.
$\hat{k}$	Unit vector in the propagation direction.
k_o	Propagation constant in free space.
$K(.,.)$, $K(\cdot\|\cdot)$	Kernel of integration for an integral operator.
κ, κ_i	Dielectric constant; ...of medium i.
$\ell_i(x)$	Lagrangian polynomial.

λ	(i) Coefficient of the free term in a Fredholm Integral Equation of the second kind. (ii) Eigenvalue of a Helmholtz equation. (iii) Wavelength of a time-harmonic electromagnetic field.
M_{ij}	Minors of the differential surface cross product determinant.
μ	Permeability.
$\mu(\cdot)$	Real valued double-layer source density function.
N	(i) Arbitrary integer; usually the limit of a range of computations. (ii) Set of Neumann boundaries.
n	Surface normal; usually at field point.
n'	Surface normal at source point.
$\hat{n}$	Unit normal vector; usually at field point.
$\hat{n}'$	Unit normal vector at source point.
M	Arbitrary integer; usually the limit of a range of computations.
ν	Order of singularity.
ω	Angular frequency.
Ω	Domain of a function.
$\vec{P}$	Dipole moment vector.
P_1, P_2	Beginning and end of a uni-variate B-spline element.
P_i	Discrete values on a B-spline curve.
P(x), P(ξ)	B-spline curve.
P(ξ,η),Pi(ξ,η)	Surface patches.
$P_i(x)$	Piecewise Lagrangian polynomial.
P00,P01,P10,P11	Corners of a surface patch.
$\Psi(\theta)$	Solution of Laplace's equation; arbitrary function of θ.
$\psi(r)$, $\psi(s)$	Complex valued analytic function.

r	(i) General position. (ii) Position at field point. (iii) Radial coordinate in a cylindrical system.
r'	Source point.
R	(i) Potential reference position. (ii) Distance vector. (iii) Two-dimensional region.
$R(r)$	Solution of Laplace's equation; function of the radial coordinate only.
s	Position at a surface.
s'	Position at a surface at the source point.
S	Boundary surface.
$\underline{\underline{S}}$	Square coefficient matrix resulting from the application of Galerkin's method to a boundary integral equation.
S_{pq}	Entry of the $\underline{\underline{S}}$ matrix.
$S(x)$	Spline function.
$\sigma(\cdot)$	Simple-layer source density function.
$\underline{\sigma}$	Vector of unknown coefficients of representation of a source density function.
σ	Scattering cross section.
T_i, T_{ij}	Transformations of the simplex variable to cater for the Green's function singularity.
u	Bi-variate simplex coordinate transformed twice.
$\hat{u}_r$	Unit vector in separation direction.
$\hat{u}_x$, $\hat{u}_y$, $\hat{u}_z$	Unit vectors in the Cartesian system.
$U(x,y)$	Bi-cubic spline function.
v	Bi-variate simplex coordinate transformed twice.
$\underline{v}$	Vector of spline control vertices, V_i.
V	Constant potential value.

V_i	Control vertices of a B-spline curve; i.e. coefficients used in representing a uni-variate function as a linear combination of B-spline basis functions. Also: "B-spline vertices."
$w(x)$	Weight function in quadrature integration.
ξ	Simplex variable.
ξ^*	Transformed simplex variable.
x_i	Discrete values of the independent variable of an interpolation problem.
υ	Order of singularity.

CHAPTER I

INTRODUCTION

The Boundary Element Method (BEM) has been shown to be an effective approach to the solution of boundary value problems formulated in terms of integral equations [1, 2, 3, 4]. Its application, using Lagrangian elements, has led to accurate solutions for many electrostatic and time-harmonic electromagnetic field problems. The Lagrangian (*) element methodology was demonstrated to be superior to the classical moment method [5] implementation using pulse-expansion and point-matching, in a number of instances. Increased stability and a significant reduction in the number of unknowns required to solve a given problem were among its merits.

This work has set out to further improve upon the capabilities of the BEM. The methodology that is developed here incorporates two major features that are fundamental in bringing about that improvement:

i) the spline formulation is utilized to guarantee high-fidelity geometric modelling without adding to the number of unknowns;

ii) furthermore, the number of unknowns is reduced due to the fact that, with the scheme developed here, all nodes used in element definition are shared by a large number of elements.

This reduction in the number of unknowns is a satisfactory development in the direction indicated by Lean:

(*) See Chapters 2 and 3 for formal definitions of the terms "Lagrangian", "spline", etc...

"The main drawback of the present (i.e. Lagrangian) interpolation scheme, not really felt in two dimensions, is the requirement for more unknowns for increasing orders of interpolation. For up to a linear variation, this scheme is definitely viable since all nodes are shared by at least two or more elements. Succeeding orders need interior nodes whose data contribute to this one element only. Hence, any algorithm that allows the usage of information from exterior nodes, especially for high-order interpolation, and yet remain sufficiently flexible for general application, would be advantageous for three-dimensional problems." (1, p. 118, emphasis added.)

It is the author's contention that the spline element methodology responds precisely to this requirement.

Also investigated is the approach to a fundamental problem inherent to numerical solution methods of integral equations with kernels that have integrable singularities within the domain of integration. While traditional methods range from ignoring the singular point altogether (e.g. [6]), to handling it analytically, which is highly geometry-dependent (e.g. [7], [8]), a problem-independent and rigorous approach is provided by numerical treatment. This work contains the implementation, in the context of spline elements, of such a technique, originally developed for Lagrangian elements [1].

The issue of approximating source variations that tend to infinity in the vicinity of surface normal discontinuities, i.e. corners or edges, has also been one that requires particular attention. The present work addresses that problem by properly modifying the spline basis functions that approximate the solution. In cases where the behavior of sources is known, this knowledge is imposed directly upon the solution, the solution then reflecting the expected behavior exactly. Where such

knowledge is not analytically available, one has the capability to experiment with various modes of singular behavior imposed on the sources and to determine a configuration that best satisfies the problem requirements.

The remaining portion of this chapter presents an overview of the BEM in general.

The second chapter considers Lagrangian, Hermitian and spline interpolation, as alternative approaches to the finite-element solution of boundary integral equations. Together with the pulse expansion technique, these methods are seen to be following a conceptual succession in the direction of increased fidelity in modelling geometry and sources, decreased number of unknowns necessary to achieve such modelling, and increased computational overhead. It has been claimed (e.g. [9]) that generally, the latter feature renders the utilization of higher-order schemes (of which the spline element approach is an instance) unnecessarily onerous. One of our goals is to show that proper algorithmic development overcomes that disadvantage. In many applications, the increased computation time per element is compensated by decreased total number of unknowns. This results in reduced overall cost in relation to lower order methods that produce comparable results.

The third chapter is devoted to the derivation and implementation

of the spline elements as the fundamental feature of this work. The two-dimensional uni-variate spline elements are derived as a linear combination of four cubic spline basis functions. The three-dimensional bi-variate ones are implemented using the Coon's Patch concept [10] commonly used in computer aided geometric design and surface modelling. Some algebraic modifications yield the representation used in all three-dimensional applications throughout this work.

The fourth chapter considers Green's function and source singularities in the spline element context. Gaussian quadrature integration formulas derived for specific implementations are discussed. The usage of modified splines that cater for expected singularities of the source distribution are also considered in that chapter.

Chapter V consists of an exposition of various electromagnetic field problems solved with the BEM using spline elements. Two- and three-dimensional geometries in electrostatic and time-harmonic problems, that involve homogenous and piecewise inhomogenous media, are treated.(*)

(*) In this work, the terms "two-" and "three-dimensional" refer to problem formulation. A problem invariant along one spatial dimension would be formulated as two-dimensional. The terms "uni-variate" and "bi-variate" refer to the boundary parametrization. The contour of a two-dimensional region would be uni-variate, whereas a three-dimensional region would be bounded by a bi-variate surface. Hence, two-dimensional boundary elements are uni-variate, and three-dimensional ones are bi-variate.

1.1 The Boundary Element Method (BEM)

Many problems of engineering can be expressed as an integral equation of the form (*):

$$\int_S K(r|r')f(r')ds(r') - \lambda f(r) = g(r). \qquad (1.1)$$

If the kernel $K(r|r')$ is square-integrable, i.e. if

$$\int\int_{SS} K^2(r|r')ds(r')ds(r) = I \qquad (1.2)$$

has a finite value, then (1.1) is a Fredholm Integral Equation, and has a unique solution for $f(r)$, [11] provided that λ is not an eigenvalue and if $g(r)$ has a finite norm, i.e.

$$\int_S (|g(r)|^2 ds(r))^{\frac{1}{2}} < \infty . \qquad (1.3)$$

For the solution of this problem, this implementation of the BEM entails an application of Galerkin's technique with isoparametric elements. Both geometric variables - r, s(r) - and sources - f(r) - are represented as linear combinations of subsectional polynomic basis functions of the same order [12, 13].

On an element, i, among the total of M elements, the relevant value, Φ, - position or source, vector or scalar - is represented as a function of simplex position, ξ as:

(*) The case when $\lambda=0$ has also been solved numerically (cf. Ch.5 and Lean (1)), but lacks theoretical support (11).

$$\Phi(i, \xi) = \sum_{j=1}^{N} \alpha_j (\xi) \Phi_{ij} \qquad (1.4)$$

for all i, $1 \leq i \leq M$.

In this generalized expression, ξ represents the position over the simplex (standard) element and as such, it may be a scalar (one-dimensional boundary element) or a two-entry vector (two-dimensional boundary element). α_j represents the "shape functions" i.e. basis functions defined over the standard element and used to interpolate from Φ_{ij} to Φ, at any point, ξ, over the i'th element. The number of shape functions, N, is a characteristic of the particular interpolation scheme.

In general, the Φ_{ij} do not correspond to actual physical values of Φ at some node points and this constitutes one of the major differences of this work from previous approaches[1,7]. (See Appendix .)

Solution of the integral equation (1.1) with positive-definite self-adjoint Fredholm operators has been analyzed extensively. Mikhlin [14] has given the proof that the approximate solution constructed by the Galerkin method converges in the mean to the exact solution of this equation, if the system of basis functions is complete (*) in the sense of convergence in the mean.(**)

The Rayleigh-Ritz variational technique of solution, which, in instances where the Fredholm operator is positive-bounded-

below (***), generates a system of linear equations identical to those produced by the Galerkin technique [14] has been extensively used in the context of problems formulated as integral equations and partial differential equations (e.g. [15], [16]). In case of non-self-adjoint operators (i.e. those that have a non-symmetric kernel) as well, the Galerkin technique results in a discretized equation that corresponds to a minimized energy functional defined by the Rayleigh-Ritz technique [17].

Galerkin's method proceeds by expressing both the position, r or r', and the unknown function, f(r), in terms of expansion

---

(*) i.e. any function in the domain of the operator

$$\Gamma\{f(r)\} = \int_{r_1}^{r_2} K(r|r')f(r')dr' - \lambda f(r)$$

can be approximated to within an arbitrary precision, in the mean, by a linear combination of a finite number of basis functions.

(**) The sequence $f_n(r)$ converges in the mean to $f(r)$ as $n\to\infty$ if $\int_{\Omega}(f_n(r)-f(r))^2 d\Omega\to 0$, where Ω denotes the domain of the functions f_n and f.

(***) A symetric operator Γ is positive-bounded-below if for any function f, in its domain, $\langle\Gamma\{f\}, f\rangle \geq \Psi ||f||^2$ where Ψ is a positive constant.

functions in the form of (1.4). Summarizing (1.1) as

$$\Gamma\{f(r')\} = g(r), \tag{1.5}$$

this produces

$$\Gamma\{\sum_{j=1}^{N} \alpha_j(\xi)\ f_{ij}\} = g(\sum_{j=1}^{N} \alpha_j(\xi)\ r_{ij}), \tag{1.6}$$

for all i, $1 \leq i \leq M$. Now, inner products with the testing functions - same as the expansion functions, α_j - are performed to get

$$< \Gamma \{ \sum_{j=1}^{N} \alpha_j(\xi)\ f_{ij} \} , \sum_{k=1}^{N} \alpha_k(\xi) > = < g(\sum_{j=1}^{N} \alpha_j(\xi)\ r_{ij}), \sum_{k=1}^{N} \alpha_k(\xi) > \tag{1.7}$$

for $1 \leq i \leq M$. The inner product is defined as:

$$<u, v> = \int_S u(r).v(r)ds(r) \tag{1.8}$$

where s is the same as in (1.1). The operator, Γ, is linear [14], and upon extraction of the unknowns, f_{ij}, (1.7) represents a system of linear equations in the form:

$$\underline{\underline{S}}\ \underline{f} = \underline{b}. \tag{1.9}$$

If there are P distinct f_{ij} and corresponding r_{ij}, then $\underline{f}$ is a vector containing these P f_{ij} in any selected order; $\underline{b}$ is a vector of P entries comprising the contribution of the right-hand-side of (1.7) to each r_{ij} in the same order as the f_{ij};

and $\underline{\underline{S}}$ is a dense P*P square matrix whose entries S_{pq} correspond to the inner product of the contribution of the integral operator, $\Gamma\{.\}$ at the q'th f_{ij}, with the shape function associated with the p'th f_{ij}.

The entry S_{pq} is computed as:

$$S_{pq} = \sum_i \int_{e_i} \alpha_p(\xi) \int_S K(r(\xi)|r'(\xi'))\alpha_q(\xi')ds'(r'(\xi'))\, ds(r(\xi)) \qquad (1,10)$$

in which the summation runs over all elements, e_i connected to the p^{th} global vertex; α_p represents the shape function associated with the local vertex in e_i that maps to global vertex, p; α_q represents the shape function associated with the local vertex in any element encountered during the internal integration that maps to global vertex, q. The inner integration, arising from the Fredholm operator, is performed over primed variables, and the outer one, the inner product integration, is over un-primed variables.

Gauss quadrature formulae [18] are used throughout for integration; parametric order of quadrature being used to control precision. Generation and utilization of specially weighted formulae will be considered in Chapter 4, below.

Clearly, a number of choices for the basis functions, α_j exists. This choice is fundamental to the operation of the solution

procedure. A particular class among the possible basis functions is the subject of the next chapter.

1.2 References

(1) Lean, M. H., Electromagnetic Field Solution with the Boundary Element Method, Ph.D. Dissertation, University of Manitoba, 1981.

(2) Jeng, G. and Wexler, A., "Isoparametric Finite Element Variational Solution of Integral Equations for Three-Dimensional Fields", International Journal of Numerical Methods in Engineering, vol. 11, pp. 1455-1471, 1977.

(3) Lean, M. H., Friedman, M. and Wexler, A., "Application of the Boundary Element Method in Electrical Engineering Problems", in Developments in Boundary Element Methods -1, Banerjee and Butterfield (ed.s), Applied Science Publishers Ltd., London, 1979.

(4) Lean, M. H. and Wexler, A., "Accurate field computation with the Boundary Element Method" to be published.

(5) Harrington, R. F., Field Computation by Moment Methods, Macmillan, 1968.

(6) Oshiro, F. K. and Su, C. S., A Source Distribution Technique for the Solution of General Electromagnetic Scattering Problems - Phase 1 Report, Northrop, Norair, NOR 65-271, 1965.

(7) Jeng, G., Isoparametric, Finite-Element Boundary Integral Solution of Three-Dimensional Fields, Ph.D. Dissertation, University of Manitoba, 1977.

(8) Lachat, J. C. and Watson, J. O., "Effective numerical treatment of boundary integral equations", International Journal of Numerical Methods in Engineering, Vol. 10, pp. 991-1005, 1976.

(9) Birkhoff, G. and Fix, G. J., "Higher-order Linear Finite Element Methods", Report to the U.S. Atomic Energy Commission and the Office of Naval Research, 1974.

(10) Coons, S. A., "Surface Patches and B-Spline Curves", In Computer Aided Geometric Design, Barnhill and Riesenfeld (ed.s), Academic Press, 1974.

(11) Zabreyko, P. P., et. al., Integral Equations - a reference text, Noordhoff International Publishing, 1975.

(12) Zienkiewicz, O. C., The Finite Element Method in Engineering Science, McGraw-Hill, 1971.

(13) Wexler, A., Finite Elements for Technologists, Electrical Engineering Department Technical Report, TR80-4, University of Manitoba, 1980.

(14) Mikhlin, S. G., Variational Methods in Mathematical Physics, Pergamon Press, 1964.

(15) McDonald, B. H., Constrained Variational Solution of Field Problems, Ph.D. Dissertation, University of Manitoba, 1975.

(16) McDonald, B. H., Friedman, M. and Wexler, A., "Variational solution of integral equations", IEEE Trans. Microwave Theory and Techniques, vol. MTT-22, pp. 237-248.

(17) Jeng, G. and Wexler, A., "Self-adjoint Variational Formulation of Problems Having Non-Self-Adjoint Operators", IEEE Trans. on Microwave Theory and Techniques, vol. MTT-26, pp. 91-94, 1978.

(18) Stroud, A. H. and Secrest, D., Gaussian Quadrature Formulas, Prentice-Hall Inc., 1966.

CHAPTER II

SPLINE APPROXIMATION

2.1 The Interpolation Problem

The use of pulses and piecewise linear functions is a common theoretical tool of approximation of functions with the inherent requirement of step sizes converging to zero. The study of the ways by which this requirement could be relaxed or completely removed, through the use of higher-order polynomials, can be said to have started with a fundamental paper by Schoenberg[1]. The main developments, however, have occurred in the 1960's, and reported in the works of Ahlberg, Nilson and Walsh[2], Greville [3], DeBoor[4] and Schultz[5], among many others.

Piecewise Lagrangian, Hermite and spline interpolation schemes will be considered below, within the context of boundary element configurations applicable to the BEM.

Lagrangian Interpolation

Consider the following uni-variate interpolation problem: Given $\{x_i, f_i\}_{i=1}^{N}$, find a $g(x)$ defined on $[x_1, x_N]$, such that

$$g(x_i) = f_i, \text{ for } i = 1, \ldots, N. \tag{2.1}$$

The Lagrangian solution to this problem can be formed as

$$g(x) = \sum_{i=1}^{N} f_i \ell_i(x) \tag{2.2}$$

where

$$\ell_i(x) = \prod_{\substack{j=1 \\ j\neq i}}^{N} (x-x_j)/(x_i - x_j), \tag{2.3}$$

that is, fitting an N'th order (N - 1'st degree) polynomial to the N given points.

That the Lagrange interpolation procedure may fail to converge as N increases is a well-known result of Runge [5](*).

A piecewise-Lagrangian solution is also possible and is more practical. On each subinterval $[x_i, x_{i+k}]$, i representing the beginning node of the subinterval, a unique polynomial of order K + 1 can be found such that

$$P_i(x_{i+j}) = f_{i+j} \text{ for } j = 0, \ldots, K. \tag{2.4}$$

Taking K = 1, the set of first degree polynomials $P_i(x)$, each defined on $[x_i, x_{i+1}]$ to satisfy

$$P_i(x_i) = f_i$$

$$P_i(x_{i+1}) = f_{i+1} \tag{2.5}$$

are called the "linear finite-element functions", or the piecewise linear solution of the given problem.
Let's choose to represent an arbitrary first degree polynomial as a linear combination of two linearly independent basis functions α_1 and α_2, defined for $0<\xi<1$ as:

$$\alpha_1 (\xi) = \xi$$

$$\alpha_2 (\xi) = 1-\xi. \tag{2.6}$$

(*) E.g. given that $g(x_i) = ((10x_i-5)^2+1)^{-1}$, $0 \leq x_i \leq 1$
$i = 1, \ldots, N$, the Lagrange interpolation procedure diverges for $N \to \infty$.

Clearly, now, the independent variable can be represented as:

$$x(\xi) = x_i \alpha_1(\xi) + x_{i+1} \alpha_2(\xi) \tag{2.7}$$

where $i = 1, \ldots, N-1$, denotes the element number, and our piecewise linear solution to the problem, as

$$P_i(\xi) = f_i \alpha_1(\xi) + f_{i+1} \alpha_2(\xi). \tag{2.8}$$

Thus, (2.6) is the definition of a Linear Lagrangian Finite Element directly usable in the BEM as outlined in section 1.1, above.

Piecewise Hermite interpolation

Pose the interpolation problem as follows:

Given $\{x_i, f_i, f'_i\}_{i=1}^{N}$, i.e. 2N independent constraints, find a $g(x)$ defined on $[x_1, x_N]$ such that

$$g(x_i) = f_i$$

$$\text{and } \frac{d}{dx} g(x)\Big|_{x=x_i} = f'_i, \text{ for } i = 1, \ldots N. \tag{2.9}$$

If the solution satisfies the additional requirement that it is once continuously differentiable on x_1, x_N, and on each $[x_i, x_{i+1}]$, $1 \leq i \leq N-1$, it is a cubic polynomial, then it is called a piecewise cubic Hermite interpolant.

If such interpolants had to be used in the BEM procedure, we would define the Hermite basis $h_i(x)$, $h'_i(x)$, such that:

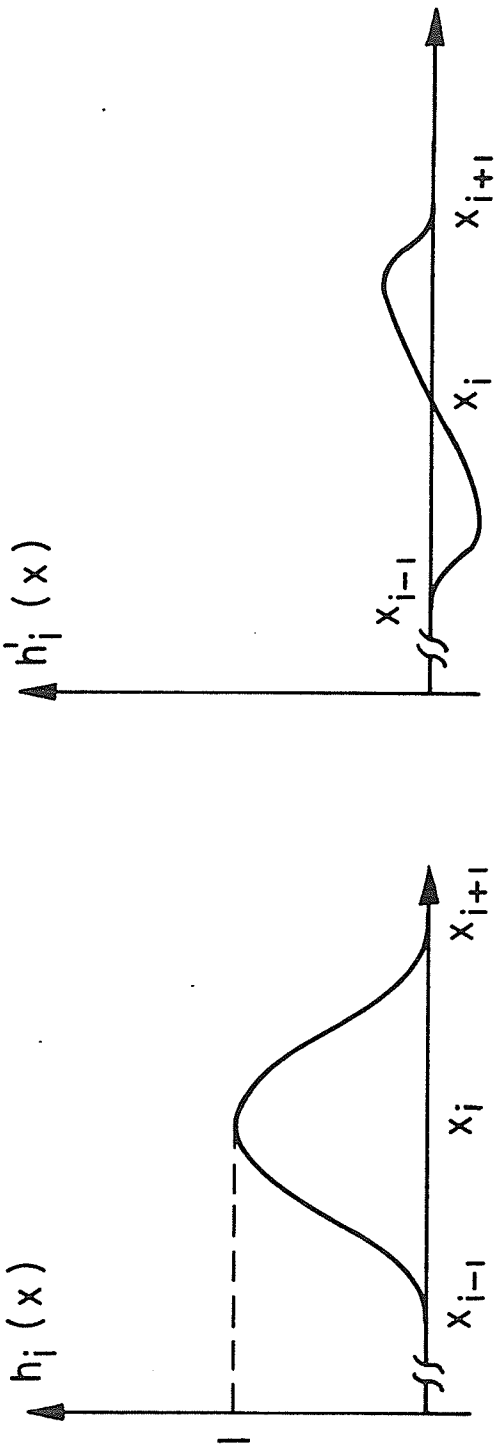

Figure 2.1. Cubic Hermite basis functions.

$$h_i(x_j) = \delta_{ij}$$

$$\frac{d}{dx} h_i(x)\Big|_{x=x_j} = 0$$

$$h'_i(x_j) = 0$$

$$\frac{d}{dx} h'_i(x)\Big|_{x=x_j} = \delta_{ij}, \text{ for } 1 \leq i, j \leq N. \tag{2.10}$$

Then, the interpolating function would be expressed as:

$$g(x) = \sum_{i=1}^{N} (f_i h_i(x) + f'_i h'_i(x)) \tag{2.11}$$

Similar to the path followed in the Lagrangian case, Hermite interpolation functions can be represented as a linear combination of the following four linearly independent basis functions (Fig. 2.1):

$$\alpha_1(\xi) = (\xi-1)^2 (2\xi + 1)$$

$$\alpha_2(\xi) = \xi^2 (3 - 2\xi)$$

$$\alpha_3(\xi) = (\xi - 1) \xi^2$$

$$\alpha_4(\xi) = (1 - \xi)^2 \xi \text{ for } 0 \leq \xi \leq 1, \tag{2.12}$$

which satisfy the stipulations of (2.10).

Now, our solution g(x), given in (2.11), can be expressed as

$$g_i(\xi) = f_i\,\alpha_1(\xi) + f_{i+1}\alpha_2(\xi) + f'_i\,\alpha_3(\xi) + f'_{i+1}\alpha_4(\xi), \quad (2.13)$$

for each interval (i.e. element) $x_i \leq x \leq x_{i+1}$, guaranteeing that the required condition, (2.9) is satisfied. Hence (2.12) defines cubic Hermite elements to be used in the BEM algorithm, if desired.

Worth noting here, is that with this approach, problem geometry definition would have to include position, x_i, as well as the variation $\left.\frac{dx}{d\xi}\right|_{x=x_i}$ at the nodes. For realistic problems, this may become quite unnecessary and cumbersome especially from the viewpoint of a user. Watson [6] has reported an implementation admitting the inconvenience of applying the Galerkin scheme. Hence, it is necessary to avoid having to specify slope information explicitly, but keep the facility to ensure slope continuity at nodes. Splines seem to address both requirements.

Cubic spline interpolation

Splines provide an interpolation procedure that yields smoother results than either Lagrange or Hermite schemes with less input

volume in comparison to the 2N independent constraints of the latter.

To construct the spline interpolant to N points, let

$\{\{x_i, f_i\}_{i=1}^{N}, f'_1, f'_N\}$ be given; i.e. N + 2 independent constraints. The cubic spline, $S(x)$, that satisfies these constraints has the following properties:

i) $S(x_i) = f_i$ for $i = 1, \ldots, N$,

$S'(x_1) = f'_1$,

$S'(x_N) = f'_N$,

ii) $S(x)$ is twice continuously differentiable over (x_1, x_N),

iii) $S(x)$ is a cubic polynomial over each (x_i, x_{i+1}), $1 \le i \le N-1$.

Existence and Uniqueness theorem [5]:

Let $h(x)$ be a Hermite interpolation function; i.e. representable as in (2.11). For given numbers $f_i = h(x_i)$, $i = 1, \ldots, N$, and $f'_1 = \frac{d}{dx}h(x)\big|_{x=x_1}$, $f'_N = \frac{d}{dx}h(x)\big|_{x=x_N}$, there exists exactly one set of numbers $f'_i = \frac{d}{dx}h(x)\big|_{x=x_i}$, for $i = 2, \ldots, N-1$, such that $h(x)$ is twice continuously differentiable over (x_1, x_N).

Stated differently, among many Hermite interpolants with arbitrary derivatives at the interior nodes, there is only one that is second order continuous, i.e. is a spline, and satisfies the end point derivative conditions.

Instead of the end-derivatives, f_1' and f_N', other constraints, for instance the fact that $f_1'' = f_N'' = 0$ may also be given, and this constitutes a well=defined procedure as well [2]. In fact, the spline interpolant, S(x), constructed under this latter constraint satisfies the minimum-curvature property, i.e. among all functions, f(x) which satisfy the interpolation condition $f(x_i) = f_i$ and have continuous second derivatives on (x_1, x_N), S(x) minimizes the integral: [5]

$$\int_{x_1}^{x_2} |S''(x)|^2 \, dx, \tag{2.14}$$

To construct the cubic spline interpolant, define the cubic B-spline basis as: (Fig. 2.2)

$$B_i(x) = \begin{cases} 0, & x \leq x_{i-2} \\ (x-x_{i-2})^3, & x_{i-2} \leq x \leq x_{i-1} \\ -3(x-x_{i-1})^3+3(x-x_{i-1})^2+3(x-x_{i-1})+1, & x_{i-1} \leq x \leq x_i \\ 3(x-x_i)^3 - 6(x-x_i)^2+4, & x_i \leq x \leq x_{i+1} \\ -(x-x_{i+1})^3+3(x-x_{i+1})^2-3(x-x_{i+1})+1, & x_{i+1} \leq x \leq x_{i+2} \\ 0, & x_{i+2} \leq x. \end{cases} \tag{2.15}$$

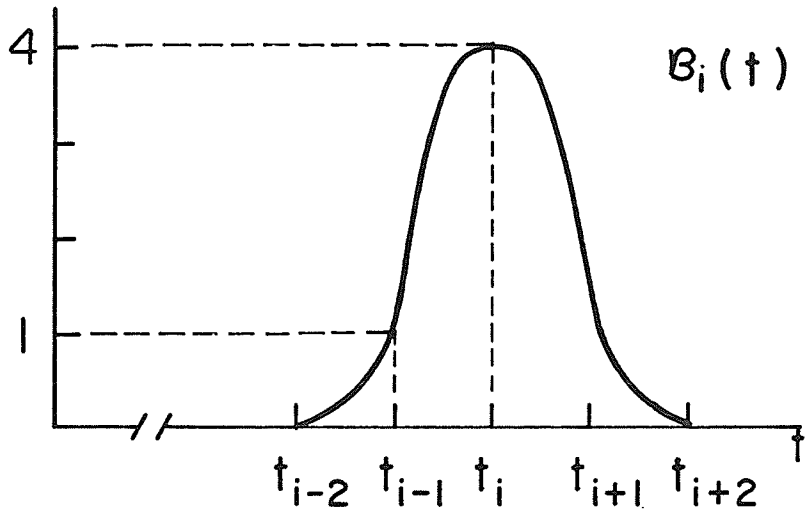

Figure 2.2 The B-spline basis function

For the special case of a uniform mesh with size h, (this restriction will be lifted automatically in the next chapter) the conditions of Table 2.1 are valid.

	x_{j-2} and others	x_{j-1}	x_j	x_{j+1}	x_{j+2} and others
$B_j(x)$	0	1	4	1	0
$B'_j(x)$	0	$3/h$	0	$-3/h$	0
$B''_j(x)$	0	$6/h^2$	$-12/h^2$	$6/h^2$	0

Table 2.1 B-spline conditions at nodes

Then if we let $S(x) = \sum_{j=0}^{N+1} V_j B_j(x)$, we must ensure that

$$f'_1 = S'(x_1) = \sum_{j=0}^{N+1} V_j B'_j(x_1) \tag{2.16}$$

$$f_N' = S'(x_N) = \sum_{j=0}^{N+1} V_j B'_j(x_N) \tag{2.17}$$

$$f_i = S(x_i) = \sum_{j=0}^{N+1} V_j B_j(x_i), \quad i = 1, \ldots, N. \tag{2.18}$$

If, alternatively, we have $f_1'' = f_N'' = 0$ given, the following two stipulations should replace (2.16) and (2.17).

$$f_1'' = S''(x_1) = \sum_{j=0}^{N+1} V_j \; B_j''(x_1) = 0 \tag{2.19}$$

$$f_N'' = S''(x_N) = \sum_{j=0}^{N+1} V_j \; B_j''(x_N) = 0. \tag{2.20}$$

(2.16), (2.17) and (2.18), or (2.18), (2.19) and (2.20) comprise a set of N+2 linear equations of the form

$$\underline{\underline{B}}\,\underline{v} = \underline{f}, \tag{2.21}$$

where $\underline{v} = (V_0 \; V_1 \; \cdots \; V_N \; V_{N+1})^T$,

$\underline{f} = (f_1'' \; f_1 \; \cdots \; f_N \; f_N'')^T$, or

$\underline{f} = (0 \;\; f_1 \; \cdots \; f_N \;\; 0)^T$, and

$$\underline{\underline{B}} = \begin{bmatrix} 3/h & 0 & -3/h & 0 & \cdots & & \\ 1 & 4 & 1 & 0 & \cdots & & \\ 0 & 1 & 4 & 1 & \cdots & & \\ & & & \cdots & & & \\ & & & & 1 & 4 & 1 \\ & & & & 3/h & 0 & -3/h \end{bmatrix}, \text{ or}$$

$$\underline{\underline{B}} = \begin{bmatrix} 6/_h{}^2 & -12/_h{}^2 & 6/_h{}^2 & 0 & \cdots & & \\ 1 & 4 & 1 & 0 & \cdots & & \\ 0 & 1 & 4 & 1 & \cdots & & \\ & & & \cdots & & & \\ & & & & 1 & 4 & 1 \\ & & & & 6/_h{}^2 & -12/_h{}^2 & 6/_h{}^2 \end{bmatrix}.$$

Because of the structure of the system (2.21), a solution exists [2, 5], and can be computed easily with a Gaussian Elimination procedure for banded matrices.

The "shape-function" expression for cubic splines in the form of (1.4), i.e. directly usable by the BEM, will be derived in Chapter III.

2.2 Interpolation of Surfaces

The extension of Lagrange, Hermite, and spline interpolation procedures to the case of two independent variables is achieved as follows:

For bi-linear Lagrange interpolation, the counterpart of the shape functions depicted in (2.6) can be defined as (e.g. [6]):

$$\begin{aligned} \alpha_1(\xi,\eta) &= (1-\xi)\ (1-\eta) \\ \alpha_2(\xi,\eta) &= \xi(\ 1-\eta) \\ \alpha_3(\xi,\eta) &= \xi\ \eta \\ \alpha_4(\xi,\eta) &= (1-\xi)\eta,\ 0\le\xi,\eta\le 1. \end{aligned} \qquad (2.22)$$

The expression

$$\Phi(\xi,\eta) = \sum_{i=1}^{4} \Phi_i \alpha_i \ (\xi,\eta) \qquad (2.23)$$

then maps the unit-square simplex into a global quadrilateral defined by four vertices (Fig. 2.3).

A similar extension to the bi-variate domain exists for Hermite interpolation as well [5]. We shall, however, immediately pass to bicubic splines which constitute the starting point of our three-dimensional (bi-variate) boundary elements.

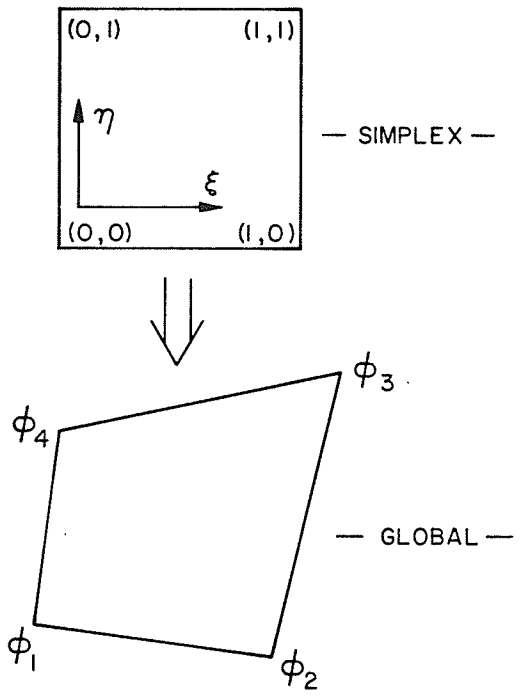

Figure 2.3. Lagrangian bi-linear mapping from a square simplex.

The original extension of the cubic spline idea to two dimensions was due to G. Birkhoff and C. DeBoor [8], who let $C_i(x)$, $i = 0, 1, \ldots, M, M+1$ be cubic spline functions such that

$$f(x) = \sum_{i=1}^{M} f_i C_i(x) + f'_1 \; C_o(x) + f'_M C_{M+1}(x) \qquad (2.24)$$

satisfies $f(x_i) = f_i$ for $i = 1, \ldots, M$,

$f'(x_1) = f'_1$, and

$f'(x_M) = f'_M$,

and $D_j(x)$, $j = 0, 1, \ldots, N, N+1$ be similar functions,

such that $$g(x) = \sum_{j=1}^{N} g_j D_j(x) + g_1' D_o(x) + g_N' D_{N+1}(x) \qquad (2.25)$$

satisfies $g(x_j) = g_j$ for $j = 1, \ldots, N$,

$g'(x_1) = g'_1$, and

$g'(x_N) = g_N$,

for given f_i, $i = 1, \ldots, M$, f_o', f_M', g_j, $j = 1, \ldots, N$, g_o', and g_M'.

Then, the function

$$U(x,y) = \sum_{i=1}^{M} \sum_{j=1}^{N} a_{ij} C_i(x) D_j(y) \qquad (2.260$$

can be uniquely constructed such that it has continuous second derivatives for $x_1 \leq x \leq x_M, y_1 \leq y \leq y_N$,

and $a_{ij} = U(x_i, y_j)$, $i=1,\ldots,M$, $j=1,\ldots,N$,

$a_{ik} = \frac{\partial}{\partial y} U(x_i, y_k)$, $i=1,\ldots,M$, $k=0,N+1$,

$a_{kj} = \frac{\partial}{\partial x} U(x_k, y_j)$, $k=0,M+1$, $j=1,\ldots,N$,

$a_{ij} = \frac{\partial^2}{\partial x \partial y} U(x_i, y_j)$, $i=0,M+1$, $j=0,N+1$. (2.27)

Hence, given the values at all mesh-points, and the partial derivatives at the boundary mesh-points, plus the cross-derivatives at the four corners, the bicubic spline interpolant is uniquely defined. Furthermore, among all functions whose fourth derivatives exist, U(x,y) minimizes

$$\iint_R \left(\frac{\partial^4 U}{\partial x^2 \partial y^2}\right)^2 dxdy + \int_E \left(\frac{\partial^2 U}{\partial s^2}\right)^2 ds \qquad (2.28)$$

where R indicates integration over the region $[x_1, x_N] \times [y_1, y_N]$ and E denotes integration over the boundary of R, with ∂S signifying the tangential derivative. This, again, is the "smoothest" interpolation property.

Bicubic splines have been extensively used in surface modelling, design and computer graphics. A recent bibliographic work (9) provides an exhaustive survey of publications in the area until mid-1981. Major developments that have been

influential in our implementation include the idea of "surface interpolation from curve networks" first introduced by Gordon [10] and later fully utilized by Riesenfeld [11], and the idea of Coon's Patch formulation [12]. The term "transfinite interpolation" was used [13] to describe the general class of interpolation schemes which, unlike classical methods which match a function at a finite number of given points, match the multi-variate function to be approximated, at a non-denumerable (transfinite) number of points. That is, not points but curves are interpolated. The Coon's Patch is a special case of transfinite interpolation.

2.2. 1. The Coons Patch

Our aim is to construct a one-to-one mapping of the unit square (bi-variate simplex) to a given three-dimensional surface to be approximated. As noted above, interpolation can proceed from given points alone, or, better yet, from curves known to lie on that surface. Assume that four boundary curves of the surface to be interpolated are given as F0 (η), F1 (η), F0 (ξ), F1 (ξ) (Figure 2.4), and the four corners, P00, P01, P10, P11.

We wish to construct a vector-valued function, $P(\xi,\eta)$ such that

$$P(0,0) = P00$$

$$P(0,1) = P01$$

$$P(1,0) = P10$$

$$P(1,1) = P11$$

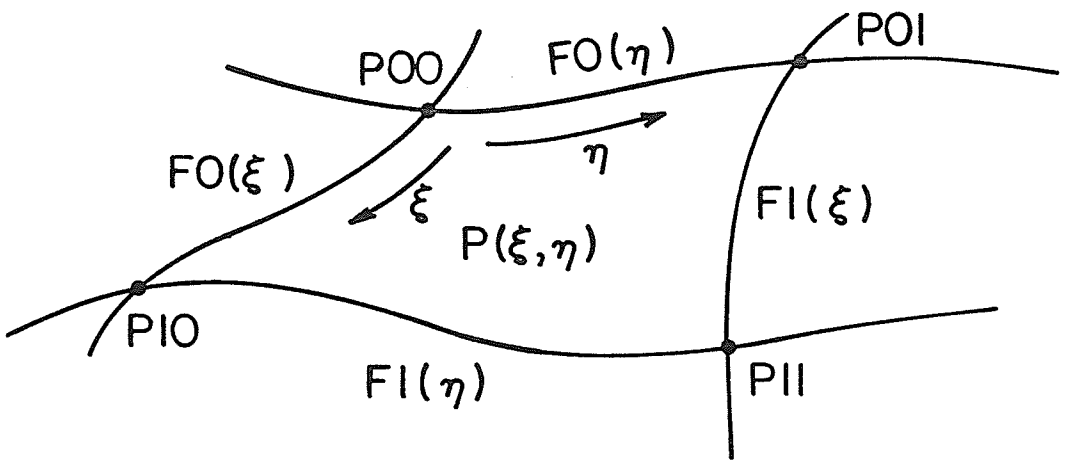

Figure 2.4. A Coons Patch,

$$P(0,\eta) \equiv F0\ (\eta)$$

$$P(1,\eta) \equiv F1\ (\eta)$$

$$P(\xi,0) \equiv F0\ (\xi)$$

$$P(\xi,1) \equiv F1\ (\xi). \qquad (2.29)$$

Let $\beta 0$ and $\beta 1$ be two functions defined on the interval $[0,1]$ that have the cardinality properties:

$$\beta 0(0) = 1,\ \beta 0(1) = 0$$

$$\beta 1(0) = 0,\ \beta 1(1) = 1. \qquad (2.30)$$

Now, if we define

$$C(\xi,\eta) = \beta 0(\xi)\ \beta 0(\eta) P00 + \beta 0\ (\xi)\beta 1(\eta) P01$$
$$+\beta 1(\xi)\beta 0(\eta) P10 + \beta 1(\xi)\beta 1(\eta) P11, \qquad (2.31)$$

$C(\xi,\eta)$ interpolates to the four given corners. For instance, with the simple choice

$$\beta 0(\xi) = 1 - \xi$$

$$\beta 1(\xi) = \xi, \qquad (2.32)$$

it is identical to the bi-linear Lagrangian element defined by (2.22) and (2.23).

But, in addition, we define

$$E(\xi,\eta) = \beta 0\ (\xi)\ F0\ (\eta) + \beta 1\ (\xi)\ F1\ (\eta)$$
$$+ \beta 0\ (\eta)\ F0\ (\xi) + \beta 1\ (\eta)\ F1\ (\xi), \qquad (2.33)$$

which interpolates to the four boundary curves, and form the general Coons Patch:

$$P(\xi,\eta) = E(\xi,\eta) - C(\xi,\eta). \qquad (2.34)$$

By simple evaluation at $\xi = 0$ or 1 and/or $\eta = 0$ or 1, with only the condition (2.30) imposed on $\beta 0$ and $\beta 1$, it is clear that $P(\xi,\eta)$ thus constructed satisfies (2.29). Stated in words, $E(\xi,\eta)$ maps each edge of the simplex to the corresponding edge of the surface to be interpolated; but as the "effect" of each boundary is "weighted" through the functions $\beta 0$ and $\beta 1$, and is added to the whole, the corners where two boundaries meet are added twice - thus the subtraction of $C(\xi,\eta)$.

Note that the only condition imposed on the so-called blending functions, $\beta 0$ and $\beta 1$, so far, were the cardinality conditions, (2.30).

As further stipulations are imposed on these functions, the Coons Patch defined in (2.34) can accomodate the crucial requirements of continuity at edges and smoothness. In particular, choosing spline functions that satisfy (2.30) together with:

$$\beta''0(0) = \beta''1(0) = \beta''0(1) = \beta''1(1) = 0, \qquad (2.35)$$

(2.34) represents a second-derivative continuous mapping of the square simplex to the global surface patch. Gordon [14] has proven that the spline-blended interpolant, $P(\xi,\eta)$, to a bi-variate function $F(\xi,\eta)$ with given univariate boundary curves $F(0,\eta)$, $F(1,\eta)$, $F(\xi,0)$ and $F(\xi,1)$, satisfies the inequality

$$||F(\xi,\eta) - P(\xi,\eta)|| \leq A.||\frac{\partial^8}{\partial\xi^4\partial\eta^4} F(\xi,\eta)|| \qquad (2.36)$$

provided that the fourth derivative with respect to either variable exists. In this expression, A is some constant independent of F, and the L^2 - norm

$$||F(\xi,\eta)|| \stackrel{\Delta}{=} \int_0^1\int_0^1 |F(\xi,\eta)|^2 d\xi d\eta \qquad (2.37)$$

is implied. In fact, if interpolation from a network of curves, and not the unit square, is implemented, the upper bound on the error norm is of $O(h^8)$, where h denotes the mesh size that the curve network depicts.

One last step in the direction of the three-dimensional cubic spline boundary element relates to the recognition of the fact that the boundary curves used in the Coons

Leaf blank to correct

numbering

Patch expression, in our application, can not be explicitly available. In case of surface modeling, positional information is available, and in the case of sources, node values are sought for. Hence, the boundary curves as well are obtained via univariate cubic spline interpolation. That is, in describing a three-dimensional surface element, first, the boundaries (which correspond to $\xi = 0$, $\xi = 1$, $\eta = 0$ and $\eta = 1$ edges of the simplex) are interpolated from specified points using the procedure outlined in section 2.1.3, above, and then, the Coons Patch based on these boundaries is obtained. Gordon [14] has shown that this procedure, again implemented on a mesh of specified points which are interpolated, first, to boundary curves, and then to a surface, converges of order $O(h^4)$, as the mesh size, h, is reduced.

2.3 References

(1) Schoenberg, I. J., "Contribution to the problem of approximation of equidistant data by analytic functions", Parts A and B, Quarterly of Applied Mathematics, vol. 4, pp. 45-99, 112-141, 1946.

(2) Ahlberg, J. H., Nilson, E. N. and Walsh, J. L., The Theory of Splines and Their Applications, Academic Press, 1967.

(3) Greville, T. N. E., Theory and Applications of Spline Functions, Academic Press, 1969.

(4) DeBoor, C., "On Calculating with B-Splines", Journal of Approximation Theory, vol. 6, pp. 50-62, 1972.

(5) Schultz, M. H., Spline Analysis, Prentice-Hall, 1973.

(6) Watson, J. O., "Hermitian Cubic Boundary Elements for Elastostatics", Innovative Numerical Analysis for the Engineering Sciences, Proc. 2nd Int. Symposium on Innovative Num. Anal. in App. Eng. Sci., University Press of Virginia, pp. 403-412, 1980.

(7) Zienkiewicz, O. C. The Finite Element Method in Engineering Science, McGraw-Hill, 1971.

(8) Birkhoff, G. and DeBoor, C., "Piecewise Polynomial Interpolation and Approximation", Approximation of Functions, H. L. Garabedian (ed.), Elsewier, 1965.

(9) Barsky, B. A., "Computer-Aided Geometric Design: A Bibliography with Keywords and Classified Index", IEEE Trans. Computer Graphics and Applications, July 1981, pp. 67-108.

(10) Gordon, W. J., "Spline blended surface interpolation through curve networks", Journal of Mathematical Mechanics, vol. 18, pp. 931-952, 1969.

(11) Riesenfeld, R. F., Applications of B-Spline Approximation to Geometric Problems of Computer Aided Design, Ph.D. Dissertation, Syracuse University, New York, 1973.

(12) Coons, S. A., "Surface Patches and B-Spline Curves", Computer Aided Geometric Design, Barnhill and Riesenfeld (ed.s), Academic Press 1974.

(13) Gordon, W. J. and Hall, C.A., "Construction of curvilinear co-ordinate systems and applications to mesh generation", International Journal for Numerical Methods in Engineering, vol. 7, pp. 461-477, 1973.

(14) Gordon, W. J., "Distributive Lattices and the Approximation of Multivariate Functions", Approximations with Special Emphasis on Spline Functions, Schoenberg (ed.), Academic Press, 1969.

CHAPTER III

THE BEM WITH CUBIC SPLINE ELEMENTS

3.1 Two-dimensional spline elements

Consider the uni-variate B-spline basis function defined as in (2.15), in which

$$B_i(x_j) = \begin{cases} 4 & \text{if } j = i, \\ 1 & \text{if } j = i \pm 1, \\ 0 & \text{otherwise;} \end{cases}$$

$$B_i(x) = 0 \quad \text{for } x \geq x_{i+2} \text{ and } x \leq x_{i-2},$$

and $B_i(x)$ is twice continuously differentiable (Fig. 2.2).

The expression

$$P(x) = \frac{1}{6} \sum_{j=1}^{4} V_{i+j-2} B_{i+j-2}(x), \text{ for } x_i \leq x \leq x_{i+1}, \; i = 1, \ldots, N-1, \quad (3.1)$$

is said to represent a B-spline curve controlled by the vertices V_{i+j-2}. Clearly, the condition

$$\frac{1}{6}(V_{i-1} + 4 V_i + V_{i+1}) = P_i, \text{ for } i = 1, \ldots, N \quad (3.2)$$

guarantees that such a curve passes through, i.e. interpolates to any number, N, of points P_i. Vertices V_o and V_{N+1} that (3.2) calls for can be arbitrarily located.

Due to the nature of the basis functions used in this linear combination, the resulting curve is:

i) a cubic polynomial in each interval $x_{j-1} \leq x \leq x_j$, $j = 2, \ldots, N$;

and

ii) second-derivative continuous for all x, $x_1 \leq x \leq x_N$.

Within the interval $x_i < x < x_{i+1}$, only the four basis functions included in expression (3.1) are non-zero (Fig. 3.1). Hence, that expression can be used to define a mapping from the simplex $[0,1]$ to global space $[P_i, P_{i+1}]$ if $x_i = 0$ and $x_{i+1} = 1$. Thus, the summation

$$P(\xi) = \frac{1}{6} \sum_{j=1}^{4} \alpha_j (\xi) V_{i+j-2} \tag{3.3}$$

where

$$\alpha_1 (\xi) = \xi^3 + 3\xi^2 - 3\xi + 1$$

$$\alpha_2 (\xi) = 3\xi^3 - 6\xi^2 + 4$$

$$\alpha_3 (\xi) = -3\xi^3 + 3\xi^2 + 3\xi + 1$$

$$\alpha_4 (\xi) = \xi^3 \tag{3.4}$$

defines a uni-variate boundary element for $0 \leq \xi \leq 1$, $P_i \leq P(\xi) \leq P_{i+1}$. In (3.3), the B-spline control vertices, V_{i+j-2} are equivalent to the ϕ_{ij} in expression (1.4). (*)

(*) See Appendix.

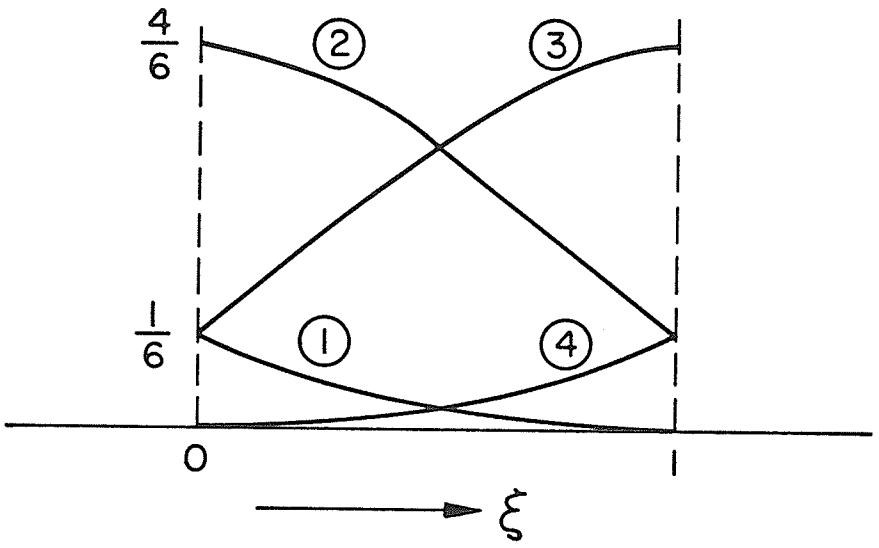

Figure 3.1. The four cubic spline shape functions on an element.

In the application of the BEM, the element definition, (3.3), is used in the discretization of the integral equation to be solved. As noted in section 1.1, this calls for the evaluation of a boundary integral along an incremental vector, $\overline{\mathbf{dl}}$ (Fig. 3.2).

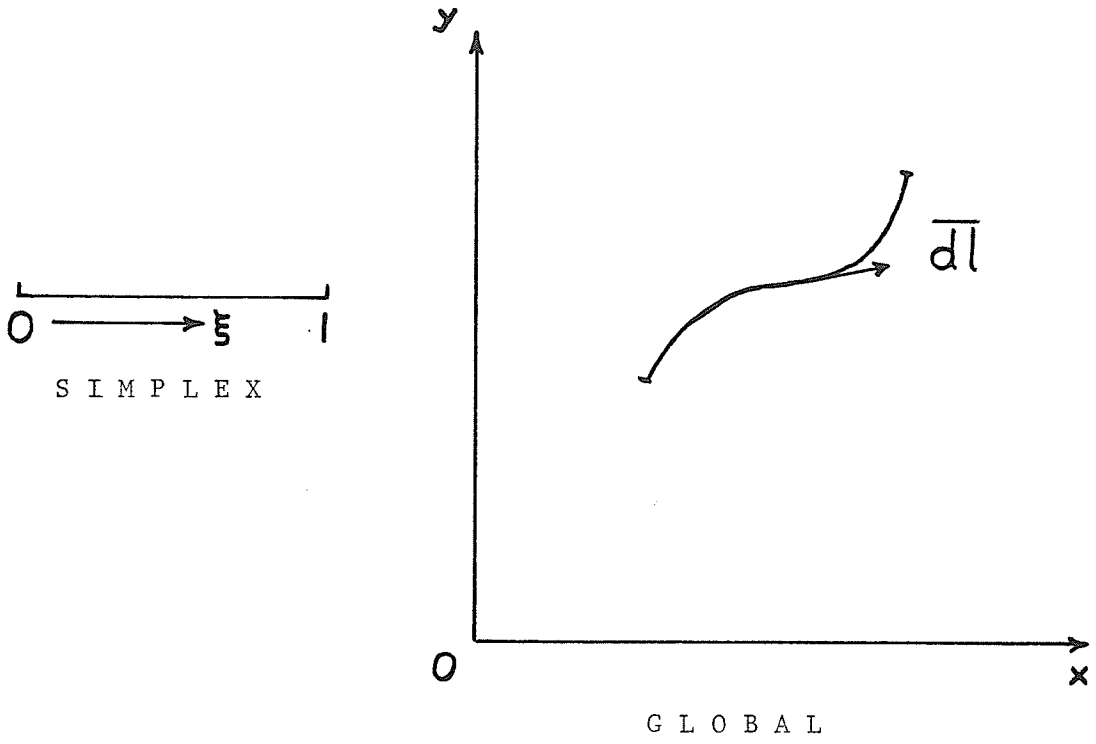

Figure 3.2. The two-dimensional boundary element mapping.

Applying expression (3.3) to the position, $\bar{r}$, evaluating $\overline{dl}$ requires the computation of

$$\overline{dl} = \frac{\partial x}{\partial \xi} \, d\xi \hat{u}_x + \frac{\partial y}{\partial \xi} \, d\xi \hat{u}_y \tag{3.5}$$

and the incremental length, or Jacobian of transformation, is:

$$J = \sqrt{\frac{\partial x}{\partial \xi}^2 + \frac{\partial y}{\partial \xi}^2} \, . \tag{3.6}$$

In this evaluation, both the x-component and the y-component of the position vector, $\bar{r}$, is expressed in the form of (3.3).

3.2 Three-dimensional spline elements

Explicitly stated,

$$P(\xi,\eta) = \beta 0(\eta)F0(\xi)+\beta 1(\eta)F1(\xi)+\beta 0(\xi)F0(\eta)+\beta 1(\xi)F1(\eta)$$
$$-P00\beta 0(\xi)\beta 0(\eta)-P01\beta 0(\xi)\beta 1(\eta)-P10\beta 1(\xi)\beta 0(\eta)-P11\beta 1(\xi)\beta 1(\eta) \tag{3.7}$$

is a Coons patch, as defined above in Section 2.2, that blends the four boundary curves $F0(\xi)$, $F1(\xi)$, $F0(\eta)$, $F1(\eta)$ by means of the blending functions $\beta 0(\cdot)$ and $\beta 1(\cdot)$ (Fig. 2.4). It can easily be shown that the bi-variate surface defined this way contains the boundary curves, and is second-derivative continuous in the ξ- and η- directions, as long as the boundary curves themselves are continuous.

To verify this statement, consider Fig. 3.3, where two adjacent patches are depicted. Let the two patch equations be given as

$$P_1(\xi,\eta) = F0(\xi)\beta0(\eta) + F1(\xi)\beta1(\eta) + F0(\eta)\beta0(\xi) + F1(\eta)\beta1(\xi) - P1\beta0(\xi)\beta0(\eta) - P2\beta1(\xi)\beta0(\eta) - P3\beta1(\xi)\beta1(\eta) - P4\beta0(\xi)\beta1(\eta) \tag{3.8}$$

and

$$P_2(\xi,\eta) = F1(\xi)\beta0(\eta) + F2(\xi)\beta1(\eta) + F2(\eta)\beta0(\xi) + F3(\eta)\beta1(\xi) - P4\beta0(\xi)\beta0(\eta) - P3\beta1(\xi)\beta0(\eta) - P6\beta1(\xi)\beta1(\eta) - P5\beta0(\xi)\beta1(\eta). \tag{3.9}$$

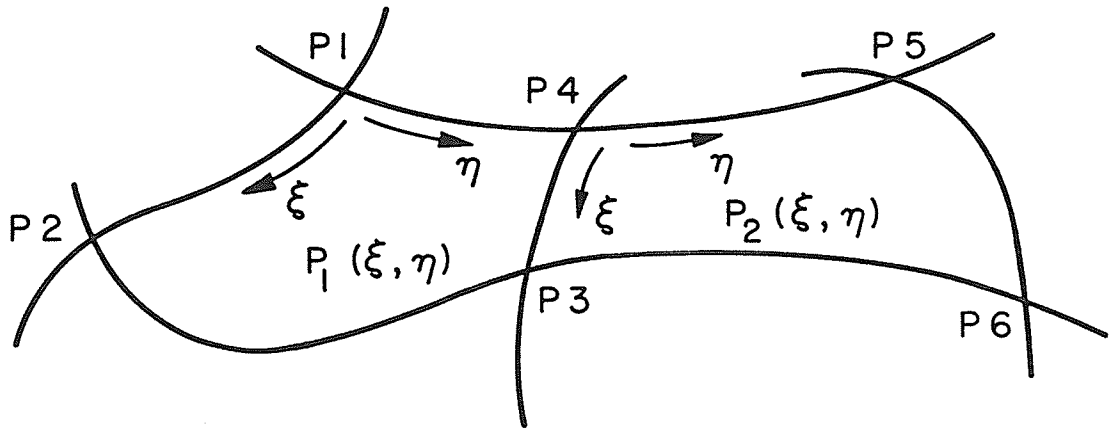

Figure 3.3. Continuity of the Coons Patch.

Now examine partial derivatives at patch edges:

$$\left.\frac{\partial P_1}{\partial \eta}\right|_{\substack{\xi=\xi \\ \eta=1}} = F0'(\eta=1)\beta 0(\xi) + F1'(\eta=1)\beta 1(\xi), \tag{3.10}$$

$$\left.\frac{\partial P_2}{\partial \eta}\right|_{\substack{\xi=\xi \\ \eta=0}} = F2'(\eta=0)\beta 0(\xi)+F3'(\eta=0)\beta 1(\xi). \tag{3.11}$$

So, as $F0'(\eta=1) = F2'(\eta=0)$ (3.12)

and $F1'(\eta=1) = F3'(\eta=0)$ due to the assumed continuity of the boundary curves from patch to patch,

$$\left.\frac{\partial P_1}{\partial \eta}\right|_{\substack{\xi=\xi \\ \eta=1}} = \left.\frac{\partial P_2}{\partial \eta}\right|_{\substack{\xi=\xi \\ \eta=0}}, \tag{3.13}$$

i.e. first derivative continuity is preserved over the boundary. Similarly, for the second derivatives,

$$\left.\frac{\partial^2 P_1}{\partial \eta^2}\right|_{\substack{\xi=\xi \\ \eta=1}} = F0''(\eta=1)\beta 0(\xi)+F1''(\eta=1)\beta 1(\xi) \tag{3.14}$$

and

$$\left.\frac{\partial^2 P_2}{\partial \eta^2}\right|_{\substack{\xi=\xi \\ \eta=0}} = F2''(\eta=1)\beta 0(\xi) + F3''(\eta=1)\beta 1(\xi) \tag{3.15}$$

thus, preserving

$$\left.\frac{\partial^2 P_1}{\partial \eta^2}\right|_{\substack{\xi=\xi \\ \eta=1}} = \left.\frac{\partial^2 P_2}{\partial \eta^2}\right|_{\substack{\xi=\xi \\ \eta=0}} \tag{3.16}$$

based on the assumption that, in turn, the boundary curves are second-derivative continuous over patch edges.

The cross-derivatives can also be tested for continuity; viz:

$$\left.\frac{\partial^2 P_1}{\partial\eta\partial\xi}\right|_{\substack{\xi=\xi \\ \eta=1}} = F0'(\eta=1)\beta 0'(\xi) + F1'(\eta=1)\beta 1'(\xi) \tag{3.17}$$

$$\left.\frac{\partial^2 P_2}{\partial\eta\partial\xi}\right|_{\substack{\xi=\xi \\ \eta=0}} = F2'(\eta=1)\beta 0'(\xi) + F3'(\eta=0)\beta 1'(\xi) \tag{3.18}$$

so,

$$\left.\frac{\partial^2 P_1}{\partial\eta\partial\xi}\right|_{\substack{\xi=\xi \\ \eta=1}} = \left.\frac{\partial^2 P_2}{\partial\eta\partial\xi}\right|_{\substack{\xi=\xi \\ \eta=0}} ; \tag{3.19}$$

i.e., the cross-derivatives are also continuous over patch boundaries. In particular, the cross-derivatives vanish at patch corners, a fact clearly seen by substituting $\xi = 0$ or $\xi = 1$ in (3.17) or (3.18). The "pseudo-flats" thus introduced violate neither interpolatory, nor continuity stipulations; nor

have they caused any numerically detectable mis-representation (see Appendix, and Chapter 5.)

Even though up to this point we have shown that the Coon's Patch expression (3.7) provides the means for a second-derivative-continuous surface representation, we still have to obtain an expression of the form of (1.4) to be used in the BEM implementation.

Each of the four edges of the patch can be represented in the form of (3.3), in terms of four B-spline vertices, V_i, and four uni-variate B-spline shape functions, α_i. At each corner of the patch, a pair of edge curves intersect, which means that a relationship of the form

$$P_{mn} = V_i + 4V_{i+1} + V_{i+2} = V_j + 4V_{j+1} + V_{j+2} \qquad (3.20)$$

should hold for the patch corners symbolized by mn = 00, 01, 10, and 11, with the V_i's and V_j's representing the vertices of the two intersecting edges.

Thus, when (3.3) is substituted into (3.7) for each edge of the surface element, we have 16 vertices, 4 controlling each edge; plus 4 corner points, P_{mn}; i.e. P00, P01, P10 and P11. But using the 8 relationships summarized in (3.20), 8 of these vertices and points can be eliminated. That elimination, clearly

is not unique. But keeping the corner points in the expression is preferred - retaining symmetry.

The resulting bi-variate boundary element definition has the form:

$$P(\xi,\eta) = \frac{1}{6} \sum_{j=1}^{12} V_j A_j \ (\xi,\eta) \qquad (3.21)$$

where A_j are the bi-variate B-spline shape functions which incorporate the uni-variate shape functions associated with the four boundaries, as well as the blending functions in expression (3.7). Here, V_j are the bi-variate B-spline control vertices. V_1, ..., V_8 correspond to uni-variate B-spline vertices of the boundary curves (i.e. the V_{i+j-2} in expression (3.3)), and V_9, ..., V_{12} are the corner points of the patch.

The obvious advantage brought about by this approach is that a bi-cubic polynomic approximation is obtained, ensuring second-derivative continuity over boundaries, by means of only 12 coefficients - in contrast to the 16 arbitrary coefficients that a classical bicubic approximation of the form,

$$P(\xi,\eta) = \sum_{j=0}^{3}\sum_{k=0}^{3} a_{jk}\xi^j\eta^k \qquad (3.22)$$

would require. The only price that is paid is vanishing cross-derivatives at patch corners, as mentioned earlier.

The explicit expressions, after elimination and re-arranging, for the bi-variate B-spline shape functions are:

$$A_1(\zeta,\eta) = \alpha_1(\zeta)\ \beta0(\eta) - \frac{4}{15}\alpha_2(\zeta)\ \beta0(\eta) + \frac{1}{15}\alpha_3(\zeta)\ \beta0(\eta)$$

$$A_2(\zeta,\eta) = \alpha_4(\zeta)\ \beta0(\eta) + \frac{1}{15}\alpha_2(\zeta)\ \beta0(\eta) - \frac{4}{15}\alpha_3(\zeta)\ \beta0(\eta)$$

$$A_3(\zeta,\eta) = \alpha_1(\zeta)\ \beta1(\eta) - \frac{4}{15}\alpha_2(\zeta)\ \beta1(\eta) + \frac{1}{15}\alpha_3(\zeta)\ \beta1(\eta)$$

$$A_4(\zeta,\eta) = \alpha_4(\zeta)\ \beta1(\eta) + \frac{1}{15}\alpha_2(\zeta)\ \beta1(\eta) - \frac{4}{15}\alpha_3(\zeta)\ \beta1(\eta)$$

$$A_5(\zeta,\eta) = \alpha_1(\eta)\ \beta0(\zeta) - \frac{4}{15}\alpha_2(\eta)\ \beta0(\zeta) + \frac{1}{15}\alpha_3(\eta)\ \beta0(\zeta)$$

$$A_6(\zeta,\eta) = \alpha_4(\eta)\ \beta0(\zeta) + \frac{1}{15}\alpha_2(\eta)\ \beta0(\zeta) - \frac{4}{15}\alpha_3(\eta)\ \beta0(\zeta)$$

$$A_7(\zeta,\eta) = \alpha_1(\eta)\ \beta1(\zeta) + \frac{4}{15}\alpha_2(\eta)\ \beta1(\zeta) - \frac{1}{15}\alpha_3(\eta)\ \beta1(\zeta)$$

$$A_8(\zeta,\eta) = \alpha_4(\eta)\ \beta1(\zeta) + \frac{1}{15}\alpha_2(\eta)\ \beta1(\zeta) - \frac{4}{15}\alpha_3(\eta)\ \beta1(\zeta)$$

$$A_9(\zeta,\eta) = -\beta0(\zeta)\ \beta0(\eta) + \frac{24}{15}\alpha_2(\zeta)\ \beta0(\eta) - \frac{6}{15}\alpha_3(\zeta)\ \beta0(\eta) + \frac{24}{15}\alpha_2(\eta)\ \beta0(\zeta) - \frac{6}{15}\alpha_3(\eta)\ \beta0(\zeta)$$

$$A_{10}(\zeta,\eta) = -\beta0(\zeta)\ \beta1(\eta) + \frac{24}{15}\alpha_2(\zeta)\ \beta1(\eta) - \frac{6}{15}\alpha_3(\zeta)\ \beta1(\eta) + \frac{24}{15}\alpha_3(\eta)\ \beta0(\zeta) - \frac{6}{15}\alpha_2(\eta)\ \beta0(\zeta)$$

$$A_{11}(\zeta,\eta) = -\beta1(\zeta)\ \beta0(\eta) + \frac{24}{15}\alpha_3(\zeta)\ \beta0(\eta) - \frac{6}{15}\alpha_2(\zeta)\ \beta0(\eta) + \frac{24}{15}\alpha_2(\eta)\ \beta1(\zeta) - \frac{6}{15}\alpha_3(\eta)\ \beta1(\zeta)$$

$$A_{12}(\zeta,\eta) = -\beta 1(\zeta)\ \beta 1(\eta) + \frac{24}{15}\ \alpha_3(\zeta)\ \beta 1(\eta) - \frac{6}{15}\ \alpha_2(\zeta)\ \beta 1(\eta)$$

$$+ \frac{24}{15}\ \alpha_3(\eta)\ \beta 1(\zeta) - \frac{6}{15}\ \alpha_2(\eta)\ \beta 1(\zeta)\ , \qquad (3.23)$$

in which the uni-variate B-spline shape functions, $\alpha_i(\cdot)$ are the same as in (3.4). The blending functions, $\beta 0(\cdot)$ and $\beta 1(\cdot)$, shown in Fig. 3.4 are defined, in turn, as cubic splines:

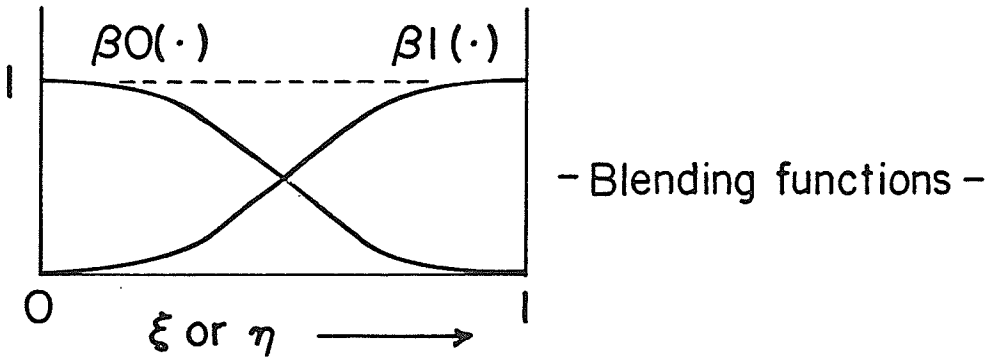

Figure 3.4. Cubic spline blending functions.

$$\beta 0(\zeta) \begin{cases} = \frac{1}{6}(-\zeta^3 + 6) & , \quad 0 \leq \zeta \leq 1/3 \\ = \frac{1}{6}(54\zeta^3 - 81\zeta^2 + 27\zeta + 3) & , \quad 1/3 \leq \zeta \leq 2/3 \\ = \frac{1}{6}(-27\zeta^3 + 81\zeta^2 - 81\zeta + 27) & , \quad 2/3 \leq \zeta \leq 1 \end{cases}$$

and

$$\beta 1(\zeta) \begin{cases} = \frac{1}{6}\zeta^3 & , \quad 0 \leq \zeta \leq 1/3 \\ = \frac{1}{6}(-54\zeta^3 + 81\zeta^2 - 27\zeta + 3) & , \quad 1/3 \leq \zeta \leq 2/3 \\ = \frac{1}{6}(27\zeta^3 - 81\zeta^2 + 81\zeta - 21) & , \quad 2/3 \leq \zeta \leq 1 \ . \end{cases} \quad (3.24)$$

As in the two-dimensional case with uni-variate boundaries, integration called for by the BEM has to be performed with respect to an incremental area vector, $\overline{ds}$, which is (Fig. 3.5):

$$\overline{ds} = \overline{dr_1} \times \overline{dr_2} \quad (3.25)$$

The incremental vectors in the two uni-variate directions can be obtained from (3.21), and represented in the Cartesian co-ordinate system as:

$$\overline{dr_1}(\xi) = \frac{\partial x}{\partial \xi} d\xi \, \hat{u}_x + \frac{\partial y}{\partial \xi} d\xi \, \hat{u}_y + \frac{\partial z}{\partial \xi} d\xi \, \hat{u}_z \quad (3.26)$$

and $$\overline{dr_2}(\eta) = \frac{\partial x}{\partial \eta} d\eta \, \hat{u}_x + \frac{\partial y}{\partial \eta} d\eta \hat{u}_y + \frac{\partial z}{\partial \eta} d\eta \hat{u}_z \quad (3.27)$$

The Jacobian of transformation, then, which is equal to the magnitude of the incremental area vector, is

$$J = \left| \overline{dr_1}\ (\xi) \times \overline{dr_2}\ (\eta) \right|$$

$$= \sqrt{M_{31}{}^2 + M_{32}{}^2 + M_{33}{}^2} \qquad (3.28)$$

in which M_{ij} are the minors of

$$A = \begin{vmatrix} \frac{\partial x}{\partial \xi} & \frac{\partial y}{\partial \xi} & \frac{\partial z}{\partial \xi} \\ \frac{\partial x}{\partial \eta} & \frac{\partial y}{\partial \eta} & \frac{\partial z}{\partial \eta} \\ 1 & 1 & 1 \end{vmatrix} \qquad (3.29)$$

taken along the last row.

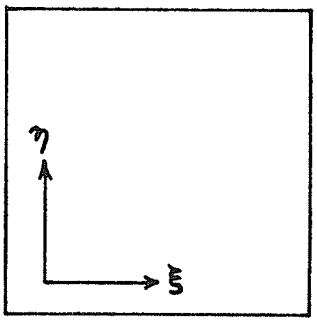

S I M P L E X

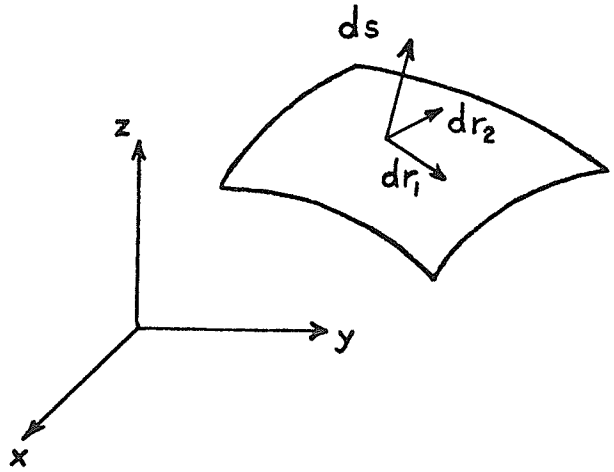

G L O B A L

Figure 3.5. The three-dimensional boundary element mapping.

Although they furnish the basis for an efficient boundary element methodology, the particular schemes of cubic spline element definition developed here do not guarantee a uni-valent mapping from the simplex to a global element. An investigation of the Uni-variate (expressions (3.3) and (3.4)) and bi-variate ((3.21) and 3.23))cubic spline elements reveals that anomalous mappings that correspond to a vanishing Jacobian of transformation (given in (3.6) and (3.28)) may result from distorted global element configurations (Fig. 3.6). An algorithm that would generate a uni-valent mapping for all configurations seems to be impossible to design [1]. Thus, using heavily distorted elements would risk improper operation of this algorithm (Fig. 3.6), which is the case for most iso-parametric schemes [2].

3.3 A hybrid algorithm: Splines for geometry, Lagrangian elements for sources.

The original stimulation for the development of cubic spline boundary elements was centered on the need to achieve a high degree of fidelity in modeling problem geometries. Especially in regard to precise evaluation of actual boundary sources and near-field affects, absence of spurious creases and cusps is crucial. Step-function appoximation or even higher-order Lagrangian schemes do not generally guarantee smooth connection of elements [e.g. 3, p. 45, figure 2.10]. Splines, on the other hand, effectively remove this hindrance.

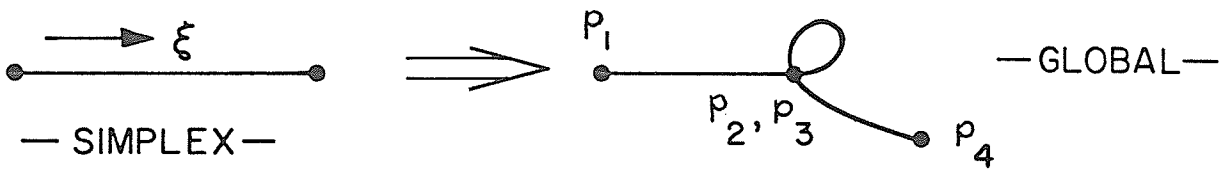

(2-D)

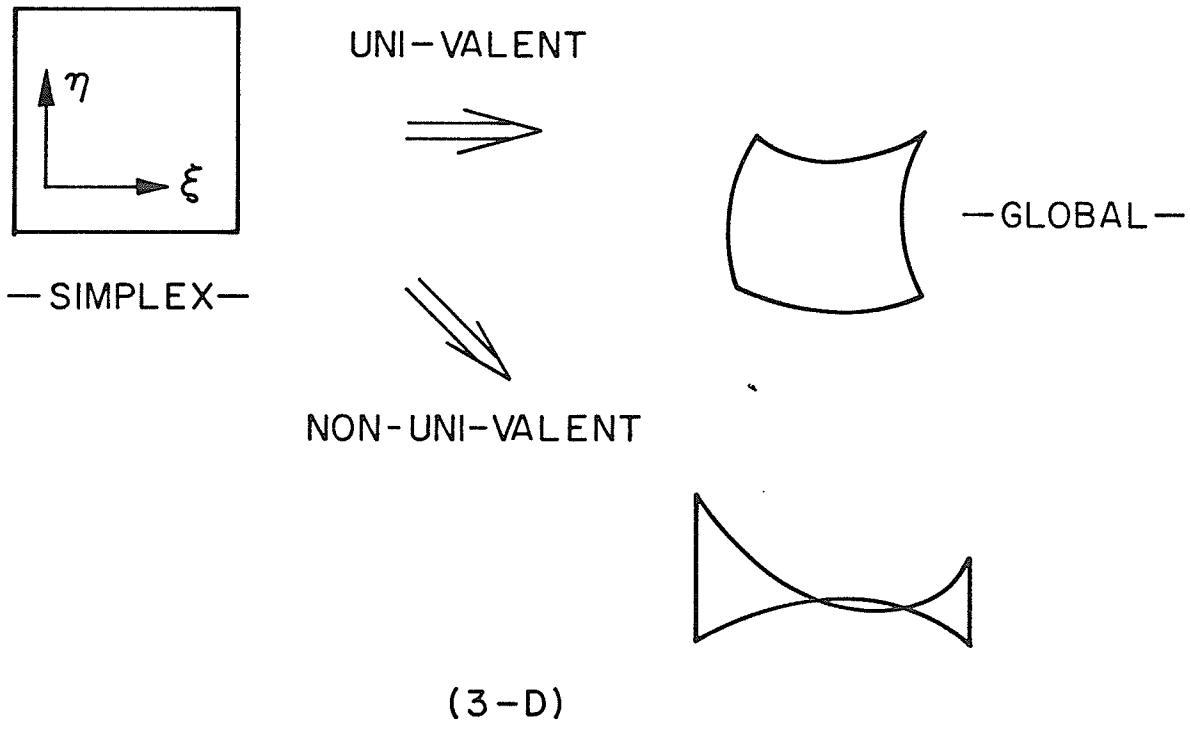

(3-D)

Figure 3.6. Anomalies of the cubic spline mapping.

With the aim of modelling problem geometries "smoothly" while keeping the source representation as simple as possible, a hybrid algorithm was implemented and tested: no longer an iso-parametric scheme (where geometry and sources are modelled to the same order of polynomic approximation), this consists of a cubic spline boundary element configuration for the geometry, and Lagrangian elements for the sources. The basis functions used for expansion and testing in the Galerkin scheme (see section 1.1) were all Lagrangian, of selectable polynomic orders. Details of the BEM implementation of Lagrangian elements are to be found in (4), (5), (6), etc.

Results obtained from this test will be presented in Chapter V and comparisons will be drawn against the solution of identical problems with the BEM using cubic splines for both geometry and sources.

3.4 References

(1) Gordon, W. J., and Hall, C. A., "Construction of curvilinear co-ordinate systems and applications to mesh generation", International Journal for Numerical Methods in Engineering, vol. 7, pp. 461-477, 1973.

(2) Zienkiewicz, O. C., The Finite Element Method in Engineering Science, McGraw-Hill, 1971.

(3) Prentner, P. M., Splines and Variational Methods, John Wiley & Sons, 1975.

(4) Lean, M. H., Electromagnetic Field Solution with the Boundary Element Method, Ph.D. Dissertation, University of Manitoba, 1981.

(5) Jeng, G. and Wexler, A., "Isoparametric Finite Element Variational Solution of Integral Equations for Three-Dimensional Fields", International Journal of Numerical Methods in Engineering, vol. 11, pp. 1455-1471, 1977.

(6) Lean, M. H., Friedman, M., and Wexler, A., "Application of the Boundary Element Method in Electrical Engineering Problems" in Developments in Boundary Element Methods -1, Banerjee, P.K. and Butterfield, R. (eds.), Applied Science Publishers Ltd., England, 1979.

CHAPTER IV

TREATMENT OF SINGULARITIES

Two fundamental problems that have to be addressed by the BEM will be discussed in this chapter: (i) evaluation of the diagonal entries of the system matrix in equation (1.9) when the integration kernel has a singular point within the domain of integration, and (ii) approximation of the solution function when it has a finite number of singularities within the domain of approximation, by a finite number of polynomic or "modified polynomic" basis functions.

4.1 Kernel singularity

The basic equation that the BEM has to solve was given above as:

$$\int_S K(r|r')\, f(r')\, ds(r') - \lambda f(r) = g(r), \qquad (1.1)$$

and the conditions for the existence of a unique solution for arbitrary g(r) were stated in (1.2) and (1.3), namely that the kernel of integration, $K(r|r')$ be square-integrable over S, and that the right-hand-side, or the "excitation" be bounded. Furthermore, it was stated that λ should not be an eigenvalue of the operator, i.e.

$$\int_S K(r|r')\, f(r')\, ds(r') - \lambda f(r) = 0 \qquad (4.1)$$

should have only the trivial solution,

$$f(r) \equiv 0. \qquad (4.2)$$

In most applications relating to electromagnetic field problems, the kernel has a singularity when the source-point, r', coincides with the field-point, r. Kellog [1] has extensively discussed the integrability of these kernels and the existence of principle-value integrals of singular integrands.

Specifically, it has been shown that [2, 3] If the kernel has the form

$$K(r|r') = \frac{A(r|r')}{R^{\nu}} \quad , \quad 0<\nu< m/2 \tag{4.3}$$

where the domain of integration, S, is a bounded surface in (m + 1)-dimensional Euclidean space, with $A(r|r')$ a bounded function, and R, the Euclidean distance between the points r and r', then (1.1) is a Fredholm equation, i.e. $K(r|r')$ is square-integrable. The same is true for a logarithmic kernel [4], i.e. if the kernel has the form

$$K(r|r') = A(r|r') \ln R \quad , \tag{4.4}$$

in two-dimensional space. In fact, it is true that [3] even when $0<\nu<m$ with everything else the same as stated for (4.3), the Fredholm theory still applies although the kernel is no longer square-integrable; i.e. (1.1) has a unique solution. Such equations are said to possess a <u>weak singularity</u>.

In all applications of the BEM investigated within the scope of this work, integration kernels were either of the forms (4.3) or (4.4), or asymptotically approaching those forms.

A number of approaches have been reported in relation to the particular method of catering for the effects of such "integrable" singularities in the solution scheme.

The most popular schemes utilize analytical evaluation of the singular integral. Either the method of "subtraction and addition" of the singular term and then evaluating the singular integral over a planar domain [5,6], or the technique of "dividing out" the singular term [7] has been used. The former scheme has been successfully implemented and produced accurate results over curved geometries, coupled with a local planarization and parametrization scheme in the vicinity of the singular point. In the simpler and more classical instance of using a pulse-expansion scheme, analytic integration is even more straight forward as the function to be approximated, being assumed constant over an element, does not effect the integrand [8].

More recently, a purely numerical scheme which has the advantages of being problem-independent and not requiring planarization has been developed. That technique, described

(9) in the context of Lagrangian elements in two- and three-dimensional spaces, is easily extendable for application in the cubic spline environment. An outline of the technique follows.

Gaussian quadrature integration (10) is utilized to evaluate all integrals depicted in the discretized equation (1.7). That is, the formula

$$\int_a^b w(x)f(x)dx \simeq \sum_{i=1}^{N} A_i f(x_i) \qquad (4.5)$$

is applied in which N denotes the pre-set order of quadrature, and x_i and A_i signify evaluation points and weights, respectively. w(x) stands for the weighting function which characterizes the particular quadrature formula being used. For a specific choice of w(x), a particular set of orthogonal polynomials are generated using the Gram -Schmidt orthogonalization procedure, whose real roots, x_i, and corresponding weights, A_i, minimize the error incurred in (4.5). In fact, if f(x) is polynomic of order M, $M \leq N$, then (4.5) is exact. The general form

$$w(x) = (1-x)^{\nu} (1+x)^{\upsilon} \; ; \; \nu,\upsilon > -1 \qquad (4.6)$$

gives rise to the family of Gauss-Jacobi polynomials which include w(x) = 1, the Gauss-Legendre weight. Also available are formulas for

$$w(x) = \ln|x|. \qquad (4.7)$$

In computation of S_{pq}, the general entry of the system matrix in the BEM, the following integral, given in (1.10), has to be evaluated:

$$S_{pq} = \sum_{i} \int_{ei} \alpha_p(\xi) \int_S K(r|r') \alpha_q(\xi') ds' ds. \qquad (4.8)$$

When the inner and outer ("source" and "observation") integration elements coincide, evaluation of the integration kernel becomes problematic. As noted above, an integrable singularity is encountered, and has to be properly tackled. The cases of two- and three-dimensional problems are similarly dealt-with; but the particularities of the element configurations warrant separate consideration.

4.1.1 Two-dimensional problems

The element whose contribution over itself is to be computed is bisected about p, the Gauss quadrature point of the outer integral (Fig. 4.1). A quadrature scheme that is weighted with the dominant behavior of the singular kernel is selected. For two-dimensional problems invariant along the axial dimension, usually the kernel is logarithmic, or approaches logarithmic behavior for small arguments; hence a logarithmically weighted quadrature formula is used for singularity treatment. The quadrature points and weights thus generated are transformed by

$$T_1: \xi^* = p(1 - \xi);\ 0 \leq \xi^* \leq p \ , \text{ and} \qquad (4.9)$$

$$T_2: \xi^* = (1 - p)\xi + p;\ p \leq \xi^* \leq 1 \ , \qquad (4.10)$$

to position the quadrature points so that p is approached on both sides logarithmically. Scaling the respective weights by (1-p) and p ensures that the original formula given[10] for

$$-\int_0^1 \ln|x|\, f(x)\, dx \simeq \sum_{i=1}^{N} A_i f(x_i) \qquad (4.11)$$

will be valid now for

$$-\int_0^p \ln|x-p| f_1(x)dx \simeq \sum_{i=1}^{N} A_i f_1(x_i),$$

and

$$-\int_p^1 \ln|x-p| f_2(x)dx \simeq \sum_{i=1}^{N} A_i f_2(x_i), \quad 0\leq p\leq 1. \qquad (4.12)$$

The functions that are sampled resemble:

$$f_1(\xi_i^*) = \frac{k(r|r'(\xi_i^*))}{\ln\{\frac{\xi_i^*-p}{1-p}\}}\ \alpha_q(\xi_i^*)\ |J||T_1|$$

$$f_2(\xi_i^*) = \frac{k(r|r'(\xi_i^*))}{\ln\{\frac{p-\xi_i^*}{p}\}}\ \alpha_q(\xi_i^*)\ |J||T_2|. \qquad (4.13)$$

Chain rule of integral calculus is being used, viz:

$$\int f(g)\, dg = \int f(g(x))\, \frac{dg}{dx}\, dx, \qquad (4.14)$$

In summary, the contribution to the system matrix of an element over itself is computed by bisecting the element about each Gauss quadrature point of the outer integral, and adding the contributions to the inner integral of the two portions

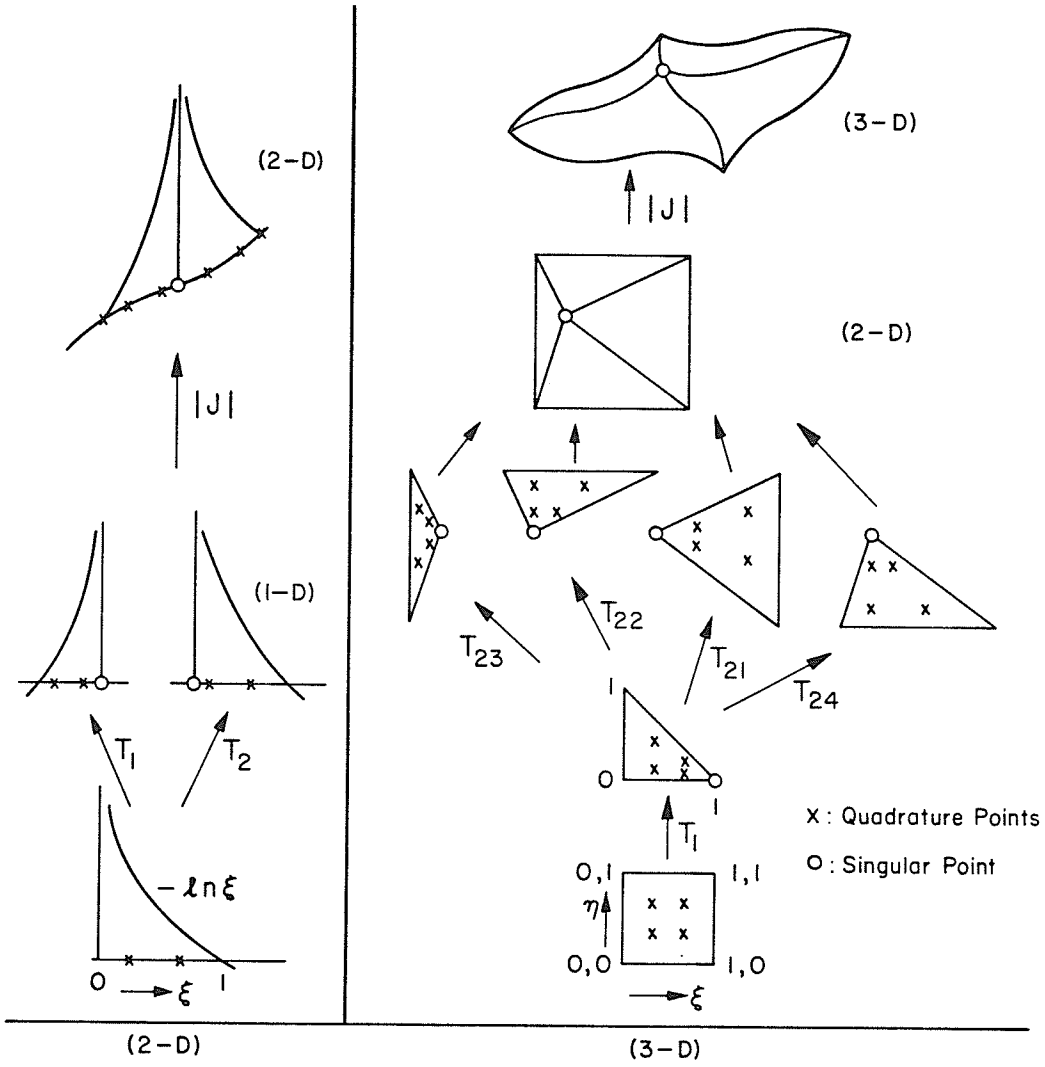

Figure 4.1. Catering for kernel singularities.

thus formed. Sampling the integral at the bisection point is thus avoided, and furthermore, as a properly weighted quadrature formula is used at this stage, high precision is achieved.

4.1.2 Three-dimensional problems

The self-element is partitioned into four triangles (Fig. 4.1) about the quadrature point of the outer integral. To obtain the sampling locations over the four partitions, a bi-variate quadrature formula generated by the product rule over a simplex unit square (bottom of Fig. 4.1) is utilized. That square is first transformed to a simplex triangle by collapsing the ξ=1 edge via the transformation

$$\begin{aligned} T1: \quad \xi^* &= \xi \\ \eta^* &= \eta\,(1-\xi) \end{aligned} \tag{4.15}$$

Where η^* and ξ^* represent the co-ordinate system on the simplex triangle. The Jacobian of transformation for T1 is:

$$|T1| = \begin{vmatrix} \frac{\partial \xi^*}{\partial \xi} & \frac{\partial \xi^*}{\partial \eta} \\ \frac{\partial \eta^*}{\partial \xi} & \frac{\partial \eta^*}{\partial \eta} \end{vmatrix} = \begin{vmatrix} 1 & 0 \\ -\eta & (1-\xi) \end{vmatrix} = (1-\xi). \tag{4.16}$$

The second step consists in transforming the simplex triangle to each of the four portions of the unit square representing the global element. The collapsed, $\xi^* = 1$, point has to correspond to the singular point, (x_p, y_p). The following linear transformations are utilized:

$$T_{21}: \quad u = (x_p - 1)\,\xi^* + 1$$
$$v = (y_p - 1)\,\xi^* - \eta^* + 1$$
$$|T_{21}| = (1-x_p), \tag{4.17}$$

$$T_{22}: \quad u = x_p\xi^* + \eta^*$$
$$v = (y_p - 1)\xi^* + 1$$
$$|T_{22}| = (1-y_p), \tag{4.18}$$

$$T_{23}: \quad u = x_p\xi^*$$
$$v = y_p\xi^* + \eta^*$$
$$|T_{23}| = x_p, \tag{4.19}$$

$$T_{24}: \quad u = (x_p - 1)\xi^* - \eta^* + 1$$
$$v = y_p\xi^*$$
$$|T_{24}| = y_p. \tag{4.20}$$

... And the final transformation involves going from the square bi-variate simplex to the global element through the cubic spline element mapping, described in section 3.2 above.

Gauss quadrature sampling is performed, now , on the following expression, again using the chain rule of integral calculus:

$$f(\xi_i, \eta_i) = k(r|r')\alpha_q(u',v')|T_1|\ |T_{2N}|\ |J|$$

in which

$$r' = r'(u', v'), \text{ via transformation } |J|, \tag{4.22}$$

$$u' = u'(\xi^*, \eta^*)$$

$$v' = v(\xi^*, \eta^*) \text{ via transformation } T_{21}, T_{22},$$

$$T_{23} \text{ or } T_{24}, \tag{4.23}$$

and

$$\xi^* = \xi^*(\xi_i, \eta_i)$$

$$\eta^* = \eta^*(\xi_i, \eta_i) \text{ via transformation } T_1. \tag{4.24}$$

While it is possible, at this juncture, to utilize a weighted quadrature scheme reflecting the form of the singularity, the fact that transformation T1 regularizes the kernel behavior by introducing the $(1-\xi)$ factor on the numerator removes that necessity.

The following numerical test cases illustrate the procedure and provide an estimate on the accuracy involved.

E.g. (i) $K(r|r') = 1$ for all r and r',

$J(u, v) = 1$ for all u, v, i.e. integrating the constant unity function over the unit square (Fig. 4.2,)

Using two-point quadrature, sampling locations and weights are (10, p.100):

$$x_1 = 0.2113,\ y_1 = 0.2113,\ w_1 = 0.25$$

$$x_2 = 0.2113,\ y_2 = 0.7887,\ w_2 = 0.25$$

$$x_3 = 0.7887,\ y_2 = 0.2113,\ w_3 = 0.25$$

$$x_4 = 0.7887,\ y_2 = 0.7887,\ w_4 = 0.25, \tag{4.25}$$

The integrals over the respective triangular portions (see (4.21)) are:

$$I_1 = \sum_{i=1}^{4} J^* (1-\xi_i) * 0.25 = 0.7887 * (0.7887 + 0.7887 + 0.2113 + 0.2113) * 0.25 = 0.7887 * 0.5 \quad (4.26)$$

and similarly,

$$I_2 = 0.2113 * 0.5,\ I_3 = 0.2113 * 0.5,\ I_4 = 0.7887 * 0.5. \quad (4.27)$$

Thus,

$$I = \Sigma I_i = (0.7887 + 0.2113 + 0.2113 + 0.7887) * 0.5 = 1.0, \quad (4.28)$$

which is exactly equal to the volume of the unit cube, as expected.

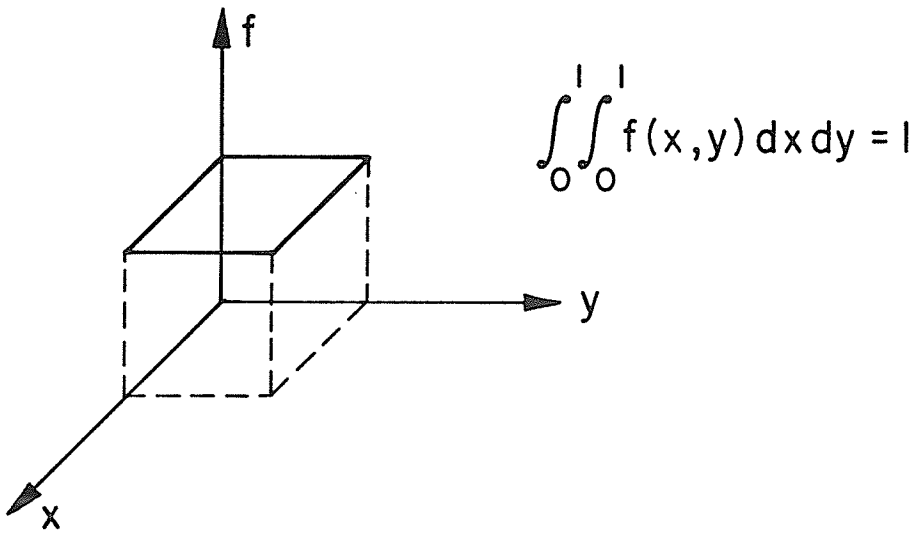

Figure 4.2 Integration of the unity function over the unit square

E.g. (ii) $K(r|r') = u'$, where $r' = (u', v')$,

$J(u,v) = 1$ everywhere, i.e. integrating a unit ramp function over the unit square (Fig. 4.3). Again using two-point quadrature over the simplex,

For I_1, $|T_{21}| = (1 - x_p) = 0.7887$

$$u = 1 - 0.7887*\xi.$$

$I_1 = u_1|T_{21}|(1-\xi_1)w + u_2|T_{21}|(1-\xi_2)w + u_3|T_{21}|$
$(1-\xi_3)w + u_4|T_{21}|(1-\xi_4) = 0.7887*0.25*(0.7887*0.8333 +$
$0.2113*0.3778)*2 = 0.2907,$ (4.29)

for I_2, $|T_{22}| = (1-y_p) = 0.7887$

$$u = 0.2113\xi + \eta(1-\xi).$$

$$I_2 = |T_{22}|w\,(\,(1-\xi_1)(0.2113\xi_1 + \eta_1(1-\xi_1)\,) +$$
$$(1-\xi_2)(0.2113\xi_2 + \eta_2(1-\xi_2)\,) +$$
$$(1-\xi_3)(0.2113\xi_3\,\eta_3(1-\xi_3)\,) +$$
$$(1-\xi_4)(0.2113\xi_4 + \eta_4(1-\xi_4)\,)\,)$$
$$= 0.1592,$$ (4.30)

for I_3, $|T_{23}| = x_p = 0.2113$

$$u = 0.2113\xi.$$

$$I_3 = |T_{23}|w(1-\xi_1)\,0.2113\xi_1 + (1-\xi_2)\,0.2113\xi_2)*2$$
$$= 0.0074,$$ (4.31)

and for I_4, $|T_{24}| = y_p = 0.2113$

$$u = (x_p - 1)\,\xi - \eta(1-\xi) + 1$$
$$= 1 - \eta(1-\xi) - 0.7887\xi.$$

$I_4 = 0.2113*0.25(\,(1-\xi_1)\,1-\eta_1(1-\xi_1) - 0.7887\xi_1 + 1-\eta_2(1-\xi_2)$
$-0.7887\xi_2 + (1-\xi_3)\,1-\eta_3(1-\xi_3)-0.7887\xi_3 + 1-\eta_4(1-\xi_4)-0.7887\xi_4$
$= 0.04266.$ (4.32)

... And adding the integrals over the four triangular portions, given in (4.29), (4.30), (4.31) and (4.32),

$$I = \Sigma I_i = 0.5 \tag{4.33}$$

which again, is exact as expected.

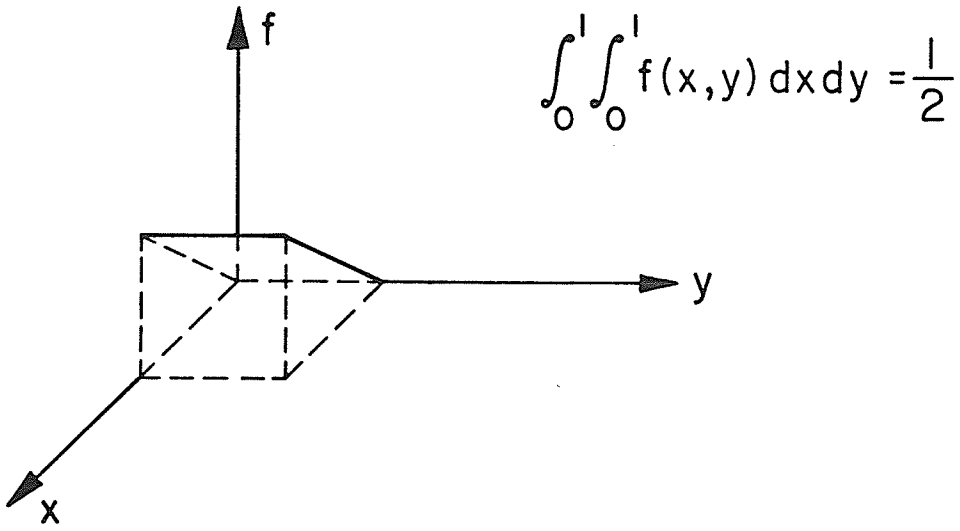

Figure 4.3 Integration of the unit ramp over the unit square.

E.g. (iii) Lastly, the integration kernel of many three-dimensional problems,

$$K(r|r') = \frac{1}{|r_o - r'|} = \frac{1}{\sqrt{(x'-x_o)^2+(y'-y_o)^2}} \tag{4.34}$$

with the singular point, r_o at (0.2113,0.2113), will be numerically integrated over a unit-square region. As the integration region coincides with the simplex square, we have a unity Jacobian of transformation.

Analytical integration is possible for this flat patch, and using the expression given by Jeng,[6,p.28] we get

$$I = 3.03174 \tag{4.35}$$

for the exact value of the integral.

A two-point quadrature integration results in

$$I = 3.1508, \tag{4.36}$$

and a three-point scheme produces the value

$$I = 3.0028, \tag{4.37}$$

These results represent 4% and less than 1% error, respectively. As most of the three-dimensional problems to be considered below involve a similar integration kernel, this example can be considered as a measure of the degree of accuracy of handling the Green's function singularity in those applications.

4.2 Source singularities due to geometry

Singularities occurring at sharp edges in electromagnetics have been the subject of research for a long time. In one of the earlier works, Lord Rayleigh [11] investigated the behavior of electromagnetic fields at edges and studied the singular behavior of the component normal to the edge. In the 1940's, Bouwkamp [12] and Meixner [13] developed the "edge-condition" which states that the electromagnetic energy density must be integrable over any finite domain even if this domain contains singularities of the electromagnetic field; that is, the electromagnetic energy in any finite domain must be finite. Meixner's report [14] in 1954 further developed the area and summarized the principles of field behavior in the proximity of dielectric and conducting wedges of arbitrary angle. He proved that the components of $\overline{E}$ and $\overline{H}$ fields parallel to the edge are finite, and derived the functional dependence of the magnitudes of the normal components on the distance from the edge tip and the wedge angle. Quite a while later, Hurd [15, 16] and J. B. Andersen & V. V. Solodukhov [17] modified Meixner's principles and showed that while Meixner's results hold for the electrostatic case of a perfect conductor, his basic assumptions are questionable for the case of a penetrable body in a dynamic field. The particular problem of

electromagnetic scattering from a dielectric wedge, investigated by the latter researchers will be further considered below, and numerical results presented.

After Meixner, Jones [18] and Braunbek [19] established the principle that the diffraction field of electromagnetic waves in the vicinity of plane-screen corners of arbitrary angle can be found by solving Laplace's equation - without having to modify Meixner's "edge-condition".

With regard to the numerical solution of elliptic partial differential equations for singular fields, the works by Motz [20], Lehman [21] and Wait & Mitchell [22] signified an important evolution. The former work used a Finite Difference operator modified to cater for the irregular behavior around the singularity; Lehman's work relied on finding the asymptotic behavior around the edge analytically, and utilized expansion functions reflecting that form as the basis for the solution that is sought for; the latter study utilizes bilinear basis functions similar to those considered above in section 2.2, supplemented by the addition of singular functions of the form of expected field behavior. Wait and Mitchell also successfully implemented a finite-element mesh refinement step to further improve convergence.

Later treatises on the subject include Prof. G. Birkhoff's

paper [23] in which numerous special purpose finite elements are developed to cater for a number of different partial differential equation problems, mainly involving nuclear reactor physics. A more general treatment by Kondrat'ev [24] develops the form of the singularity for a rather wide class of elliptic problems.

Also developed later were algorithms for deriving special purpose interpolatory schemes particularly applicable to modeling singular behavior [25].

Methods based on conformal mappings [26], which seem to restrict the scope of applicability, have produced highly reliable results where appropriate mappings were available. Especially suited to integral equation formulations, these methods can be used even when problem geometry cannot be directly transformed, but the singular behavior approaches that of a standard transformable configuration. The only drawback on this account appears to be the necessity of analytical treatment prior to numerical solution.

A different approach has been followed by Ying Lung-An [27] and Thatcher [28] independently. While posing a problem of nomenclature, ("infinite similar" as opposed to "infinitesimal")

Ying's method seems highly innovative: in the neighborhood of the singularity, a countable infinity of mutually similar triangular elements are placed, and the resulting system matrix is computed by an algorithm that makes use of infinite matrix series computed as a function of their eigenvalues which are proven to lie within the unit circle [23].

The major forms of singularity of sources that we shall be dealing with can be examined via a simple consideration of the governing Laplace or Helmholtz equations [30].

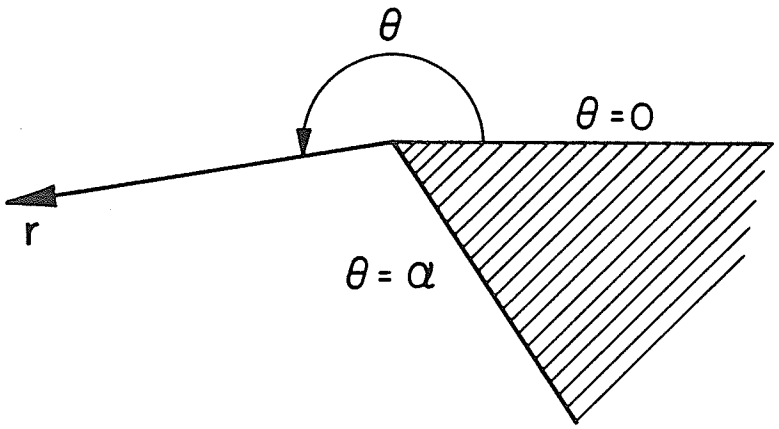

Figure 4.4 Two-dimensional wedge geometry

Restricting our attention to variation in two dimensions only, Laplace's equation

$$\nabla^2\Phi = 0 \tag{4.37}$$

is separable in cylindrical co-ordinates, r and Θ (Fig. 4.4):

$$r^2\frac{\partial^2\Phi}{\partial r^2} + r\frac{\partial\Phi}{\partial r} + \frac{\partial^2\Phi}{\partial\Theta^2} = 0, \tag{4.38}$$

its solution being

$$\Phi(r,\Theta) = R(r)\Psi(\Theta), \tag{4.39}$$

with

$$r^2\frac{d^2R}{dr^2} + r\frac{dR}{dr} - s^2R = 0 \tag{4.40}$$

and

$$\frac{d^2\Psi}{d\Theta^2} + s^2\Psi = 0. \tag{4.41}$$

The general solution is the sum of all linearly independent solutions,

$$\Phi(r,\theta) = \Sigma\ (a_s r^s \sin s\Theta + b_s r^s \cos s\Theta) \tag{4.42}$$

summation extending over all real s that satisfy the boundary conditions.

E.g. If given $\Phi = 0$ at $\Theta = 0$ and $\Theta = \alpha$,

then

$$\Phi(r,\Theta) = \sum_{k=1}^{\infty} a_k r^{k\frac{\pi}{\alpha}} \sin\frac{k\pi}{\alpha}\Theta. \tag{4.43}$$

Or, if given $\Phi = 0$ at $\Theta = 0$ and $\frac{\partial\Phi}{\partial n} = 0$ at $\Theta = \alpha$,

then

$$\Phi(r,\theta) = \sum_{k=0}^{\infty} a_k r^{(k+\frac{1}{2})\frac{\pi}{\alpha}} \sin(k+\tfrac{1}{2})\tfrac{\pi}{\alpha}\theta, \qquad (4.44)$$

etc...

To ensure regular behavior of Φ at r=0 (Meixner's condition), only k>0 is possible. But still, when $\alpha>\Pi$, the leading term of the <u>derivative</u> (i.e. electric field intensity) will be singular, of order $r^{\frac{\pi}{\alpha}-1}$, for the first example, and $r^{(\frac{3\pi}{2\alpha}-1)}$ for the second.

A similar look at the Helmholtz equation,

$$\nabla^2\Phi + \lambda\Phi = 0 \qquad (4.45)$$

reveals that the general solution will have the form:

$$\Phi(r,\Theta) = \Sigma J_s(\sqrt{\lambda}\, r)\,(a_s \cos s\Theta + b_s \sin s\Theta) \qquad (4.46)$$

summed over all real s that satisfy given boundary conditions. Again, s>0 to have finite potential at the origin, but the $r^{\frac{\pi}{\alpha}-1}$ singularity exists for low frequency fields with boundary conditions as in the first example.

In this work, such singularities are incorporated into the numerical solution via a technique that can be said to follow the line of researchers like Motz, Lehman, Wait and Mitchell. The expected form of the singularity is additively imposed on the basis functions of the solution around the singular position.

4.2.1. Two-dimensional elements

Assume that the source function, f(r) is expected to vary as

$$f(r) \rightarrow \frac{1}{|r-r_o|^{\nu}} \tag{4.47}$$

when $r \rightarrow r_o$, denoting the singular position, and $\nu \leq 1$ is the order of the singularity. For the case of a uni-variate boundary, i.e. a two-dimensional problem, let the singular position correspond to the $\xi = 1$ point on the simplex, without losing generality.

The constraints that delineate the behavior of the modified shape functions, then, are:

(i) The value, slope and curvature of each of the new shape functions should match the original "non-singular" function as $\xi \rightarrow 0$; and

(ii) As $\xi \rightarrow 1$, each new shape function should either behave as $\frac{1}{(1-\xi)^{\nu}}$, or vanish.

Using an additive modification scheme, the "singular shape functions" are thus constructed as:

$$\alpha_1(\xi) = \xi^3 + 3\xi^2 - 3\xi + 1 \quad \text{(unchanged)},$$
$$\alpha_{2,3,4}(\xi) = (\xi-1)(a\xi^2 + b\xi + c) + \frac{1}{(1-\xi)^{\nu}} \tag{4.48}$$

with

$c = -3$

$b = c+\nu$

$a = b+6+ \frac{\nu(\nu+1)}{2}$ for α_2,

$c = 0$

$b = \nu-3$

$a = b-3+ \frac{\nu(\nu+1)}{2}$ for α_3, and

$c = 1$

$b = c + \nu$

$a = b + \frac{\nu(\nu+1)}{2}$ for α_4 (Figure 4.5). (4.49)

The fact that the required constraints are satisfied can be verified directly through substitution and differentiation.

The modified shape functions for the case of an element with singular source behavior at $\xi = 0$ can be obtained from those constructed above by replacing ξ with $(1 - \xi)$ and making use of symmetry. That is, for singularity at $\xi = 0$, the modified functions will be:

$\alpha_4(\xi) = \xi^3$ (unchanged),

$$\alpha_{1,2,3} = (-\xi)\ (\bar{a}\ \xi^2 + \bar{b}\ \xi + \bar{c}) + \frac{1}{\xi^{\upsilon}} \qquad (4.50)$$

with the values of $\bar{a}$, $\bar{b}$, $\bar{c}$ for α_1, α_2, α_3 the same as those of a, b, c for α_4, α_3, and α_2 in (4.49), respectively.

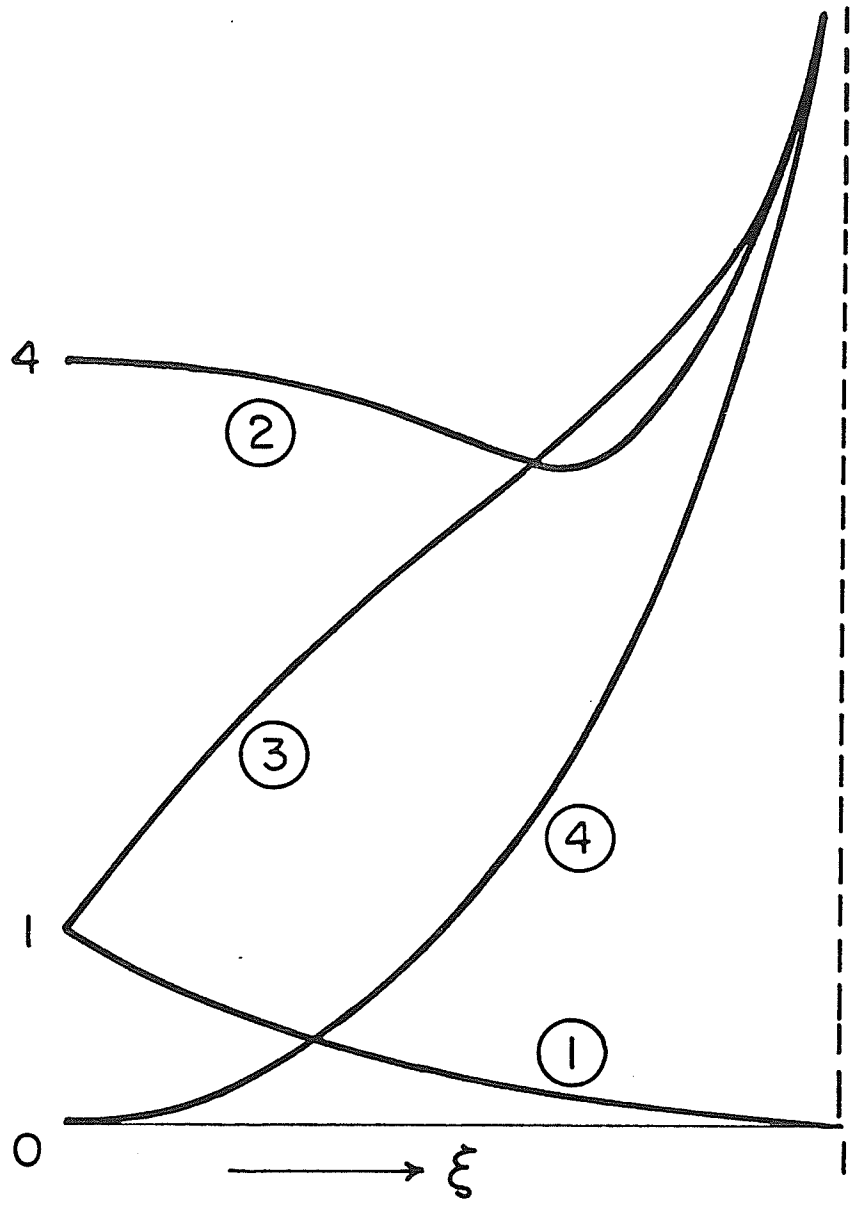

Figure 4.5. Modified shape functions for singularity at $\xi=1$.

As element definitions are thus selectively modified for cases involving singular behavior of sources, the numerical quadrature scheme applied in the evaluation of integrals may also require alteration. The Gauss-Legendre scheme (section 4.1.1.) with a weight function of unity may no longer provide sufficient precision in the integration of an integrand varying singularly. Table 4.1 presents the results of a test involving the integration of the four modified shape functions by two separate numerical schemes. Obviously, the higher the order of singularity, the greater the extent to which a Gauss quadrature scheme that reflects the singular form is needed to remain within acceptable precision. Four-point quadrature was used for numerical integration. The symbols stand for:

$$I_1 = \int_0^1 (-\xi^3 + 3\xi^2 - 3\xi + 1)\, d\xi$$

$$I_{2,3,4} = \int_0^1 (\xi-1)(a\xi^2 + b\xi + 1) + \frac{1}{(1-\xi)^{\upsilon}}\, d\xi \qquad (4.51)$$

with a, b, c as given in (4.49). Approximate integration was based on the formulas [10]:

$$\underline{\text{Gauss-Legendre (4 points)}}: \quad \int_0^1 f(\xi)d\xi = \sum_{i=1}^{4} A_i f(\xi_i) \qquad (4.52)$$

$$\underline{\text{Gauss-Jacobi (4 points)}}: \quad \int_0^1 \frac{1}{(1-\xi)^{\upsilon}} g(\xi)d\xi = \sum_{i=1}^{4} A_i g(\xi_i) \qquad (4.53)$$

$$\text{in which } g(\xi) = f(\xi).(1-\xi)^{\nu},$$

with A_i and ξ_i pre-specified.

Integrand	Exact Value	Gauss-Legendre Value	Gauss-Legendre Error	Gauss-Jacobi Value	Gauss-Jacobi Error	Order of Singularity(υ)
I_1	0.25	0.25	-	0.25	-	1/4
I_2	3.0078	2.981	.89%	3.0075	0.01%	
I_3	2.2578	2.231	1.19%	2.2562	0.07%	
I_4	0.5078	0.4974	2.04%	0.5085	0.14%	
I_1	0.25	0.25	-	0.25	-	1/3
I_2	3.1481	3.0940	1.58%	3.1478	0.01%	
I_3	2.3981	2.3440	2.07%	2.3961	0.08%	
I_4	0.64815	0.5940	3.54%	0.6491	0.14%	
I_1	0.25	0.25	-	0.25	-	1/2
I_2	3.5938	3.4	5.39%	3.5934	0.01%	
I_3	2.8438	2.65	6.69%	2.8412	0.09%	
I_4	1.0938	0.9	17.7%	1.0952	0.13%	

Table 4.1. Quadrature integration of modified spline shape functions

At this juncture various issues have to be confronted:

i) A general purpose BEM algorithm must be capable of utilizing different Gauss quadrature schemes at different stages of operation. Similar to invoking a logarithmically weighted formula for the treatment of kernel singularity (see section 4.1.1), a Gauss-Jacobi formula should be substituted for the Gauss-Legendre quadrature when singularities due to geometric features warrant such a measure.

ii) Furthermore, the weighted quadrature for kernel singularity and the one for "geometric" singularity will have to be used in conjunction. Evaluation of the "self-element" contribution to the system matrix for an element possessing a singular end point would require such operation.

iii) Lastly, with the stipulations presented up to this point, an element that has singular source behavior at both ends would require "doubly-modified" shape functions. Our straightforward response to this issue has been that such configurations shall not be allowed. That is, uni-variate elements with singular source behavior at both ends are not permitted; problem model has to contain at least two adjoining elements between two locations of singularity. Thus an element can have a singularity at either the $\xi = 1$ point or the $\xi = 0$ point, but not both.

Consideration of issues (i) and (ii), which become even more complicated for bi-variate elements (see Section 4.2.2

below), can be the subject of further research. Our response has been that as opposed to selective use of Gauss-Jacobi formulas as problem singularities require, increased overall orders of Gauss-Legendre quadrature will be preferred. The practical situation where a number of different orders of singularity have to be imposed on the solution (e.g. different angular edges on a metallic body such as a ship, etc.) precludes the possibility of generating the weighted formulas necessary to cater for each and every distinct behavior type. Increased order of Gauss-Legendre quadrature, on the other hand, improves precision without having to resort to specialization. Moreover, "double-modification" necessity, alluded to as issue (ii) above, is thus removed.

A general conclusion is, then, that higher quadrature orders will be necessary for the solution of problems with singular corners or edges, in comparison to those with smooth geometries.

4.2.2. Three-dimensional elements.

Extension of the "modified spline" idea to the bi-variate case is fairly straightforward. Only one edge in each direction is permitted to acquire singular behavior. The uni-variate shape functions, α_i, that occur in expressions (3.3) are replaced by appropriately modified functions described in section 4.2.1 above. This can be done only in one direction, for an edge

singularity, or in both directions, representing a three-dimensional corner (Fig. 4.6).

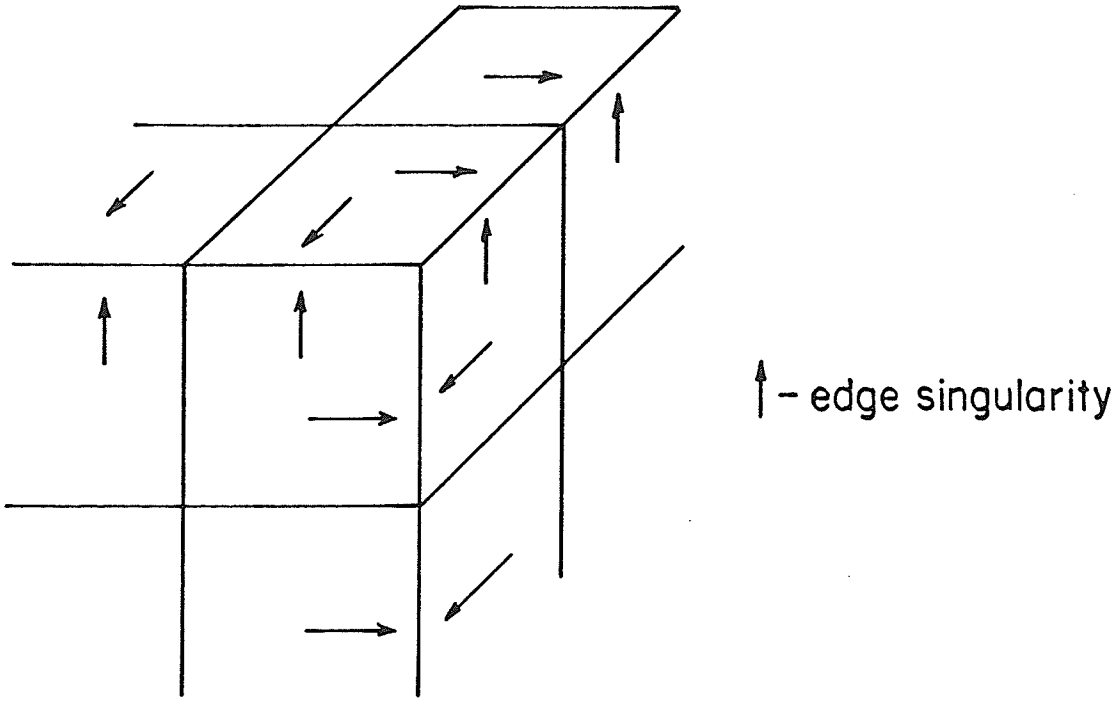

Figure 4.6 Three-dimensional geometric singularities.

For computation of integrals, a possible approach would have been to generate, in addition to bi-variate Gauss-Legendre quadrature, suitably weighted bi-variate quadrature formulae for singular behavior on one or both directions, and use the appropriate rule for integration over each element. For problems that involve only one type of singularity, e.g. only one 90° metallic edge, this would have procured high accuracy with a low number of unknowns, and low quadrature orders. This approach

is suggested but not elaborated upon [31, 32], in the similar context of modified bicubic finite elements. In the instance of the general "real-life" problem, however, the solution scheme may have to cater for numerous different types of singularities. While utilizing shape functions modified to suit the special behavior over each singular element requires only trivial computational burden, having to generate quadrature formulae to cater for the integration of each and every distinct form may become overly arduous.

A realistical approach is to prefer the more rigorous technique of weighted quadrature generation for problems that involve only one kind of singular behavior, but to resort to increased orders of bi-variate Gauss-Legendre quadrature (i.e. unweighted formulae) for the general case.

Three-dimensional problems are inherently much larger, both in terms of required computer storage and computational time, than their two-dimensional counterparts. This fundamental aspect further complicates the treatment of singularities - and provides further reason for the preference for less elaborate and time-consuming algorithmic efforts, as long as the attainable accuracy is not sacrificed.

Possibilities of a block-oriented implementation of the BEM

will be discussed later. Such an approach seems to provide the answer, in certain cases, to the enigma of being able to cater for a wide variety of special cases and remaining within the realm of as broad a generality as possible. Handling a large spectrum of singular behavior is an integral part of that requirement of general applicability.

4.3 References

(1) Kellogg, O. D., Foundations of Potential Theory, Dover Publications, 1953.

(2) Mikhlin, S. G., Integral Equations, Pergamon Press, 1964.

(3) Zabreyko, P. P., et.al., Integral Equations - a reference text, Noordhoff International Publishing, 1975.

(4) Jaswon, M. A., "Integral equation methods in potential theory - I", Proceedings of the Royal Society of London, A275, pp. 23-32, 1963.

(5) McDonald, B. H., Constrained Variational Solution of Field Problems, Ph.D. Dissertation, University of Manitoba, 1975.

(6) Jeng, G. Isoparametric Finite-Element Boundary Integral Solution of Three-Dimensional Fields, Ph.D. Dissertation, University of Manitoba, 1977.

(7) Acton, F. S., Numerical Methods that Work, Harper & Row, 1970.

(8) Harrington, R. F., Field Computation by Moment Methods, Reprinted by R. F. Harrington, R. D. 2, West Lake Road, Cazenovia, N. Y. 13035, 1968.

(9) Lean, M. H., Electromagnetic Field Solution with the Boundary Element Method, Ph.D. Dissertation, University of Manitoba, 1981.

(10) Stroud, A. H. and Secrest, D., Gaussian Quadrature Formulas, Prentice-Hall Inc., 1966.

(11) Lord Rayleigh, Scientific Papers, vol. IV, p. 288, 1903.

(12) Bouwkamp, C. J., "A note on singularities occurring at sharp edges in electromagnetic diffraction theory", Physica XII, no. 7, pp. 467-474, 1946.

(13) Meixner, J., "Die Kantenbedingung in der Theorie der Beugung electromagnetischer Wellen an vollkommen leitenden ebenen Schirmen", Annalen der Physik, vol. 6, no. 6, pp. 1-9, 1949.

(14) Meixner, J., "The behavior of electromagnetic fields at edges", New York University Institute of Mathematical Sciences, Division of Electromagnetic Research, Report No. EM-72, New York, 1952.

(15) Hurd, R. A., "The Edge Condition in Electromagnetics", IEEE Trans. on Antennas and Propagation, Succinct Papers, January 1976, pp. 70-73.

(16) Hurd, R. A. "On Meixner's edge condition for dielectric wedges", Canadian Journal of Physics, vol. 55, no. 22, pp. 1970-1971, 1977.

(17) Andersen, J. B. and Solodukhov, V. V., "Field Behavior near a dielectric Wedge", IEEE Trans. on Antennas and Propagation, vol. AP-26, no. 4, pp. 598-602, 1978.

(18) Jones, D. S., "Diffraction by an edge and by a corner", Quarterly Journal of Mechanics and Applied Mathematics, vol. V, pp. 363-378, 1952.

(19) Braunbek, W., "On the diffraction field near a plane-screen corner", IRE Trans. Antennas and Propagation, vol. AP-4, pp. 219-223, 1956.

(20) Motz, H., "The treatment of singularities in relaxation methods", Quarterly of Applied Mathematics, vol. 4, pp. 371-377, 1946.

(21) Lehman, R. S., "Developments at an Analytic Corner of Solutions of Elliptic Partial Differential Equations", Journal of Mathematics and Mechanics, vol. 8, no. 5, pp. 727-760, 1959.

(22) Wait, R., and Mitchell, A. R., "Corner Singularities in Elliptic Problems by Finite Element Methods", Journal of Computational Physics, vol. 8, pp. 45-52, 1971.

(23) Birkhoff, G., "Angular Singularities of Elliptic Problems", Journal of Approximation Theory, vol. 6, pp. 215-230, 1972.

(24) Kondrat'ev, V. A., "Boundary problems for elliptic equations with conical or angular points", Transactions of the Moscow Mathematical Society, vol. 17, pp. 105-128, 1968.

(25) Hughes, T.J.R. and Akin, J. E., "Techniques for developing special finite element shape functions with particular reference to singularities", International Journal for Numerical Methods in Engineering, vol. 15, pp. 733-751, 1980.

(26) Shafai, L., "An improved integral equation for the numerical solution of two-dimensional diffraction problems", Canadian Journal of Physics, vol. 48, pp. 954-963, 1970.

(27) Ying Lung-an, "The Infinite Similar Element Method for Calculating Stress Intensity Factors", Scientia Sinica, vol. 21, no. 1, pp. 19-43, 1979.

(28) Thatcher, R. W., "The Use of Infinite Grid Refinements at Singularities in the Solution of Laplace's Equation", Numerical Mathematics, vol. 25, pp. 163-190, 1976.

(29) Han Hou-de and Ying Long-an, "An Iterative Method in the Infinite Element", Department of Mathematics and Mechanics, Peking University, 1980.

(30) Decreton, M. C., Treatment of Singularities in the Finite Element Method, M.Sc. Thesis, University of Manitoba, 1972.

(31) Birkhoff, G. and Fix, G.J., "Higher-order Linear Finite Element Methods", Report to the U.S. Atomic Energy Commission and The Office of Naval Research, 1974.

(32) Fix, G. J., et. al, "On the Use of Singular Functions with Finite Element Approximations", Journal of Computational Physics, vol. 13, pp. 209-228, 1973.

CHAPTER V

APPLICATIONS

In this chapter, implementation of the BEM with cubic spline elements will be discussed for numerous problems of electromagnetic field theory. Electrostatic field problems that involve the solution of Laplace's or Poisson's equation under Dirichlet and/or Neumann boundary conditions, and time-harmonic problems of the solution of the Helmholtz equation will constitute the two major categories that will be considered.

Alternative approaches available for the purpose of arriving at an integral equation formulation of the boundary-value problems under consideration will be first summarized in general terms, and later, for each application, one approach will be followed.

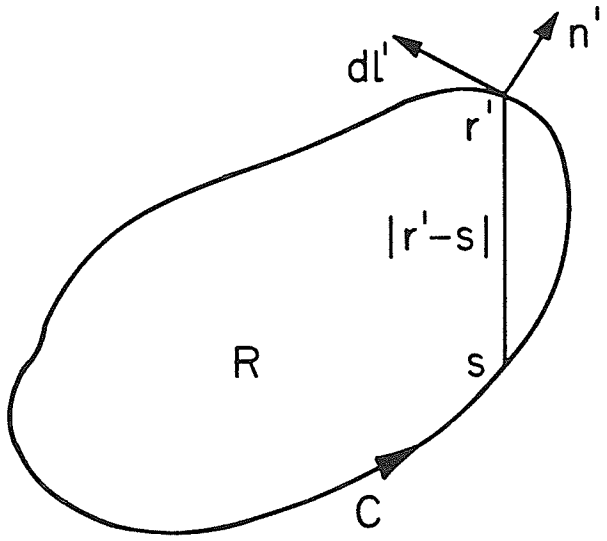

Figure 5.1. Two-dimensional problem configuration

5.1. Alternative formulations.

The governing equation for the Dirichlet problem (Fig. 5.1.) is:

$$\nabla^2\Phi\ (x,\ y) = 0 \text{ for } (x,\ y) \in R \tag{5.1}$$

under the constraint that

$$\Phi(x,\ y) = g(x,\ y) \text{ for } (x,\ y) \in C\,. \tag{5.2}$$

If we let (*) [1]

$$r = x + jy$$

the function $\Phi(x, y)$ which is harmonic in the simply connected domain, R, can be regarded as the real part of a certain analytic function, $\psi(r)$ which has no singular points inside R. The solution entails finding $\psi(r)$. Now let

$$\psi(r) = \frac{1}{2\Pi j} \int_C \frac{\mu(r')}{r'-r}\, dr' \tag{5.4}$$

which is a Cauchy-type integral in which $\mu(r')$ will be assumed a real function. Determination of this unknown density function, $\mu(r')$ will complete our solution.

If the point r in (5.4) tends towards a certain point, s, on the boundary C from inside R, by the Cauchy integral principle we have:

$$\psi(s) = \tfrac{1}{2}\,\mu(s) + \frac{1}{2\Pi j} \int_C \frac{\mu(r')}{r'-s}\, dr'. \tag{5.5}$$

Taking the real part of (5.5),

$$\tfrac{1}{2}\mu(s) + \frac{1}{2\Pi} \operatorname{Im}\{\int_C \frac{\mu(r')}{r'-s}\, dr'\} = g(s) \tag{5.6}$$

because

$$\operatorname{Re}\{\psi(s)\} = \Phi(s), \tag{5.7}$$

(*) The classical argument that follows is essentially two dimensional as it relies on the theory of functions of a single complex variable. This way, problems formulated in two spatial dimensions only are rigorously solved. In cases where the simplification due to invariance

as specified earlier. But since $\mu(r')$ is assumed real,

$$\tfrac{1}{2}\mu(s) + \frac{1}{2\Pi}\int_C \mu(r')\ \mathrm{Im}\left\{\frac{dr'}{r'-s}\right\} = g(s), \tag{5.8}$$

The integration kernel being

$$\mathrm{Im}\left\{\frac{dr'}{r'-s}\right\} = \mathrm{Im}\left\{d(\ln(r'-s)\ )\right\} \tag{5.9}$$

in which

$$r'-s = |r'-s|e^{j\theta}$$

can be substituted. But then,

$$\mathrm{Im}\ \{d(\ln(r'-s)\ )\} = \mathrm{Im}\ \{d(\ln|r'-s|e^{j\theta})\}$$

$$= d\theta$$

which, in turn is (referring to Fig. 5.1),

$$d\Theta = \frac{\partial\Theta}{\partial l'}\ dl' \tag{5.12}$$

From the Cauchy-Riemann relations, now,

$$\frac{\partial\Theta}{\partial l'} = \frac{\partial \ln|r'-s|}{\partial n'}\ , \tag{5.13}$$

in which n' denotes the outward directed normal to the boundary curve, C. Thus, if we define,

$$G(s,r') = -\frac{1}{2\Pi}\ln|r'-s| \tag{5.14}$$

we have

$$\mathrm{Im}\left\{\frac{dr'}{r'-s}\right\} = -2\Pi\ \frac{\partial G}{\partial n'}\ dl'. \tag{5.15}$$

As long as the boundary, C, has continuous curvature, this integration kernel is continuous and in fact, we have the Fredholm <u>second kind</u> integral equation:

---

in one dimension is absent, the more "physical" approach of potential-due-to-a-source, to be considered later, may be more direct.

$$\tfrac{1}{2}\mu(s) - \int_C \mu(r') \frac{\partial G}{\partial n'} dl' = g(s) \qquad (5.16)$$

the solution of which will directly lead us, through (5.4) and (5.7) to our unknown function, $\Phi(x, y)$.

Equation (5.16) is termed the double-layer potential formulation of the Dirichlet problem. It can be directly obtained by considering the electrostatic potential $\Phi(r)$ at a point r, due to a unit dipole oriented along n', located at r', and summing up the effects of a continuous distribution, $\mu(s)$, of such dipoles. Equating the effect at the boundary to the given boundary potential, g(s), directly yields equation (5.16).

An alternative formulation would result from the consideration of the potential due to a simple-layer of sources: the potential at r due to a point source at r' is given in two-dimensional Cartesian space by:

$$\Phi(r) = -\frac{1}{2\Pi} \ln|r'-r| \qquad (5.17)$$

if the strength of the point source is ε_o in free space. A distribution, $\sigma(s)$, of such charges over a contour, C gives rise to a potential

$$\Phi(r) = -\frac{1}{2\Pi} \int_C \sigma(r') \ln|r'-r| dl'. \qquad (5.18)$$

In particular, at the boundary, this reduces to

$$g(s) = -\frac{1}{2\Pi} \int_C \sigma(r') \ln|r'-s| dl', \qquad (5.19)$$

which, with the previous definition of the function, G, is

$$\int_C \sigma(r')G(s,r')\,dl' = g(s), \tag{5.20}$$

which is a Fredholm integral equation of the first kind.

The formulation based on a simple-layer source distribution for the Neumann problem can be obtained from direct differentiation of (5.18). The normal derivative of the potential at an observation point, r, along the outward-directed boundary normal, n, can be represented by:

$$\frac{\partial \Phi}{\partial n}(r) = -\frac{1}{2\Pi}\int_C \sigma(r')\frac{\partial}{\partial n}\ln|r'-r|\,dl' \tag{5.21}$$

as long as the observation point along the normal does not lie on the boundary. When it does, however, it can be shown by a parallel argument to the development of the double-layer formulation for the potential, that there is a discontinuity equal to the value of the source distribution. That is,

$$\frac{\partial \Phi}{\partial n}(s)_+ = \int_C \sigma(r')\frac{\partial G}{\partial n}(s,r')dr' - \tfrac{1}{2}\sigma(s) \tag{5.22}$$

if s is approached from the outside of C (i.e. against the orientation of n,) and

$$\frac{\partial \Phi}{\partial n}(s)_- = \int_C \sigma(r')\frac{\partial G}{\partial n}(s,r')dr' + \tfrac{1}{2}\sigma(s) \tag{5.23}$$

if the boundary is approached from the inside. Thus,

$$\frac{\partial \Phi}{\partial n-}(s) - \frac{\partial \Phi}{\partial n+}(s) = \sigma(s) \tag{5.24}$$

representing the jump in the value of the normal derivative of the simple-layer potential. Obviously, for a given

$$\frac{\partial \Phi}{\partial n}(s) = h(s) \tag{5.25}$$

at either side of the boundary, (5.22) or (5.23) constitutes the integral equation formulation of the Neumann problem. Once the $\sigma(s)$ is determined, any potential

$$\Phi(r) = \int_C \sigma(r')G(r,r')dr' + \Phi_o \tag{5.26}$$

Φ_o being an arbitrary constant, will be a solution.

A third alternative formulation is provided by the application of Green's Theorem, and is, in fact, equivalent to the superposition of the simple-layer and double-layer formulations outlined above.

For the solution of Laplace's equation, (5.1), in the configuration of Fig. 5.1, consider the Green's function that satisfies

$$\nabla^2 G\ (r,r') = -\delta(r-r') \tag{5.27}$$

where δ denotes the Dirac delta function. Writing (5.1) in terms of source coordinates, r', multiplying it by $G(r,r')$ and (5.27) by $\Phi(r')$, and subtracting the latter from the former gives:

$$G(r,r')\nabla^2\ \Phi(r') - \Phi(r')\nabla^2\ G(r,r') = \Phi(r')\delta(r-r'). \tag{5.28}$$

Integrating this expression over the two-dimensional domain over which (5.1) is to be solved, we obtain:

$$\int_R \{G(r,r')\nabla^2\Phi\ (r') - \Phi(r')\nabla^2 G(r,r')\}\ ds' = \begin{cases} \Phi\ (r) & \text{if } r \in R, \\ 0 & \text{otherwise,} \end{cases} \tag{5.29}$$

by definition of the Dirac delta function. Now, invoking

Green's theorem, we obtain the equivalent boundary-integral formulation:

$$\int_C \{ G(r,r') \frac{\partial \Phi}{\partial n'} (r') - \Phi(r') \frac{\partial G}{\partial n'} (r,r') \} dl' = \begin{cases} \Phi(r) & \text{if } r \in R, \\ 0 & \text{otherwise,} \end{cases} \quad (5.30)$$

in which n' is the normal directed outwards, dl' denotes integration along the contour C, for source co-ordinates; and r denotes any observation point inside R. When r is on the boundary, C, due to the stipulation that

$$\int_C \Phi(r') \delta (r-r') dl' = \tfrac{1}{2} \Phi(r) \text{ if } r \in C, \quad (5.31)$$

we have

$$\int_C \{ G(r,r') \frac{\partial \Phi}{\partial n'} (r') - \Phi(r') \frac{\partial G}{\partial n'} (r,r') \} dl' = \tfrac{1}{2} \Phi(r), \quad r \in C. \quad (5.32)$$

Hence, this formulation can be summarized as:

$$\Phi(r) = \gamma \int_C \{ G(r,r') \frac{\partial \Phi}{\partial n'} (r') - \Phi(r') \frac{\partial G}{\partial n'} (r,r') \} dl' \quad (5.33)$$

in which

$$\gamma = \begin{cases} 0 \text{ if } r \notin R, \\ 1 \text{ if } r \in R, \; r \notin C, \text{ and} \\ 2 \text{ if } r \in C. \end{cases}$$

In particular, for the Dirichlet case when $\Phi(r)$, $r \in C$ is given, the Fredholm equation:

$$\int_C G(r,r') \frac{\partial \Phi}{\partial n'} (r') dl' = \frac{1}{2} \Phi(r) + \int_C \Phi(r') \frac{\partial G}{\partial n'} (r,r') dl' \quad (5.34)$$

represents the problem.

All consideration above was devoted to the two dimensional problem configuration of Fig. 5.1. The Green's function was defined earlier as:

$$G(r,r') = -\frac{1}{2\Pi} \ln|r'-r|. \tag{5.14}$$

Similar arguments hold, and the formulations are valid for three-dimensional space, with

$$G(r,r') = \frac{1}{4\Pi} \frac{1}{|r'-r|} \tag{5.35}$$

and boundary integrals taken over incremental surfaces instead of lines.

The fact that the formulation of (5.30) represents direct superposition of simple and double-layer potentials is clear when the term

$$\Phi_1 = \int_C G(r|r') \frac{\partial \Phi}{\partial n'} (r')dl' \tag{5.36}$$

is identified as the simple-layer potential due to a density $\sigma(s) = \frac{\partial \Phi}{\partial n}(s)$, and the term

$$\Phi_2 = \int_C -\Phi(r') \frac{\partial G}{\partial n'} (r,r')dl' \tag{5.37}$$

is recognized the double-layer potential due to a density $\mu(s)=-\Phi(s)$. As the boundary is approached, the simple-layer potential is continuous but the double-layer potential has a discontinuity of $\frac{1}{2}\mu(s)$, hence the boundary relation (5.32) follows when $r \varepsilon C$.

Of these three alternative formulations, the simple-layer that results in eq'n. (5.20) seems to provide the most straightforward and least costly approach to the Dirichlet problem. It is advantageous

over the double-layer formulation of equation (5.16) insofar as computational savings are incurred by the absence of the extra term in the equation. The classical preference [1,2] for Fredholm's second kind equations that involve that term is unwarranted as long as proper treatment of kernel singularities lead the way to avoiding ill-conditioned system matrices in Fredholm's first kind integral equations [3,4].

Green's Theorem formulation, while yielding accurate results in terms of potentials directly, without the introduction of intermediate source terms, requires special logic to determine region topologies and modify the equations to be used to obtain unknowns in different regions. Furthermore, as (5.34) illustrates, the excitation term requires more computational effort. This latter formulation, on the other hand, results in a block-structured system matrix for multi-region problems as the equation entails integration over one closed region alone. This feature may be a definite advantage especially in multi-media problems, especially if a block-oriented linear equation solution scheme is available for use.

The Neumann problem, being the dual of the Dirichlet problem posed in terms of a simple-layer distribution, provides an instance where a double-layer formulation would be implemented. The excitation term is straightforward , and the integration kernel identical to the free-space Green's function for the simple-layer formulation of the Dirichlet case. The resulting integral equation is identical

to (5.20), but to obtain the potential field, further efforts are necessary. The Green's Theorem alternative in this case requires a similar effort in setting up the integral equation, but produces surface potentials directly.

5.2 Electrostatic field problems

5.2.1. Parallel plate capacitor

The infinite strip capacitor problem constitutes the first test of the developed methodology. The half strip length and half plate separation were taken as unity (see Fig. 5.2). The exact capacitance for this configuration is known [5] as 18.72 $pF/_m$. The charge accumulation on the plates is expected [6, p.569] to vary as:

$$\sigma_s(r) \to \frac{1}{r^{\frac{1}{2}}} . \qquad (5.38)$$

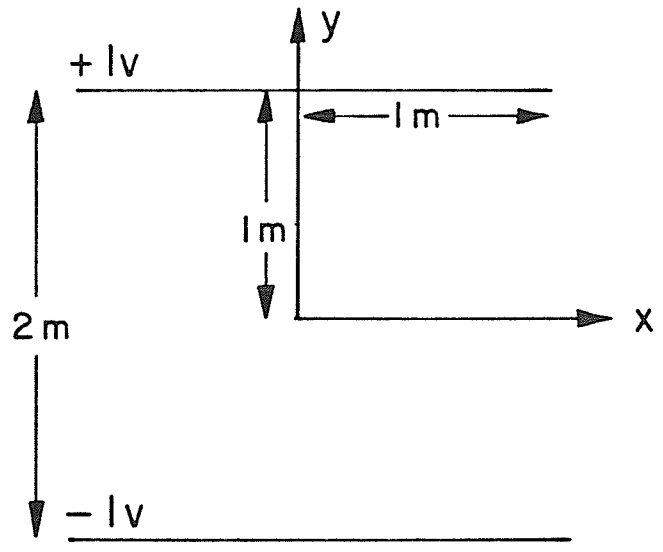

Figure 5.2 The Parallel plate capacitor.

The positive quadrant $x \geq 0$, $y \geq 0$ was modelled using quarter-symmetry, with +1 volt imposed on the y=1 plate. The Fredholm first-kind equation for the plate charge can be written for this configuration as

$$\frac{1}{\varepsilon_0} \int_0^1 \sigma(x')\, G(x,1|x',1)dx' = 1 \qquad (5.39)$$

in which a modified Green's function that incorporates problem symmetry is utilized:

$$G(x,y|x',1) = -\frac{1}{2\Pi} \ln \left(\frac{[(x-x')^2+(y-1)^2]\ [(x+x')^2+(y-1)^2]}{[(x-x')^2+(y+1)^2]\ [(x+x')^2+(y+1)^2]} \right)^{\frac{1}{2}} \qquad (5.40)$$

To solve this problem, 3 uni-variate boundary elements,(*) involving 6 unknowns, were used along a half-plate of the capacitor. The BEM with spline elements was applied, with an edge singularity of $\frac{1}{r^{\upsilon}}$, in which $\upsilon = 0.5$, imposed on the shape functions over the edge element.

Capacitance was calculated from the total energy, E, as:

$$C = \frac{2E}{V^2} \qquad (5.41)$$

Here, as in the other electrostatic field applications, the capacitance, or twice the energy content divided by the square of the applied constant potential, was computed as a simple vector dot product:

(*) See Appendix for an exemplary straight-line element.

Remembering that the basic equation to be solved has the form (section 1.1):

$$\langle \Gamma \underline{f}, \underline{\alpha} \rangle \underline{\sigma} = \langle \underline{g}, \underline{\alpha} \rangle \tag{5.42}$$

and the solution, σ is the expansion coefficient vector for the charge distribution, the product of the right-hand-side of this equation and its solution gives nothing but

$$\underline{\sigma}^T . \langle \underline{g}, \underline{\alpha} \rangle = \int_S \sigma(s) g(s) ds \tag{5.43}$$

because of the linearity of the integration operation. But by definition, this last term is twice the electrostatic energy stored in the capacitor. Hence, to determine the capacitance once the charge distribution has been ascertained, we use:

$$C = \frac{\underline{\sigma}^T . \langle \underline{g}, \underline{\alpha} \rangle}{V^2}, \tag{5.44}$$

that is the dot product of the right-hand-side and the solution of the system equation, divided by the constant applied potential difference, squared,

The results for the capacitance values are presented in Table 5.1, and the computed charge distribution is compared with the analytical prediction in Figure 5.3.

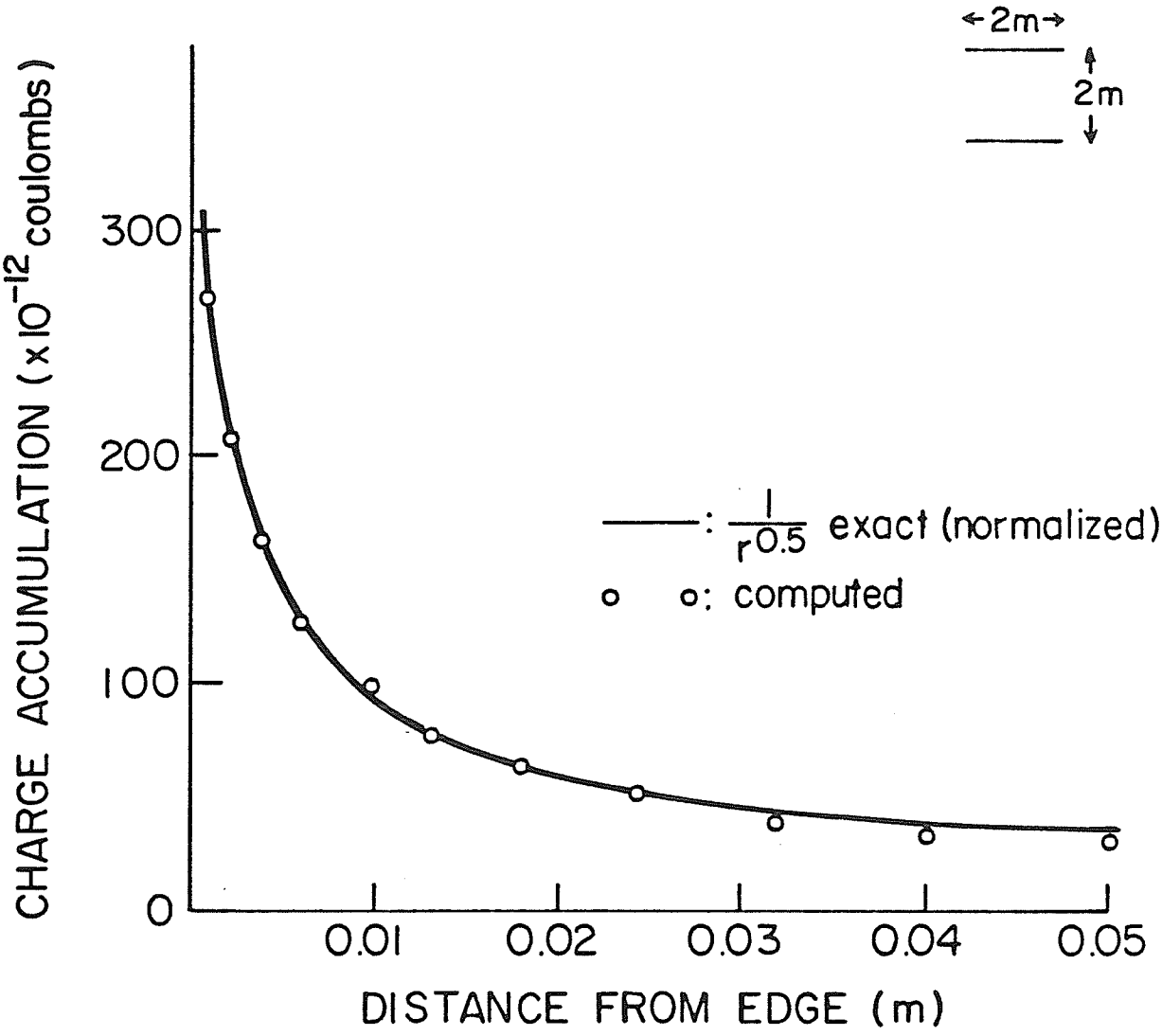

Figure 5.3. Charge accumulation on the parallel plate capacitor.

The accuracy of these results, especially with regard to the computed charge distribution, should be compared against those obtained by earlier researchers.

McDonald, et. al. [7] reported similar accuracy in capacitances and "medium-range" field values with either 50 pulses or 5 unknowns (4 pulses) and one singular function. Lean [4] has obtained a smooth singular behavior of charges using fourth order Lagrangian elements with five unknowns and a singular term. The results we have obtained, again with six unknowns including the singularity term, show a good match of the charge distribution with analytic prediction.

Integration quadrature order	Capacitance (pF)
4	18.78
5	18.752
6	18.737
8	18.718

Table 5.1. Parallel plate capacitance as computed by the BEM with cubic splines, 6 unknowns, $\frac{1}{r^{1/2}}$ singularity imposed.

5.2.2. Coaxial capacitor

The only difference between the solution scheme applied for this problem and that used for the parallel plate capacitor was that quarter-symmetry was not utilized here. In spite of circular geometry, the small size of the problem permitted the solution of the complete problem within a configuration that involved only 16 unknowns - 4 per quadrant (Fig. 5.4).

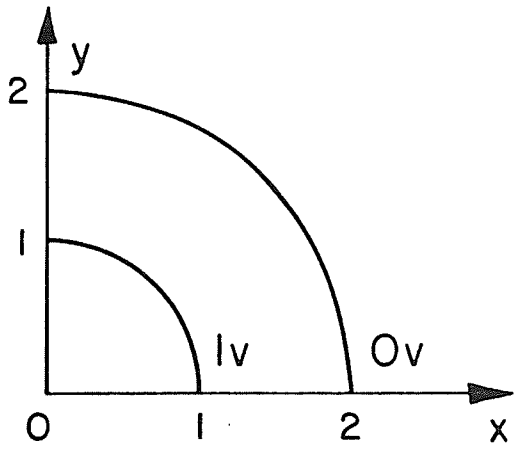

Figure 5.4. The coaxial capacitor

The exact value of the capacitance for unit length of this configuration is 80.259 pF.

For solution, the equation

$$\frac{1}{\varepsilon_0} \int_C \sigma(s')\, G(s,s')\, ds' = g(s) \tag{5.45}$$

was used with C denoting conductor contours,

$$G(r,r') = -\frac{1}{2\pi} \ln|r-r'| \,, \tag{5.46}$$

and

$$g(s) = \begin{cases} 1 & \text{on the inner conductor,} \\ 0 & \text{on the outer conductor.} \end{cases} \tag{5.47}$$

Two different algorithms were invoked for solution: one that utilized the spline element methodology for geometry modeling as well as source approximation and the "hybrid" algorithm that restricted spline usage to geometric interpolation only, and applied the Lagrangian element technique for source representation. Quarter symmetry was implemented in the latter approach. The hypothesis being tested was that the use of cubic spline shape functions for source modelling introduces too much overhead in comparison to lower-order methods such as pulse or Lagrangian polynomic expansion.

The results obtained by the two algorithms are presented in Table 5.2.

Integration quadrature order	4 (***)				6		8	
Method(*)	BSP	H,N=2	H,N=3	H,N=4	BSP	H,N=4	BSP	H,N=4
Minimized functional value	80.7611	80.7532	80.7403	80.8489	80.5042	80.4911	80.4053	80.3959
Relative execution time(**)	4.39	1	1.27	1.41	7.58	2.23	11.54	3.16

(*) BSP: BEM with cubic splines, no symmetry, 16 unknowns

H: Hybrid, quarter symmetry

N: Order of Lagrange interpolation, N=2 indicates 10 unknowns,
N=3 indicates 14 unknowns,
N=4 indicates 18 unknowns.

(**) The ratio of elapsed CPU time to the shortest such time on this table. For this problem, 1 = 0.90 sec. CPU with the WATFIV software on the Amdahl 470/V7.

(***) The expected[7] monotonic convergence as interpolation order is increased is not evident in this case, due, probably, to significant error incurred by low integration order.

Table 5.2. Solution of the coaxial capacitor problem with two algorithms.

As the table shows, computational results do not indicate an advantage of the "hybrid" method over the "pure" spline approach. Comparable execution times (regarding symmetry) are required to reach solutions of comparable accuracy. If anything, considering the empirical rule that computation time varies almost as the square of the number of elements, the "pure" spline algorithm that takes roughly four times as long as the "hybrid" are which is using a quarter of the number of unknowns, seems to be preferable (*). Furthermore, the algorithmic simplicity of not having to process two different classes of shape functions is enjoyed.

5.2.3. Rectangular infinite cylinder

In solving the exterior Dirichlet problem in two-dimensional space, the free-space Green's function is modified as:

$$G(r,r') = -\frac{1}{2\Pi} \ln|r-r'| + \frac{1}{2\Pi} \ln|R-r'| \qquad (5.48)$$

where R is a fixed distant point, to ensure that potential is regular as that reference point is approached. Without this precaution, of course, the condition of vanishing potential when r increases would be violated.

(*) Timing comparisons between the Lagrange and Spline BEM methodologies will be presented in section 5.3.5 for the more substantial application of three dimensional electromagnetic scattering .

Using the simple layer formulation, again both the "hybrid" and "pure" algorithms were used, and comparisons drawn. In addition, a "pure" spline algorithm that imposed the expected $\frac{1}{r^{1/3}}$ singularity of the charge density on the expansion functions was tested on this problem. Tables 5.3 and 5.4 summarize the results of these two tests, respectively.

Integration quadrature order	$r^{-1/3}$ singularity imposed?	energy functional
2	No	7.852
3	No	7.850
4	No	7.849
5	No	7.848
8	No	7.848
3	Yes	7.834
6	Yes	7.833
8	Yes	7.833

Table 5.3. Stored energy for the square cylinder problem as computed with singular expansion functions.

Integration quadrature order	2		3		4			5		6	
Method (*)	BSP	H,N=4 (****)	BSP	H,N=4	BSP	H,N=3	H,N=4	BSP	H,N=4	BSP	H,N=4
Minimized functional value	7.8519	n.a.	7.8497	7.9233	7.8487	7.8499	7.8669	7.8482	7.8499	7.8475	7.8489
C/R (**)	5.54	n.a.	5.13	2.4	5.17	3.22	1.25	5.16	3.05	5.14	2.89
Relative execution time (***)	1.39	n.a.	1.85	1.05	2.39	1	1.07	2.90	1.22	4.93	1.44

(*) BSP: BEM with cubic splines, no symmetry, 12 unknowns.
H: Hybrid, see Table 5.2.

(**) C/R: The ratio of charge accumulation at the corner to that at the middle.

(***) The ratio of elapsed CPU time to the shortest such time on this table.
For this problem, 1=0.41 sec. CPU with the WATFIV software on the Amdahl 470/V7.

(****) The results for this case were completely unreliable due to the inability of the low order quadrature scheme to cater for the high order interpolatory polynomial.

Table 5.4. Solution of the square cylinder problem with two algorithms.

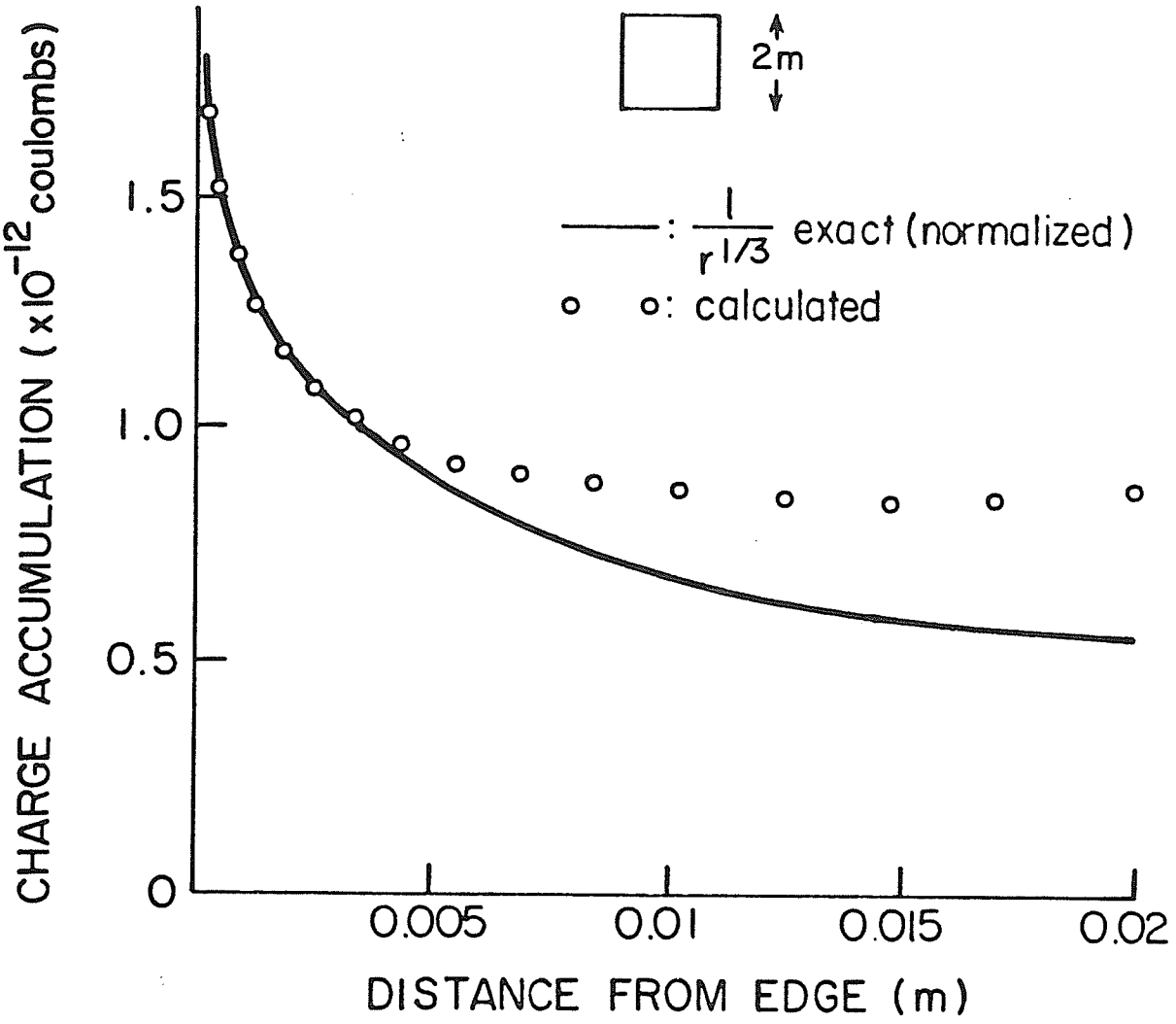

Figure 5.5. Charge accumulation on an infinite conducting square cylinder.

There is an indication of the smooth interpolation property of splines in Table 5.4: A quadrature order of 2, implying linear approximation of integrands, is not sufficient to integrate a Lagrangian cubic (N=4) polynomial, which presumably introduces spurious undulations, whereas a cubic spline is integrated fairly well.

The spline shape functions utilized to prepare Table 5.4 did not contain the added singular term; as such, the charge accumulation could not be accurately approximated at edges. The ratio of the edge accumulation to the density at the center, however, is a good indicator of performance - the spline algorithm consistently produces higher ratios than the hybrid algorithm that approximates sources by Lagrangian polynomials.

Also evident from Table 5.4 is the fact that modelling sources with splines does not necessarily increase computational overhead in comparison to Lagrangian polynomic approximation. In fact, the B-spline algorithm working over the complete geometry never took four times as long as the hybrid algorithm that was making use of symmetry to solve a four times smaller model of the problem.

Figure 5.5 shows the charge density as computed by the B-spline algorithm with shape functions modified by the added singular term. While the asymptotic form of the singularity is closely reproduced, towards the center of the sides of the square, the density deviates from the $r^{-1/3}$ curve, possibly indicating the effect of the opposite edge.

5.2.4. Polarizability of a dielectric cylinder

The potential problem for a homogenous dielectric object immersed in an incident electrostatic field in free space provides an example of a Fredholm second kind integral equation obtained via the Green's Theorem formulation outlined in section 5.1.

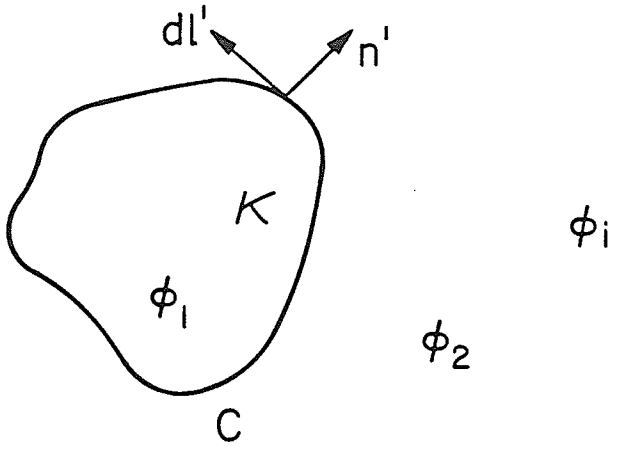

Figure 5.6 Dielectric cylinder in an incident field.

Consider the geometry of Fig. 5.6. Let Φ_1 and Φ_2 represent the potential inside and outside the dielectric, respectively. Let Φ_i be the incident or unperturbed field.
We can write

$$\Phi_1 = \Phi + \Phi_i/\kappa \tag{5.49}$$

and

$$\Phi_2 = \Phi + \Phi_i \tag{5.50}$$

where κ represents the dielectric constant of the object, and Φ stands for the perturbation potential, or the potential stemming from the induced dipoles. Now, we can invoke the formulation in (5.33) for both the inside and outside (i.e. the region bounded by the dielectric and a cylinder with infinite radius) regions, and eliminate Φ_1 and Φ_2 in terms of Φ and Φ_i:

$$\Phi(r) = \frac{\Phi_i(r)}{\kappa} - \frac{\kappa - 1}{\kappa} \int_C \Phi(r') \frac{\partial G}{\partial n'} dl' \quad \text{for r inside R,} \tag{5.51}$$

and

$$\Phi(r) = \Phi_i(r) - (\kappa - 1) \int_C \phi(r') \frac{\partial G}{\partial n'} dl' \quad \text{for r outside R.} \tag{5.52}$$

Letting r approach the boundary on both sides, we obtain, as in eq.n (5.32),

$$\Phi_i(r) = \frac{\kappa + 1}{2} \Phi(r) + (\kappa - 1) \int_C \Phi(r') \frac{\partial G}{\partial n'} dl', \tag{5.53}$$

in which

$$G(r,r') = -\frac{1}{2\pi} \ln|r - r'| \tag{5.54}$$

in two-dimensional space, as usual.

Once equation (5.53) is solved for $\Phi(r)$, the boundary potential, the dipole moment of the body can be evaluated from [8]:

$$\overline{P} = (\kappa - 1)\, \varepsilon_0 \int_C \Phi(r')\, \hat{n}'\, dl' \tag{5.55}$$

in which $\hat{n}'$ denotes the unit normal vector at the source point, r'. Polarizabilities are defined [8] as the dipole moment magnitudes for the two orthogonal incidence directions.

This problem has been solved by Mei and Van Bladel [9] and Eyges and Gianino [10] among others. It has particular significance in low frequency scattering problems. The former work has used the classical pulse expansion - point matching method with "typically 80" unknowns, and the latter has devised a method that can be called Fourier expansion-point matching which relies on analytic approximations and a 2x2 system of equations. Mei and Van Bladel's solution provides the boundary potentials and polarizabilities whereas Eyges and Gianino restrict their attention to polarizabilities, i.e. not near but far fields.

A point of detail for this application involves the integration kernel of equation (5.53). We have

$$\frac{\partial G}{\partial n'}(r,r') = \frac{1}{2\pi |r-r'|}\, \hat{n}' \cdot \frac{(r-r')}{|r-r'|} \tag{5.56}$$

which is no longer logarithmic. Hence, for the evaluation of the integral when the source and observation elements coincide

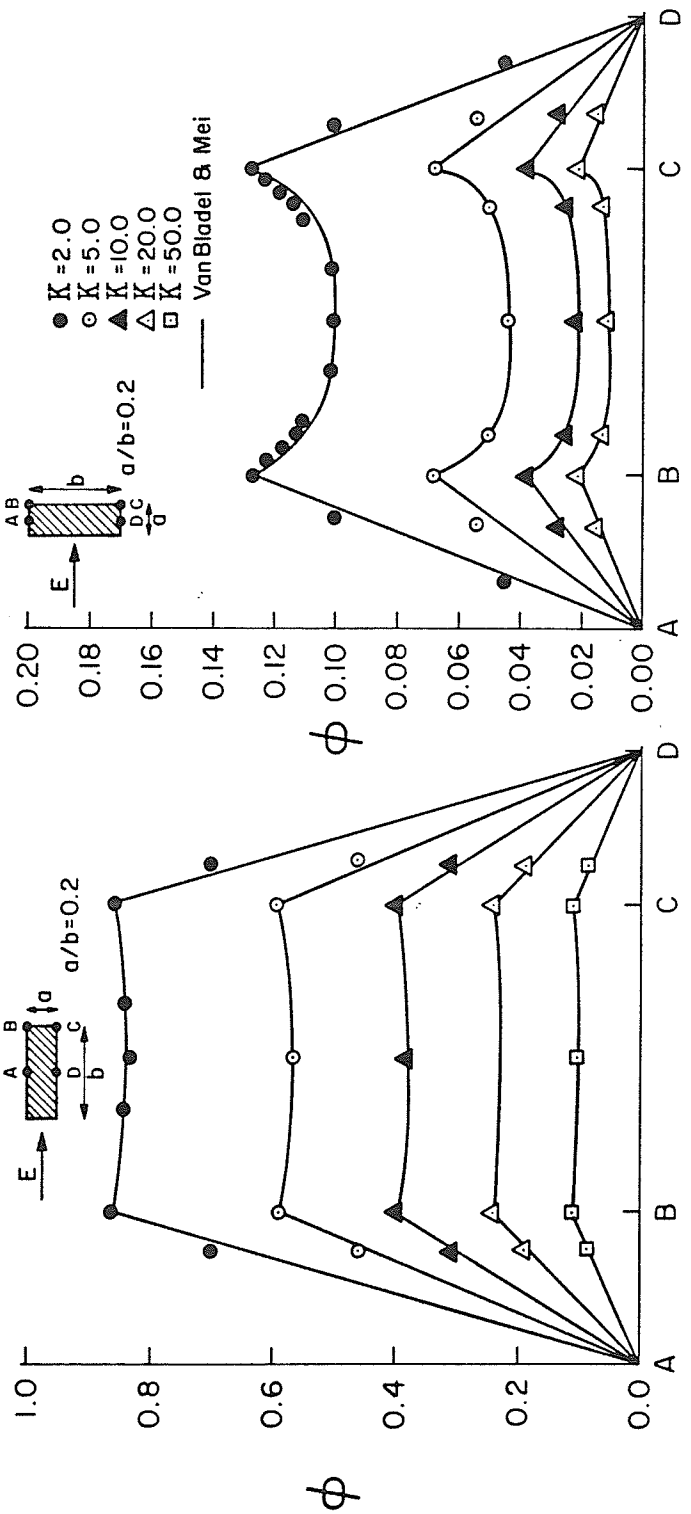

Figure 5.7. Surface potentials on a rectangular dielectric cylinder in an electrostatic field.

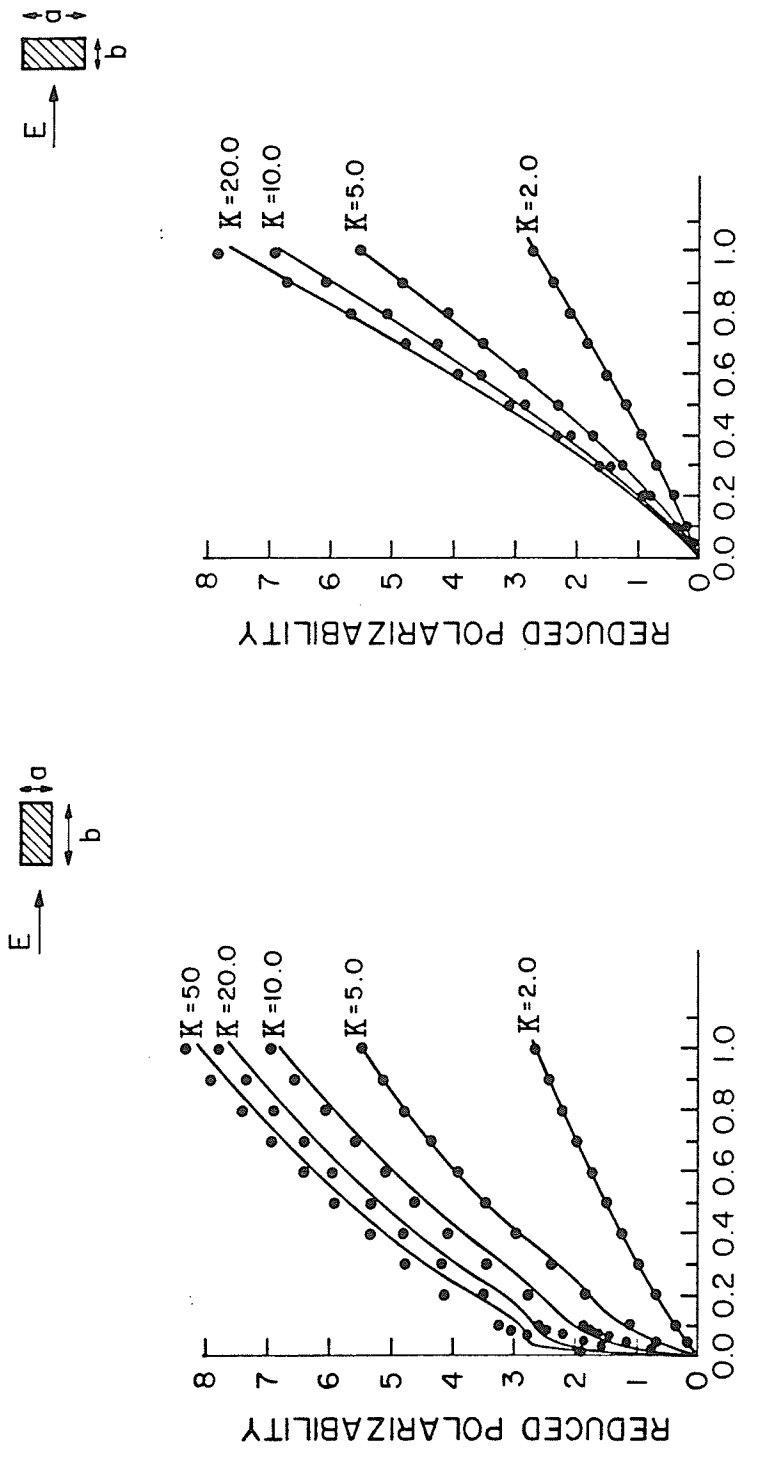

Figure 5.8. Polarizability of a rectangular dielectric cylinder in an electrostatic field.

(see section 4.1.1, above), the bisection technique is sufficient without having to resort to utilization of a logarithmically weighted Gauss Quadrature formula, as the form of the singularity is smoother than both logarithmic, and, of course, $\frac{1}{r}$ behavior. The regular Gauss-Legendre scheme yields sufficient precision.

The surface potentials, obtained with 12 unknowns only, and polarizabilities are presented in Figures 5.7 and 5.8. Comparisons with Mei and Van Bladel's results are provided only, firstly because, as noted earlier, Eyges and Gianino do not proceed from surface potentials at all, and secondly because their results for polarizabilities, being approximations geared for the far fields alone, are not any more precise than obtained here for any of the instances.

5.2.5. Conducting Sphere

The Dirichlet problem in three-dimensional space for a perfectly conducting charged object constitutes the subject of this and next subsections.

The equation

$$\int_S \sigma(s')G(s,s')\,ds' = g(s) \tag{5.57}$$

with

$$G(r,r') = \frac{1}{4\pi\epsilon_0}\,\frac{1}{|r-r'|} \tag{5.58}$$

is the Fredholm first kind equation based on the simple-layer source representation, $\sigma(s)$, applicable to the problem. $g(s) = 1.0$ was imposed; symmetry was not used.

Recovered surface potentials, computed as

$$\Phi(r) = \int_S \sigma(s')G(r,s')ds' \qquad (5.59)$$

after $\sigma(s)$ is solved for, interior potentials, and the evaluated capacitance of the sphere is presented in Table 5.5. The exact value of the capacitance is known to be $4\pi\varepsilon_0$, or 111.2626 pF, for the unit sphere.

Model Particulars(*)			Surface potentials(v)		Interior potential(v)	Capacitance (pF)
N	NG	NGS	at equator	at poles		
12	5	2	.97	.96	.99	108.084
44	3	2	.9872	.96	.997	110.229
34	4	2	.9942	.94	.999	108.71
44	4	2	.9935	.90	.999	110.027
62	4	2	.993	.96	.9997	110.344
62	4	3	.9982	.96	1.0000	110.373
15*8	4	4	.9994	.99	1.0000	111.224

(*):

N : Total number of unknowns, in the last application, 1/8th symmetry was used.

NG : Integration quadrature order

NGS: Integration quadrature order used in treating kernel singularity

Table 5.5. Results of the Dirichlet problem for the conducting sphere.

One immediate observation from Table 5.5 is that the order of Gauss quadrature used in treating kernel singularities correlates with the accuracy obtained in the evaluated capacitance. The fact that the interior potentials are closer to the exact value of 1.0 than the surface potentials is due to the discrepancy introduced in geometric modelling. Also worth noting is that a comparison of equator and pole potentials reveals the relative weakness of that particular geometric model at the poles. The particular representation using 34, 44 or 62 unknowns was one in which the quadrilateral elements were "collapsed" at the poles, becoming three-dimensional triangular patches. The 12-unknown model, on the other hand, did not have this disadvantage and displays rather remarkable accuracy considering the reduction in computational effort - one-and-a-half unknowns per spherical octant!

5.2.6. Conducting cube

The scheme of imposing expected singular behavior of boundary sources on expansion functions was put to test in a three-dimensional case for the problem of the conducting cube.

The upper- and lower-bounds for the capacitance have been calculated respectively in [11] and [12], and reproduced in [8] as:

$$72.88 < C < 74.27. \qquad (5.60)$$

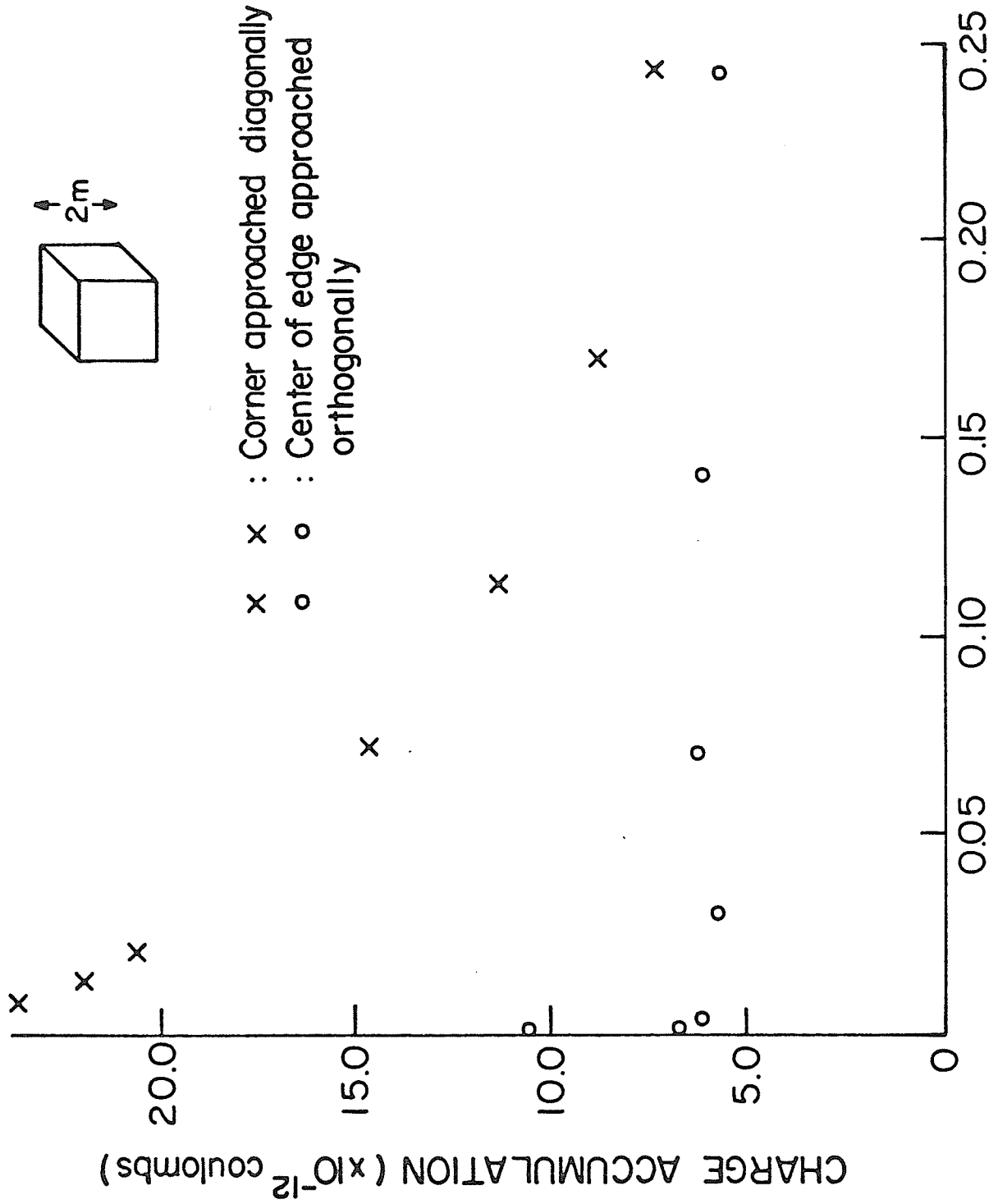

Figure 5.9. Surface charge density on a conducting cube.

Two algorithms, with and without singularly-modified expansion functions were applied for the problem. Neither the results given in [8], nor the BEM with un-modified Lagrangian elements applied by Lean [4] for the same problem claim accurate computation of surface charges. The charge profile that we have calculated is presented in Figure 5.9. Analytical results for the charge density are not available. We have imposed the $\frac{1}{r^{1/3}}$ behavior which is known for the 90^{o} conducting edge, on each of the 12 edges of the cube. The behavior at the three-dimensional corners is thus approximated by the spline blending operation (see sections 2.2 and 3.2, above) applied to univariate $\frac{1}{r^{1/3}}$ behavior in the two orthogonal directions on each face. The capacitance figures computed by the modified and unmodified spline method, as well as those reported [4] for the Lagrangian case can be found in Table 5.6.

Table 5.6 demonstrates the utility of the modified expansion function scheme in cutting down the number of unknowns necessary to achieve a certain degree of accuracy. Also obvious is the fact that the inherent magnitude of three dimensional problems warrant utilization of symmetry whenever possible.

Model Particulars(*)				Capacitance (pF)
Type	N	NG	NGS	
NS	32	4	2	72.28
S	32	4	2	72.78
S	6*8	4	2	72.90
L	7*8	4	4	72.94
L	37*8	4	4	73.13
L	31*8	4	4	73.19

(*) NS: Splines, no singular modification

S: Splines with singular elements

L: Lagrangian, without singular modification (4, p.62)

N: Total number of unknowns, NG: integration quadrature, NGS: quadrature for singularity treatment.

Table 5.6. Capacitance of the conducting cube.

5.2.7. Multiply inhomogeneous media

The mixed-boundary condition electrostatic potential problem with multiple piecewise inhomogeneities will be considered in this subsection. A general problem geometry is depicted in Figure 5.10. Using the appropriate integration kernel (Green's function) and integration procedure will ensure applicability in two- or three-dimensional space.

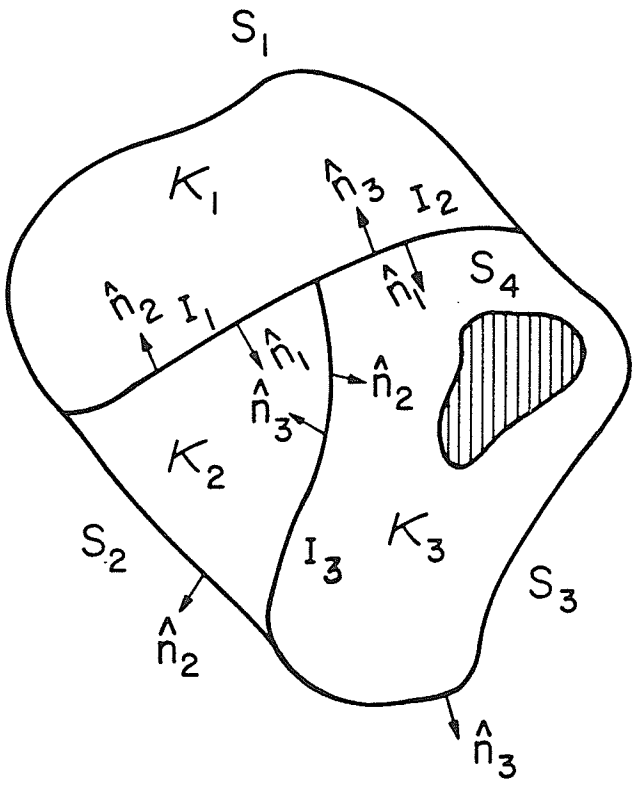

$$D = S_1 \cup S_4 \quad , \quad N = S_2 \cup S_3 \qquad I = I_1 \cup I_2 \cup I_3$$

$$S = S_1 \cup S_2 \cup S_3 \cup S_4 \cup I_1 \cup I_2 \cup I_3$$

Figure 5.10. A multi-media configuration.

Based on a simple-layer representation of sources, potential anywhere can be written as:

$$\Phi(r) = \int_S \sigma(s')G(r,s')ds', \tag{5.61}$$

with a properly evaluated $\sigma(s)$, and S as in Fig. 5.10. In two-dimensional space, the Green's function will be:

$$G(r,r') = -\frac{1}{2\Pi} \ln|r-r'|, \tag{5.62}$$

and integration will be over all contours in the problem; the three-dimensional Green's function will be:

$$G(r,r') = \frac{1}{4\Pi} \frac{1}{|r-r'|}, \tag{5.63}$$

and, surface integrals will be evaluated over all boundaries.

For boundaries on which a Dirichlet potential is specified, we can write:

$$\int_S \sigma(s')G(s,s')ds' = g(s), \quad s\varepsilon D \tag{5.64}$$

where s takes on values on the Dirichlet boundary only, and integration covers all boundaries.

Similarly, the boundaries on which a Neumann condition is prescribed will give rise to the equation:

$$\int_S \sigma(s')\frac{\partial G}{\partial n}(s,s')ds' + \tfrac{1}{2}\sigma(s) = h(s), \quad s\varepsilon N \tag{5.65}$$

in which consistent normal vector definitions have been assumed. Equation (5.65) follows from direct differentiation of (5.61) as explained above (see section 5.1).

On interfaces between two regions with differing characteristics, signified by κ_i and κ_j, two conditions should hold: first, potential across the interface should be continuous. This condition is automatically satisfied due to the adopted representation (5.61). Second, the normal component of the displacement vector (current density in case of conductors) should be continuous. That is, (with reference to Fig. 5.10):

$$\kappa_i \frac{\partial \Phi}{\partial n_i} + \kappa_j \frac{\partial \Phi}{\partial n_j} = 0 \tag{5.66}$$

This constraint can be written for $s \varepsilon I_i$, as:

$$\kappa_i \{ \int_S \sigma(s') \frac{\partial G}{\partial n_i}(s,s') + \frac{1}{2}\sigma(s)\} +$$

$$\kappa_j \{ \int_S \sigma(s') \frac{\partial G}{\partial n_j}(s,s') + \frac{1}{2}\sigma(s)\} = 0 \tag{5.67}$$

which, upon rearranging, and noting that

$$\frac{\partial G}{\partial n_i} = - \frac{\partial G}{\partial n_j}, \tag{5.68}$$

produces the equation:

$$(\kappa_i - \kappa_j) \int_S \sigma(s') \frac{\partial G}{\partial n_i}(s,s')ds' + \frac{(\kappa_i + \kappa_j)}{2}\sigma(s) = 0 \tag{5.69}$$

to be enforced with appropriate indices i and j for all $s \varepsilon I$.

Equations (5.64), (5.65) and (5.69) constitute a coupled system in terms of the unknown, $\sigma(s)$, the fictitious "source distribution" over the boundaries. The BEM discretization and solution technique can be applied to this system, resulting in a dense matrix equation.

In general, an equation of type (5.64) depicts a conductor boundary at specified potential, one of type (5.65) with homogenous right-hand-side would signify a perfect insulator, and (5.69) represents a dielectric-dielectric interface.

Implementation of a similar approach has been reported [13] for a power insulator problem possessing rotational symmetry.

A drawback of this approach, however, seems to be in the dense system matrix that it yields. As all three integrations entail coupling of all boundary elements of the system, a classical "full-size" linear equation solution scheme has to be invoked. Especially for three-dimensional problems that do not possess symmetry (e.g. an analysis of ground electrode energy dissipation over piecewise in homogenous earth strata with irregular geometries), to achieve acceptable precision of results, fairly large systems of linear equations may become unavoidable — in spite of the savings brought about by implementing a boundary-integral-equation technique as opposed to the classical finite-element or finite difference methods of solving partial differential equations.

An alternative may be discovered by investigating an approach that would yield a block-sparse matrix which would be amenable to more efficient solution schemes that have been proposed [14]. The Green's Theorem formulation discussed above (sec. 5.1) should lead towards that route.

5.3. Time-harmonic problems

Scattering and diffraction of sinusoidal electromagnetic waves by conducting or dielectric objects has been the subject of a large volume of research in the last decades. Classical partial differential equation solutions in terms of cylindrical, spherical or spheriodal wave functions [15] have been widely applied where problem geometries can be suitably classified. Low frequency approximations leading to power series solutions [16] have been studied, and the particular case of "small sphere" scattering, or Rayleigh scattering [17] can be said to have been the starting point of the interest in the area. High frequency asymptotic solutions have also been popular, leading the way to the technique of Physical Optics, PO, [18] which is based on the assumption that for small wavelengths, global geometry of the scatterer loses importance in determining the local nature of induced sources; each point on the scatterer reflects as if it were on an infinite tangent plane at the point of reflection. The Geometrical Optics approximation, which may be considered a refined version of the same approach, incorporates the global geometry information to the results of the PO approximation [19].

Integral equation formulation of scattering problems have also been classically popular [15, 17, 18], but numerical methods which permitted their solutions in arbitrarily shaped domains did not achieve their current popularity until the late 1960's. The moment method, and its particular pulse expansion-point matching form was established in the West as a fundamental tool in the solution of electromagnetic scattering problems especially after the publication of R. F. Harrington's now classical monograph [20]. Since then, a multitude of specialized problems have been tackled with that tool and accurate solutions have been obtained.

Until recently, moment-method solution of two-dimensional problems involved pulse expansion, and three-dimensional ones, wire-grid representation of solid surfaces [21]. Even flat-patch approximations seem to be a relatively novel approach [22]. BEM applications [4] have introduced iso-parametric curved elements to these models.

Our goal in studying a narrow selection of electromagnetic scattering problems has been to examine the improvements that can be introduced in terms of reduced computational costs and increased solution precision via the use of the BEM in general, and the cubic spline element methodology in particular.

5.3.1. Conducting circular infinite cylinder

Assuming a time variation of the form $e^{j\omega t}$, the fundamental Maxwell Equations for a time-harmonic electromagnetic field are:

$$-\nabla \times \overline{E} = j\omega\mu\overline{H}$$

$$\nabla \times \overline{H} = j\omega\varepsilon\overline{E} + \overline{J} \qquad (5.70)$$

where $\overline{J}$ represents the volume distribution of electric currents. Restricting our attention to TM fields, $\overline{E}$ and $\overline{J}$ vectors will be confined to the axial direction only. Then, (5.70) will lead, in a homogenous, anisotropic region, to:

$$\nabla^2 E + k^2 E = j\omega\mu J \qquad (5.71)$$

where

$$\overline{E} = \hat{u}_z E\,(x,y)$$

$$\overline{H} = \hat{u}_z H\,(x,y), \qquad (5.72)$$

in the Cartesian co-ordinate system, and

$$k = \omega\sqrt{\varepsilon\mu} = 2\Pi/\lambda. \qquad (5.73)$$

The solution to (5.71), a Helmholtz equation, can be constructed in terms of G(r,r'), the response to a point source in two-dimensional space, i.e. an infinite filament of unity current [18],

$$G(r,r') = -\frac{k\eta}{4} H_o^{(2)}(k|r-r'|), \qquad (5.74)$$

in which the characteristic impedance is given by:

$$\eta = (\mu/\varepsilon)^{\frac{1}{2}} \qquad (5.75)$$

and $H_0^{(2)}$ denotes the second kind Hankel function of order zero.

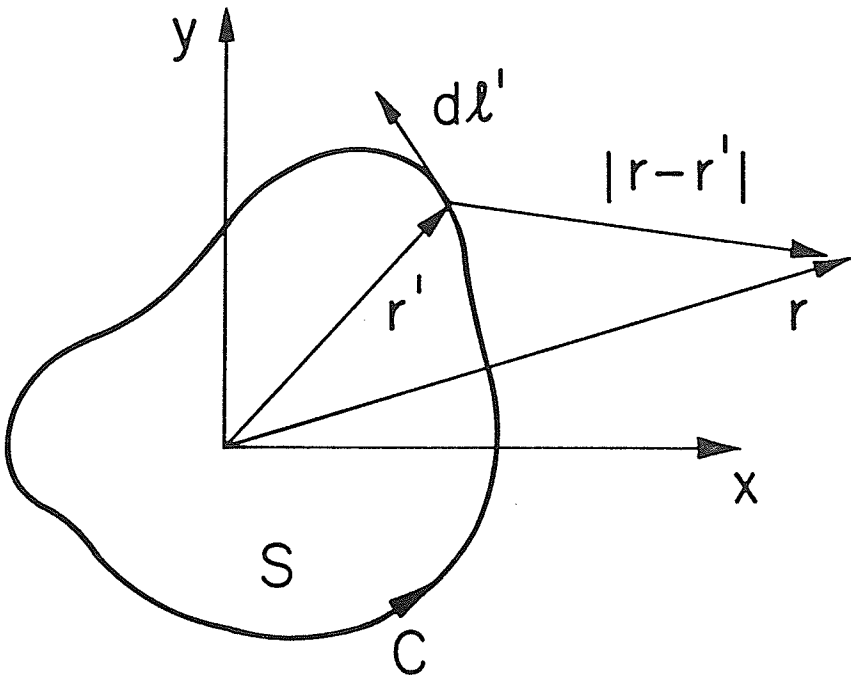

Figure 5.11. Cross section of a cylindrical scatterer.

The scattered field due the induced surface currents, $J_z(s)$ will be the sum of the contribution of all filamentary sources over the problem geometry (Fig. 5.11), i.e.

$$E_z^s(r) = \int_S J_z(s')G(r,s')ds'. \qquad (5.76)$$

For a conducting cylindrical body, the scattered field, $\bar{E}^s$, at the boundary, C, is exactly equal to the negative of the incident field, $\bar{E}^i$, so that the net total $\bar{E}$ field vanishes. Thus,

$$E_z^i(r) = -\int_C J_z(r')G(r,r')dl', \text{ for } r\epsilon C, \qquad (5.77)$$

is the Fredholm first kind integral equation formulation of the problem.

In this application, attention is focused on TM incidence and an E-field representation is used, but the TE case can easily be catered for in terms of the H-field, in a similar fashion.

The results obtained for the solution of (5.77) with the BEM with cubic splines (BSP) for the case of a unit-radius circular cylinder are presented in this subsection. Comparisons are given for a pulse expansion-point matching (PTM) solution of the same case. The tests were performed for medium-low and high frequencies, namely ka = 1.05 and ka = 5.24, corresponding to 50 MHz and 250 MHz respectively. The PTM procedure outlined by Harrington [20] was used.

A polynomic approximation of the Hankel function [23] was utilized throughout.

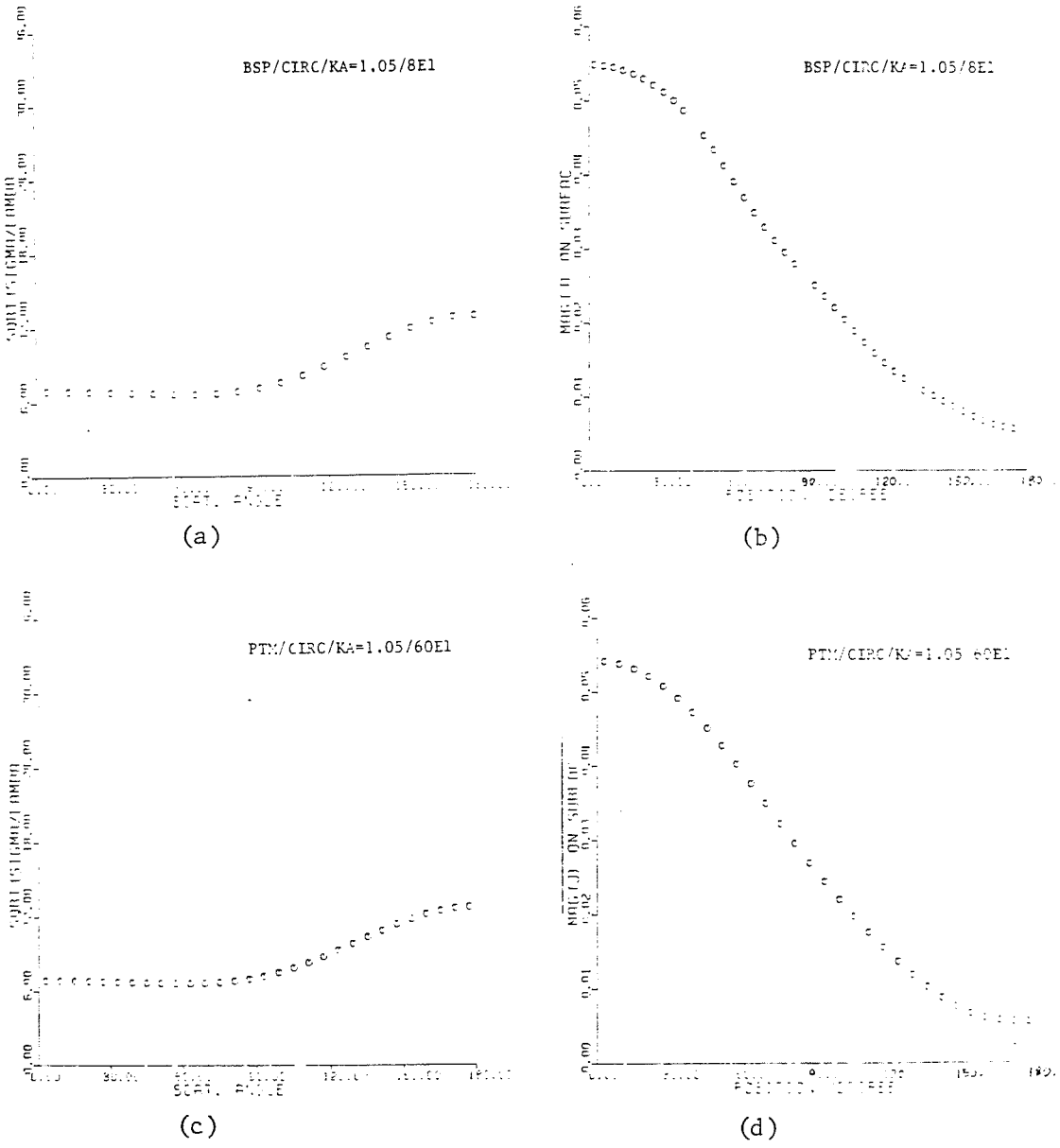

Figure 5.12. Scattering from conducting circular cylinder, low frequency. (a)Radar cross section, BEM; (b)Surface current density, BEM; (c)Radar cross section, point matching; (d)Surface current density, point matching.

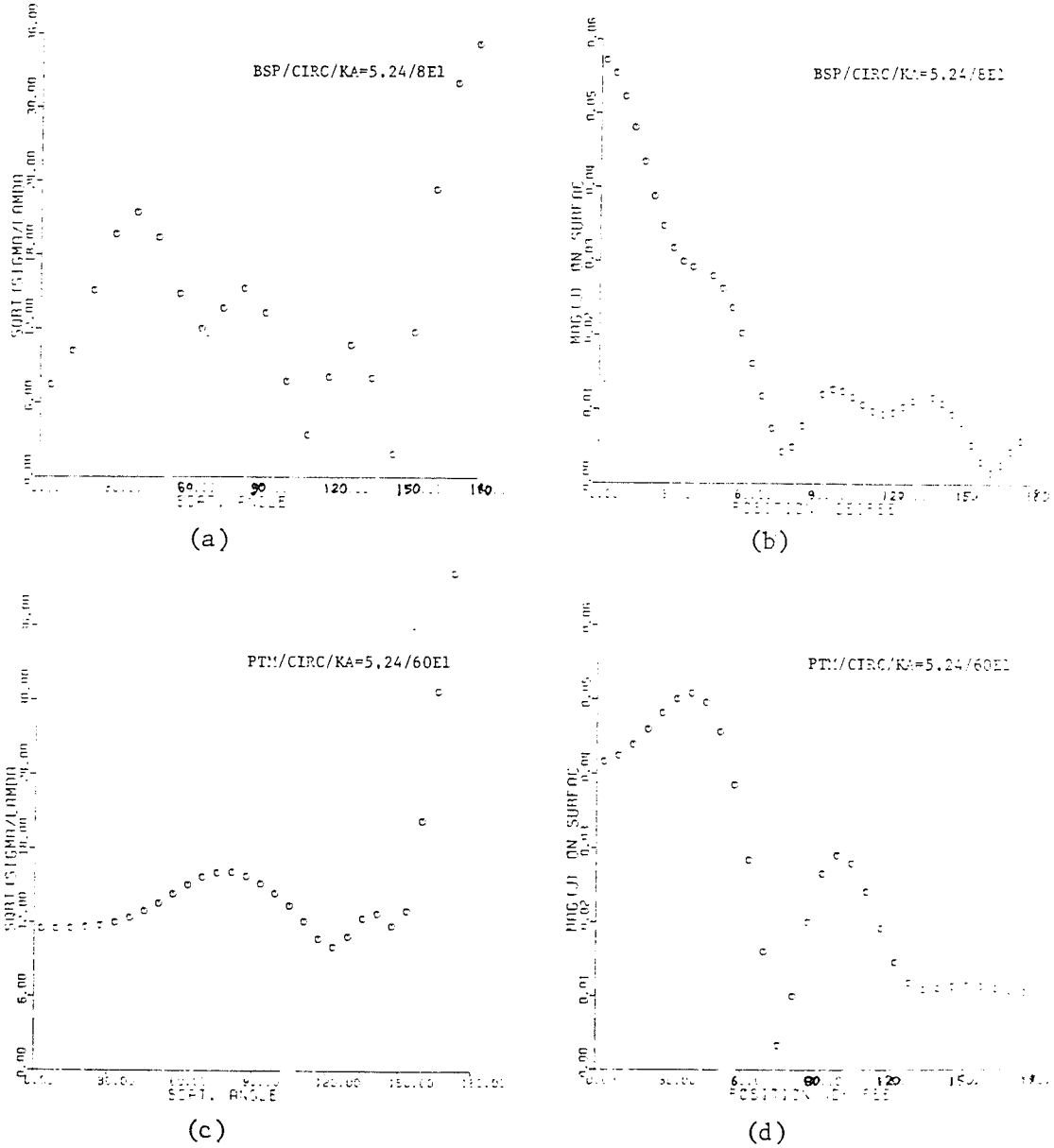

Figure 5.13. Scattering from conducting circular cylinder, high frequency.

(a)Radar cross section, BEM; (b)Surface currents, BEM;

(c)Radar cross section, point matching; (d)Surface currents, PTM.

Results in Figures 5,12 and 5.13 show that the PTM results and those of the BSP agree quite well for the lower frequency. At the higher frequency, the 8 elements of the BSP model, representing an element size of $0,66\lambda$, do not seem to be sufficient for accurate surface field computation.

A model with more elements would greatly improve accuracy at the higher frequency, as will be demonstrated in the next subsection.

5.3.2. Conducting rectangular infinite cylinder

Moment method solutions based on boundary integral relations for the problem of scattering from conductors, especially for the case of elliptic and square cylinders were reported by Mei and Van Bladel [24] and Andreasen [25] in two well-known and interesting papers, certain points in the former being the subject of some dispute [26].

The issue of edge singularity of the current density, or the magnetic field for TM incidence, was tackled in those works by using a large number of pulses especially in the proximity

of the edge, and ensuring that the integrand is not sampled right at the edge but "evenly on either side of it".

Shafai [27] developed a conformal mapping technique whereby the field singularity is directly incorporated, via the transformation of the scatterer surface to the unit circle, to the integral equation to be solved. A non-singular function is then sampled, and the coefficients involved in the transformation relate the surface current thus computed to the actual physical behavior.

Our approach to the problem of edge singularity of the surface fields has been to modify the basis of approximation to reflect the expected form of the singularity (see section 4.2, above). A $\frac{1}{r^{1/3}}$ form of behavior is expected [28], and the factor υ in the expressions (4.48) and (4.49) is chosen as $\upsilon = 1/3$. Parallel to the solution for the circular cylinder, pulse expansion - point matching (PTM) solutions with a relatively large number of approximating pulses are compared with the BSP results (Figures 5.14 and 5.15).

Obviously, the results are in agreement with those reported in the literature for the lower frequency and radar cross section computations [24, 25, 26, 27]. The PTM, however, breaks down

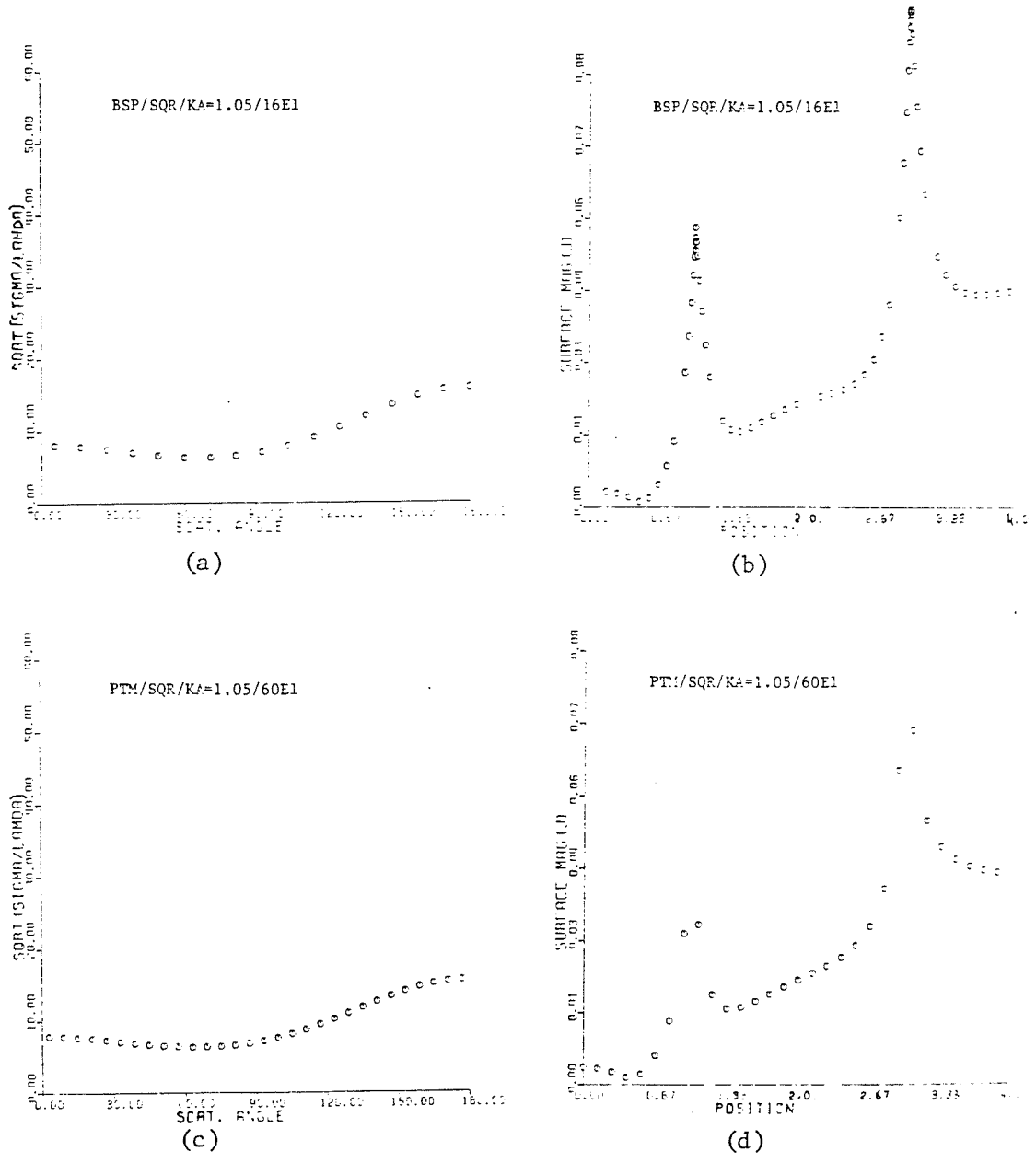

Figure 5.14. Scattering from conducting square cylinder, low frequency. (a)Radar cross section, BEM; (b)Surface current density, BEM; (c)Radar cross section, point matching; (d)Surface current density, point matching.

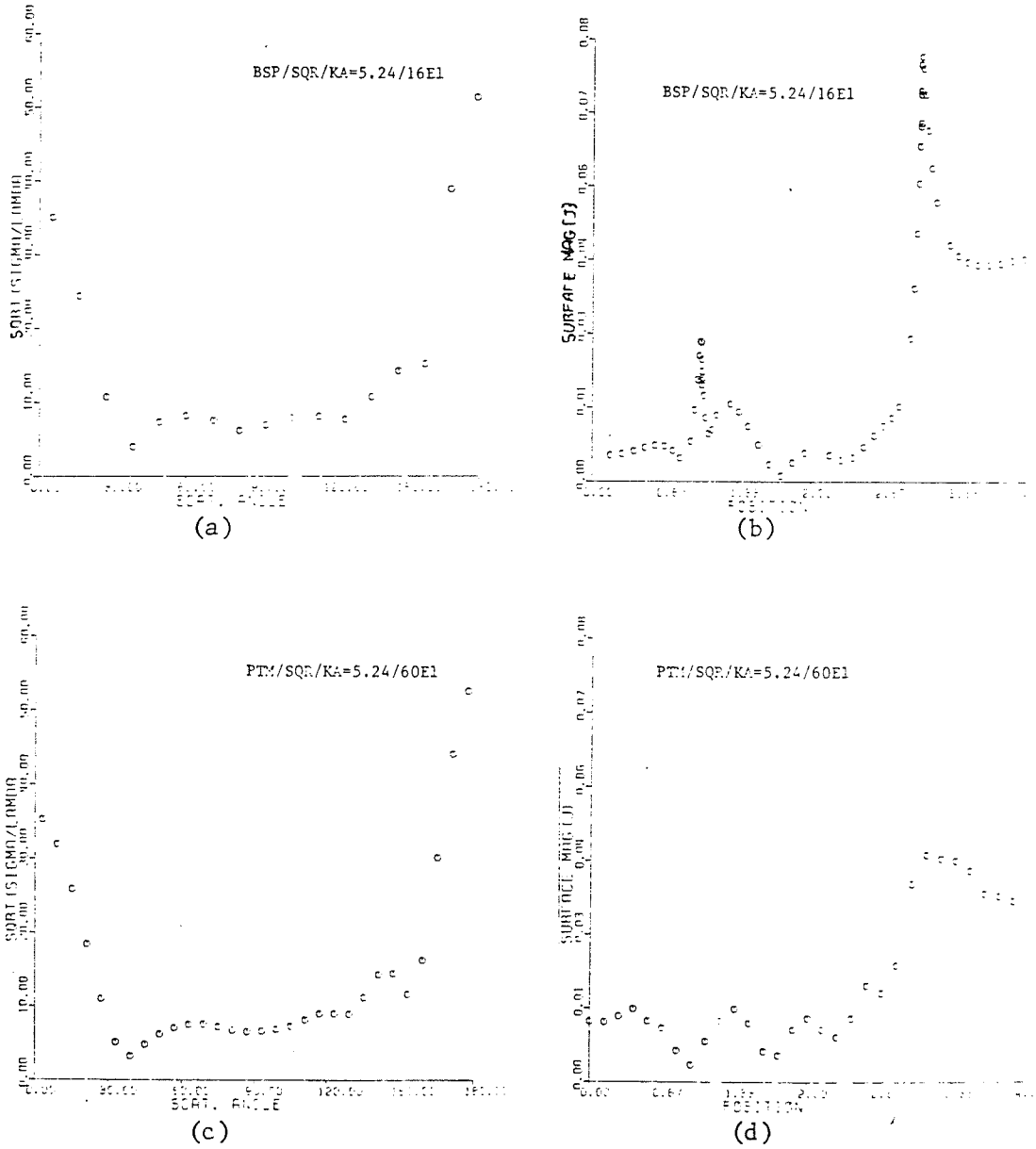

Figure 5.15. Scattering from conducting square cylinder, high frequency. (a)Radar cross section, BEM; (b)Surface current density, BEM; (c)Radar cross section, point matching; (d)Surface current density, point matching.

at the upper frequency range, especially for the surface sources - demonstrating the need for an even higher number of unknowns to model the problem. The singular behavior of surface sources is seen to be very comfortably reproduced by the modified spline model, with a relatively low number of unknowns. The total circumferential length of the square is 8 meters. At the higher frequency of 250 MH_z, the wavelength being λ = 1.196 m, this represents 6.7 wavelengths. A total of 16 elements were used, implying an average element length of 0.42λ, or an average sampling distance at 4-point Gauss quadrature, of 0.1λ. The PTM model, on the other hand represents a sampling distance of only 0.028λ. Accepted standards for reliable far-field results alone are in the vicinity of 0.17λ [21, p.346]. The accuracy of the near-field computations at the cost of sampling at every 0.1λ demonstrate the efficiency of the BEM.

5.3.3. Dielectric circular infinite cylinder

The smooth circular dielectric cylinder immersed in an incident plane TM wave in free space will be the subject of this subsection, and the square cylinder involving the problematic "wedge-scattering" issue will be considered next.

The moment-method solution of a two-dimensional surface-integral formulation of the problem was reported in 1965 [29]. While that approach possessed the ability to cater for inhomogenous bodies, it suffered relatively high computational costs. The

alternative, unimoment method [30], proposed by K. Mei in this context, is similar to the widely applicable "mutual-constraint" technique of McDonald and Wexler [31, 32]. A boundary integral equation may also be derived, as long as the dielectric is homogenous, thus effectively reducing problem dimensions. A general three-dimensional derivation was presented firstby Poggio&Miller [33]. Applications have been reported in [34], [35], and [36]. Morita has improved the technique [37] to overcome the difficulty posed when the excitation is at a resonant frequency of the interior. His Extended Boundary Condition technique is essentially an extension of the approach put forward by Waterman [38] for the problem of conducting cylinders.

Starting from the Helmholtz equation, (5.71), the Green's Theorem formulation (5.33) may be invoked for the axial component of the electric field:

$$E_z(r) = \gamma \int_S \{G(r,s') \frac{\partial E}{\partial n'} z(s') - E_z(s') \frac{\partial G}{\partial n'} (r,s')\} ds', \qquad (5.78)$$

which is valid for two regions: one, for r interior to the dielectric body, in which case

$$G_i(r,r') = -\frac{j}{4} H_o^{(2)}(k|r-r'|) \qquad (5.79)$$

with

$$k = \omega \sqrt{\varepsilon \mu}; \qquad (5.80)$$

and the second, for r exterior to it, in which case

$$G_e(r,r') = -\frac{j}{4} H_o^{(2)}(k_o|r-r'|) \tag{5.81}$$

with

$$k_o = \omega \sqrt{\varepsilon_0 \mu_0}. \tag{5.82}$$

The total field is, $E_z(r) = E_z^i(r) + E_z^s(r)$, i.e. the sum of the incident and scattered fields. Enforcing the continuity of the tangential $\bar{E}$ and normal $\bar{D}$ $(=\varepsilon\bar{E})$ fields, and writing (5.78) when r approaches the surface, we have the two coupled integral equations:

$$E_z^i(s) = \tfrac{1}{2} E_z(s) + \int_C \{G_e(s,s') \frac{\partial E_z}{\partial n'}(s') - E_z(s') \frac{\partial G_e}{\partial n'}(s,s')\} ds' \tag{5.83}$$

$$0 = \tfrac{1}{2} E_z(s) - \int_C \{G_i(s,s') \frac{\partial E_z}{\partial n'}(s') - E_z(s') \frac{\partial G_i}{\partial n'}(s,s')\} ds' \tag{5.84}$$

for s located on the boundary, C. Here G_e and G_i are as defined in (5.79) through (5.82). The incident field is given by

$$E_z^i(r) = E_o \exp(-jk_o x). \tag{5.85}$$

The solution of (5.83) and (5.84) directly gives the surface fields, a fact which demonstrates an advantage of the Green's Theorem formulation, as remarked earlier.

The analytical expression in terms of Bessel and Hankel functions for scattered surface fields is [18, p.261]:

$$E_z^s = \sum_{-\infty}^{+\infty} j^{-n} a_n e^{jn\Phi} \tag{5.86}$$

with

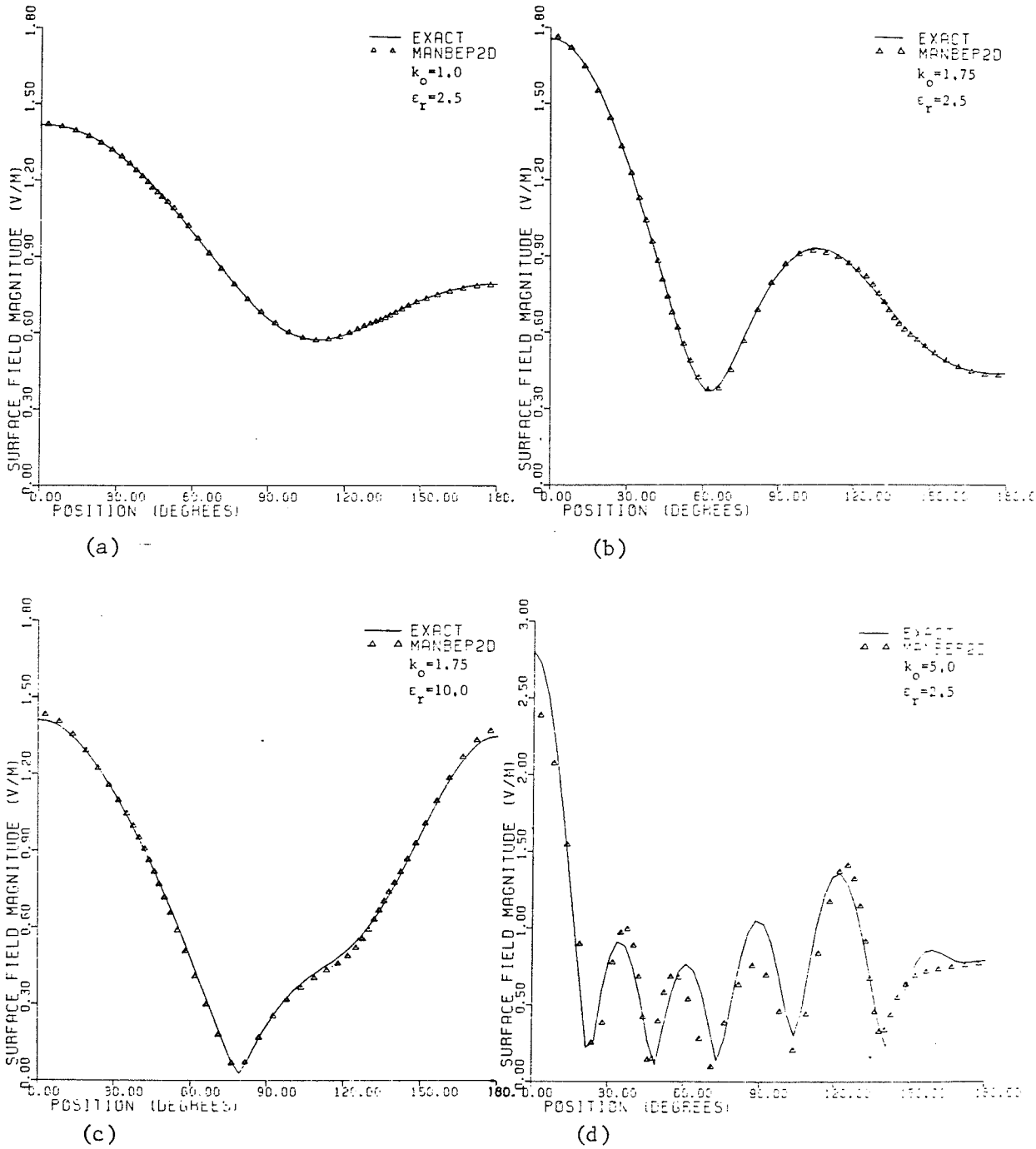

Figure 5.16. Surface fields on a dielectric circular cylinder immersed in a time-harmonic field.

$$a_n = -J_n(k_o a)\ \frac{\varepsilon J_n'(ka)/\varepsilon_o k a J_n(ka) - J_n'(k_o a)/k_o a J_n(k_o a)}{\varepsilon J_n'(ka)/\varepsilon_o k a J_n(ka) - H_n^{(2)'}(k_o a)/k_o a H_n^{(2)'}(k_o a)} \qquad (5.87)$$

in which ε and ε_0 denote the permittivity of the dielectric and free space, respectively, and k and k_o signify the wave number in dielectric and free space, respectively, as in (5.80) and (5.82).

The numerical solution of (5.83) and (5.84) was obtained, for the case of the circular cylinder, with 16 cubic spline boundary elements over the cylinder. Hankel functions of order zero and one, as called for by the G(.) and $\frac{\partial G}{\partial n}$(.) terms, were approximated by polynomials [23]. The results for various dielectric and frequency combinations are presented and compared to the exact values in Figure 5.16.

The results are definitely satisfactory. When the model starts showing signs of deterioration at k_o=5,0 and ε=2.5, the propagation constant in the dielectric is k=7.905, implying a circumferential length of 7.905λ.

The computations for k_o=1,75 are particularly useful in assessing the reliability of the solution technology for the square cylinder problem which will be considered next.

5.3.4. Dielectric square infinite cylinder

Meixner's well known work [28], cited above, presents an in-depth treatise of the problem of field singularity at a common

edge between two dielectric wedges (Fig. 5.17).

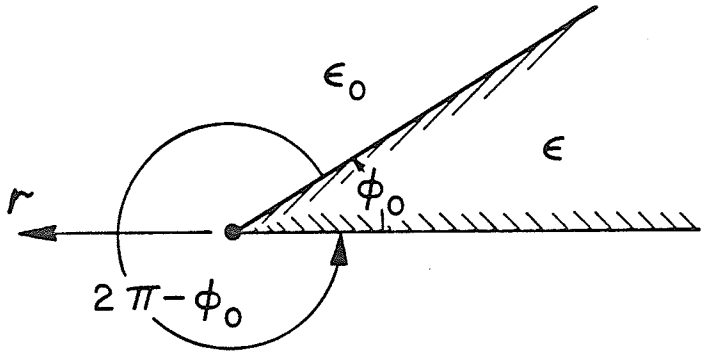

Figure 5.17 Dielectric wedge configuration

Considering a dielectric wedge in free space, Meixner's theory predicts that when $\overline{H}$ is parallel to the edge, the electric field components E_r and E_ϕ behave as r^{t-1}, where t is the lowest positive solution of

$$\frac{\varepsilon - \varepsilon_o}{\varepsilon + \varepsilon_o} = \pm \frac{\sin t\Pi}{\sin t(\Phi_o - \Pi)} . \qquad (5.88)$$

In 1970, Hurd [39] observed that

a) If $\varepsilon \neq \varepsilon_0$ and $\Phi_0 \neq 0, \Pi, 2\Pi$, there always exists a solution of (5.88) such that $0<t<1$, meaning that the Electric field is singular at r = 0, and

b) due to the symmetry of (5.88) in ε and ε_0, wedge angles of Φ_0 and $2\Pi-\Phi_0$ display the same singularity. He then went on to consider the case when $\varepsilon/\varepsilon_0$ becomes very large. Assuming that $\Phi_0<\Pi$, then, the smallest root of (5.88) approaches

$$t = \Pi/(2\Pi-\Phi_0) \qquad (5.89)$$

which gives the correct singularity for a perfectly conducting wedge (see section 4.2), but means that a wedge of Φ_0 with $\varepsilon/\varepsilon_0$ very small has the same discontinuity, due to symmetry. But it is known, by exact solutions (e.g.40) that a perfectly conducting wedge of angle $\Phi_0>\Pi$ does not have a field singularity. Thus, Meixner's theory which predicts singularity for high-dielectric constants but non-singular behavior for perfect conductors was put to question.

Bach Andersen and V. Solodukhov (41) studied the same issue, and demonstrated that obtaining conductor behavior by letting $\varepsilon \to \infty$ is often correct, but not always - when $\varepsilon/\varepsilon_0$ is infinite, equation (5.88) which is derived on the assumption that fields inside the dielectric are non-vanishing, ceases to apply. Thus, they proved that permeable wedges of angle $\Phi_0>\Pi$ have a singularity of the E-field whereas perfectly conducting wedges of the same angle do not. Upon further analysis of Meixner's theory, they also showed that while those results hold for the electrostatic case and for perfect conductors, in time-

varying configurations, Meixner's singularity predictions do not hold for dielectric wedges.

In the light of this briefly summarized controversy around the dielectric edge singularity topic, we have attempted a solution of the dielectric square cylinder scattering problem without modifying our polynomic spline basis. To determine field behavior at edges, a relatively large number of elements were packed into their vicinity. Results obtained by the computer program for the TE incidence case are presented in Figure 5.18.

Our results indicate locally discontinuous peaks at both edges. Andersen and Solodukhov used a small-radius-of-curvature approximation for edges, and reported similar peaks at the lateral edges, but not at the edge of incidence. Their numerical computations showed that the fields tend to zero there (Fig. 5.19), similar to the expectation in case of electrostatics. They were at a loss, however, to explain the deviation from the electrostatic behavior that their results demonstrated.

It can be concluded that, as Andersen and Solodukhov have also stated, the behavior of electromagnetic fields of higher frequencies in the vicinity of dielectric edges is not necessarily

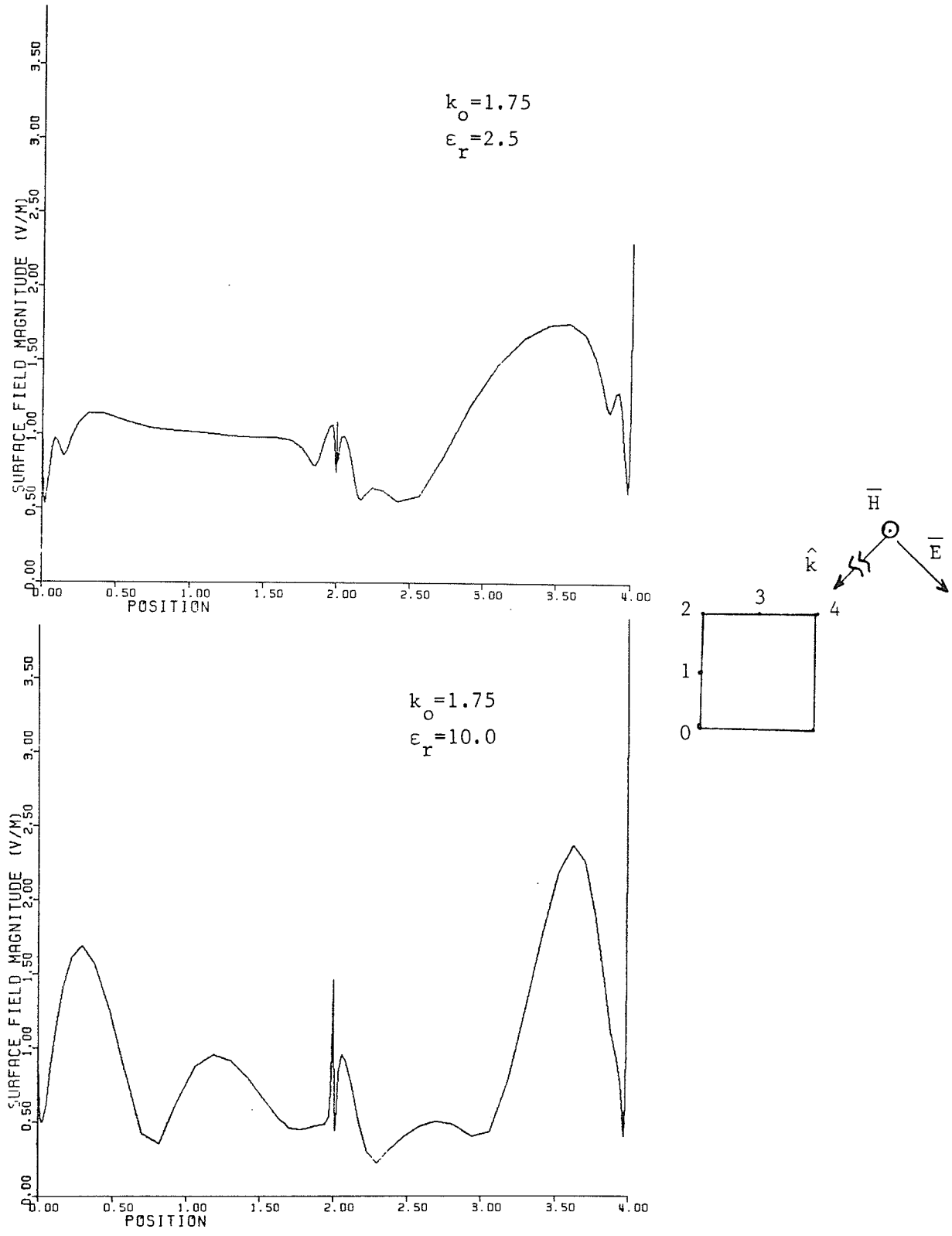

Figure 5.18. $|E_{tan}|$ for TE incidence on a square dielectric cylinder.

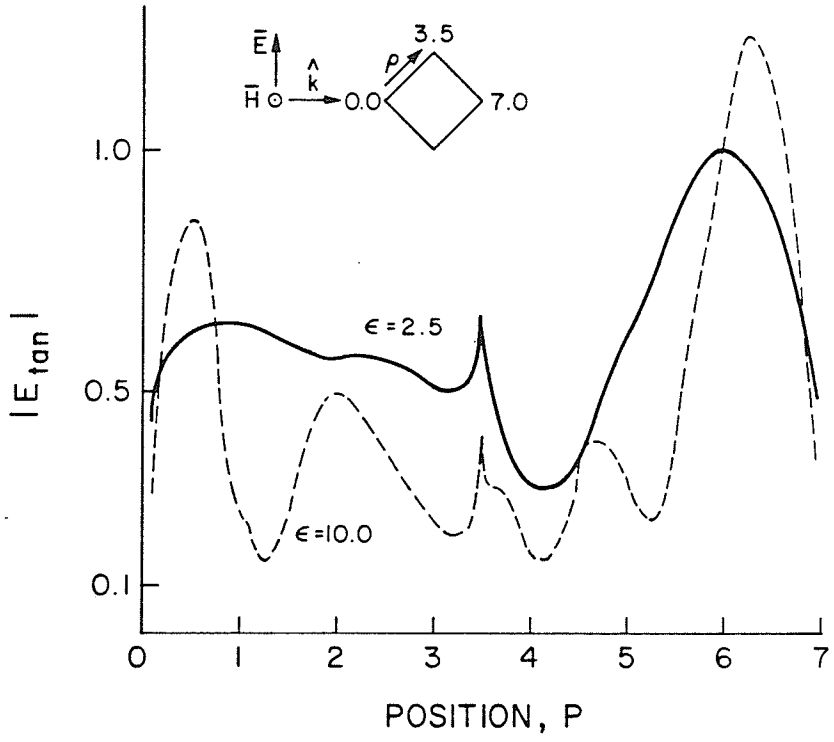

Figure 5.19. Bach Andersen and Solodukhov's results for the dielectric square cylinder [41].

as predicted for the electrostatic case. It is likely that local singularities exist in the vicinity of perfect edges, but approximations that involve even very small radii of curvature may suppress the peaks - which would explain the discrepancy between Andersen and Solodukhov's results and ours. The degree of agreement between our numerical results and the exact values for the case of the smooth circular dielectric cylinder leads us to believe that the singular behavior at both edges, predicted by our program, reflects a close approximation of the phenomenon.

5.3.5. Conducting sphere

Comprehensive analytical solutions to the problem of electromagnetic scattering from a conducting sphere are available [42], and the results for various frequencies provide a classical test for any numerical procedure for the solution of three-dimensional scattering problems.

Maxwell's equations (5.70) in a divergenceless region, give rise to the vector Helmholtz equations:

$$\nabla\times\nabla\times\bar{E}-k^2\bar{E} = 0 \qquad (5.90)$$

$$\nabla\times\nabla\times\bar{H}-k^2\bar{H} = 0 \qquad (5.91)$$

A scalar free-space Green's function, G, that satisfies

$$\nabla\times\nabla\times G\hat{a} - k^2 G\hat{a} = -\delta(r-r')\hat{a} \qquad (5.92)$$

can be utilized to construct the solution to (5.90) and (5.91), $\hat{a}$ denotes a unit vector in an arbitrary direction. Invoking the

vector form of Green's theorem (*), we can obtain

$$\overline{E}(r)\cdot\hat{a} = \gamma\int_S \{\overline{E}(s')x\nabla xG(r,s')\hat{a} - G(r,s')\hat{a}x\nabla x\overline{E}(s')\}\cdot\hat{n}ds \qquad (5.93)$$

similar to the scalar formulation summarized in (5.33), with the same definition of γ in terms of the position, r.

(5.93) holds for the $\overline{H}$ field as well, and application of the proper boundary conditions on (5.93) or its counterpart for the magnetic field results in an Electric Field Integral Equation (EFIE) or a Magnetic Field Integral Equation (MFIE), respectively. Traditional preference has generally been [33] for the MFIE in smooth-surface problems, and for the EFIE in thin cylindrical configurations.

Enforcing the condition that at the conductor boundary, the normal magnetic and tangential electric fields should vanish, i.e.

$$\hat{n}\cdot\overline{H}(r) = 0,$$
$$\hat{n}x\overline{E}(r) = 0, \text{ for } r\varepsilon S, \qquad (5.94)$$

and letting $\gamma = -2$ on S, (5.93) and its $\overline{H}$-field counterpart lead to the MFIE:

(*) $\int_V \{\overline{A}\cdot\nabla x\nabla x\overline{B} - \overline{B}\cdot\nabla x\nabla x\overline{A}\}dv = \int_S \{\overline{B}x\nabla x\overline{A} - \overline{A}x\nabla x\overline{B}\}\cdot\overline{ds}$

in which $\overline{A}$ and $\overline{B}$ are vector functions of position with continuous first and second derivatives within and on S, where S is the boundary of V.

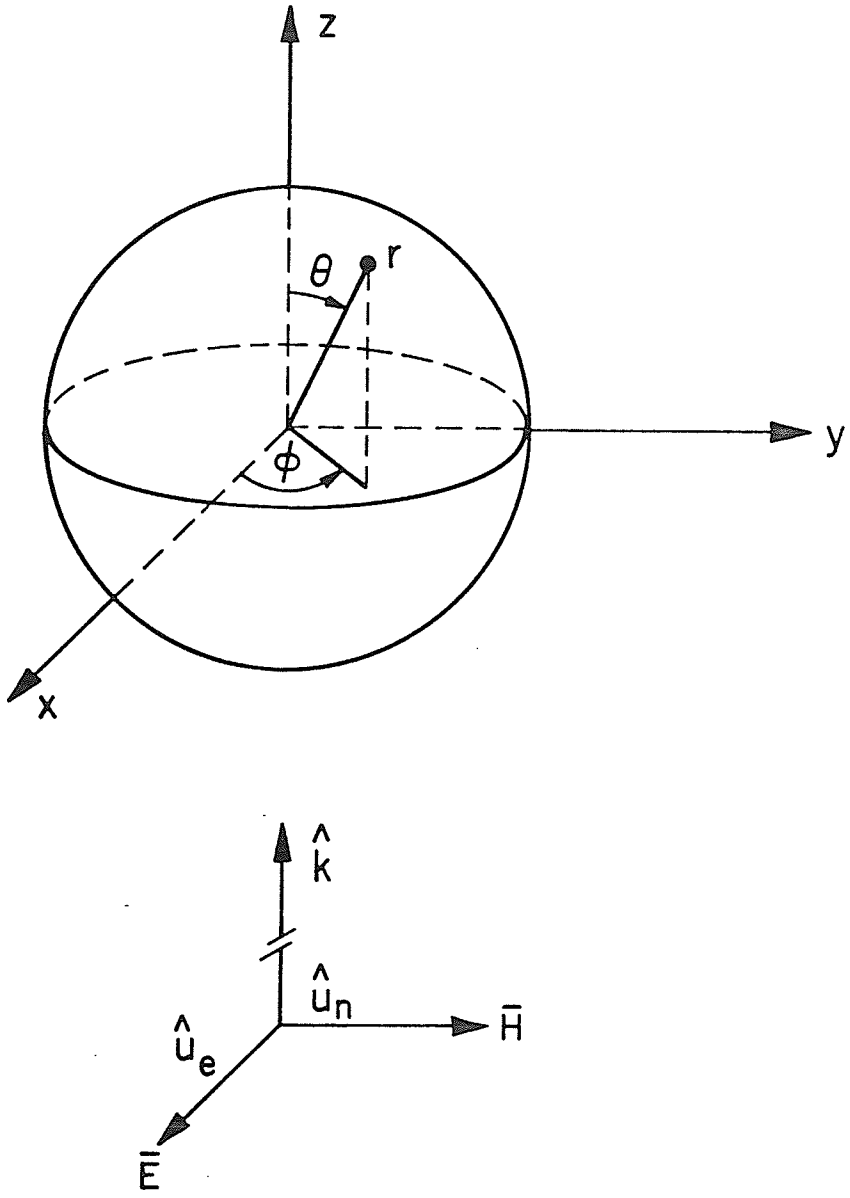

Figure 5.20. Geometry for three-dimensional scattering problems.

$$\hat{n} \times \int_S \bar{J}(s') \times \nabla' G(s,s')ds' - \tfrac{1}{2}\bar{J}(s) = -\hat{n}\times\bar{H}^i(s) \qquad (5.95)$$

in which

$$\bar{H}(r) = \bar{H}^s(r) + \bar{H}^i(r), \qquad (5.96)$$

and

$$\bar{J}(s) \triangleq \hat{n}\times\bar{H}(s) \qquad (5.97)$$

represents the equivalent surface currents, and $\nabla' G(s,s')$ denotes the gradient of the scalar function, G. Explicitly,

$$G(r,r') = \frac{e^{-jk|r-r'|}}{4\pi|r-r'|} \qquad (5.98)$$

and

$$\nabla' G(r,r') = \frac{1}{4\pi|r-r'|^2} e^{-jk|r-r'|}(1+jk|r-r'|)\hat{u}_r \qquad (5.99)$$

in which the unit vector, $\hat{u}_r$ is given by:

$$\hat{u}_r = \frac{(r-r')}{|r-r'|} . \qquad (5.100)$$

(5.95) is a Fredholm integral equation of the second kind, in terms of the equivalent surface current, $\bar{J}(s)$. Its solution leads to the scattered field through:

$$\bar{H}^s(r) = \int_S \bar{J}(s')\times\nabla' G(r,s')ds'. \qquad (5.101)$$

To compute far-field quantities, phase terms can be neglected which results in

$$\nabla' G(r,r') \to \frac{jk\, e^{jk|r|}}{4\pi|r|} e^{jk\hat{u}_r\cdot r'} \hat{u}_r \qquad (5.102)$$

where only the r^{-1} term of the binomial expansion of

$$(r-r') \rightarrow |r| - \frac{(r\cdot r')}{|r|} \tag{5.103}$$

has been retained for $r>>r'$.

The radar cross-section, defined as:

$$\sigma = \lim_{r \rightarrow \infty} 4\Pi r^2 \frac{|\bar{H}^s|^2}{|\bar{H}^i|^2} , \tag{5.104}$$

can thus be computed as:

$$\sigma = \frac{1}{4\Pi} \left| \int_S jk(\bar{J}(s') \times \hat{u}_r) e^{jk\hat{u}_r\cdot r'} ds' \right|^2 . \tag{5.105}$$

The computations have been carried out for a plane wave with unit $\bar{E}$ magnitude, incident at an arbitrary specified angle as

$$\bar{H}^i(r) = \frac{1}{\eta}\hat{u}_h \, e^{-j\hat{k}\cdot r} \tag{5.106}$$

in which $\hat{u}_h$ denotes the unit vector in the magnetic field direction, and $\hat{k}$ is the unit vector in the propagation direction (Fig. 5.20). The magnitude is scaled down by η, the intrinsic impedance of free-space.

The surface fields and scattering cross section for a unit sphere in a linearly-polarized TEM wave of unit H-field magnitude, and f = 80.9 MH_z, as computed by the BEM with cubic spline bivariate elements, are presented in Fig. 5.21. An 8-element model of the complete sphere using only 12 unknowns in the

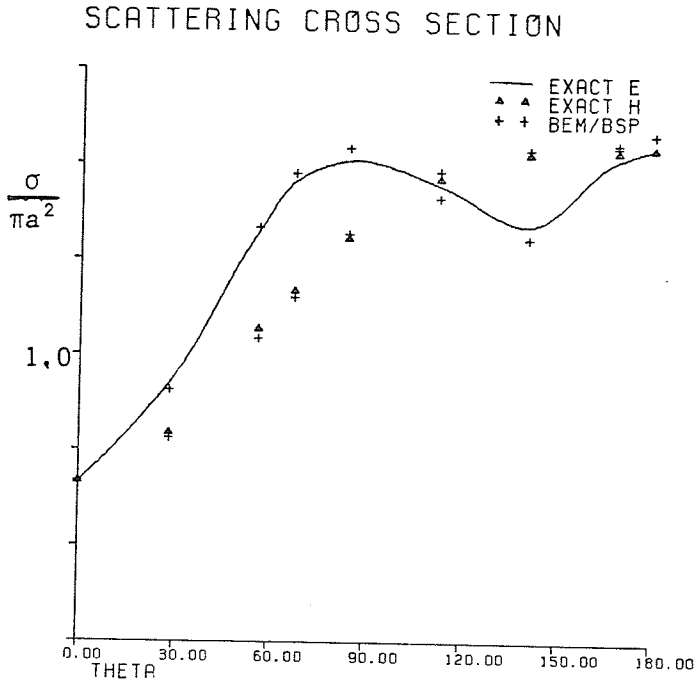

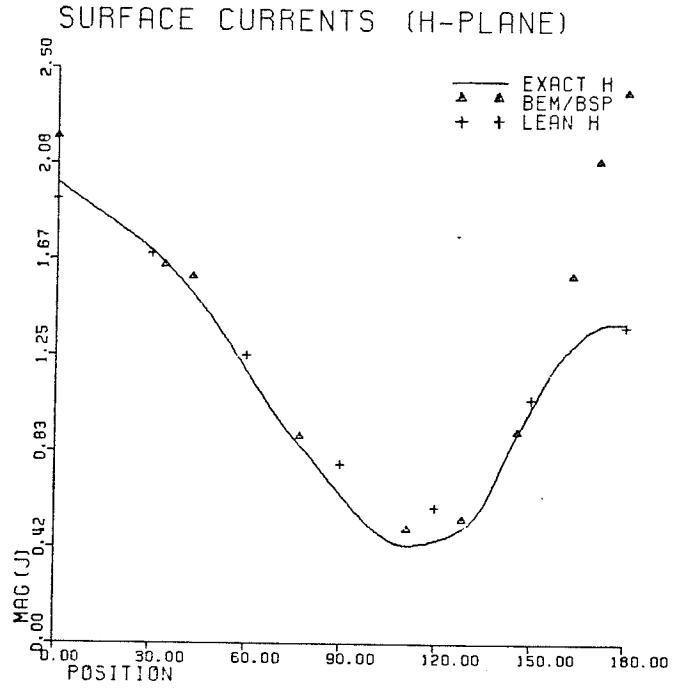

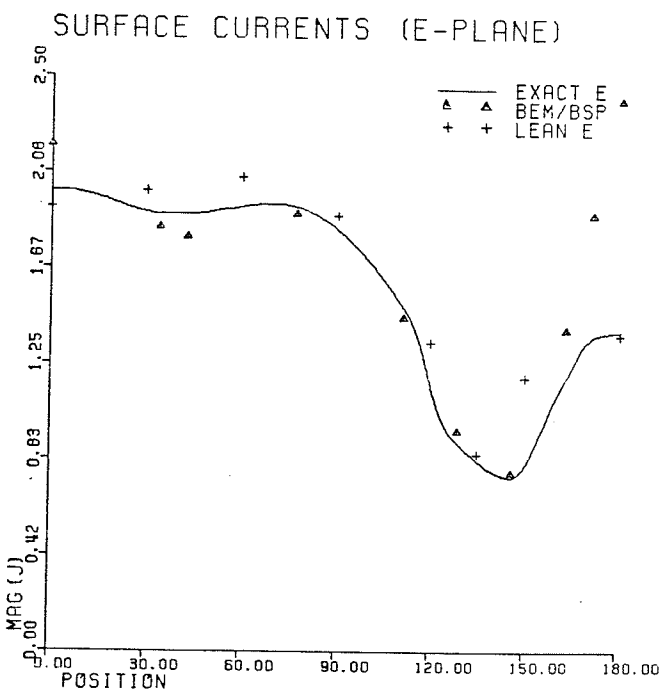

Figure 5.21. Scattering from a conducting sphere, ka=1.7,
Exact curves from King & Wu [42].

discretized BEM model was utilized. A 3-dimensional Cartesian vector form of (5.95) in this case resulted in a 36 x 36 system of equations to arrive at the solution in 49.5 cpu seconds (*) without using symmetry. A classical moment method approach to the same problem would typically require a linear equation set of the order of 264 x 264 to 360 x 360 without using symmetry [43], or 33 x 33 to 45 x 45 if 1/8 symmetry can be catered for.

In comparison to the Lagrangian element implementation of the BEM [4] as well, splines have introduced noticeable savings in this problem: similar accuracy in terms of the far-fields was reported at the same frequency and the same configuration, with a 38-node model requiring a 114 x 114 system that took 200 cpu seconds (*) for solution. To achieve accurate surface sources, improved geometrical modelling was recommended. Considering the relative cheapness of this particular spline model, the results presented in Figure 5.21 together with those of Lean[4], are quite encouraging.

5.3.6. Conducting cube

Previous work on electromagnetic scattering from a conducting cube is not readily available. The closest topics of recent interest seem to be that of scattering from a thin plate [44,45], and from three dimensional objects possessing rotational symmetry

(*) On the University of Manitoba Amdahl 470/V7 system using Fortran H software.

[45]. Poggio and Miller's relevant article [33], presents the applicable theory, but their solution technique of wire-grid modelling or flat patch approximation of sources have not been applied to the particular instance of the cube.

In our view, the aspect of the problem which makes it highly "un-appealing" is the edge singularities it involves and the immense amount of unknowns that would be required to model the irregular behavior of surface sources, due mainly to the effect of the singularities.

Having demonstrated the reliable operation of the BEM with three-dimensional cubic spline elements in the case of electromagnetic scattering from a conducting sphere, we applied that methodology to the case of the conducting cube. As verified by a number of researchers [39, 41], Meixner's edge condition [28] holds for the perfectly conducting edge immersed in a time-varying electromagnetic field. Thus, the $\frac{1}{r^{1/3}}$ form of singularity was imposed on the appropriate shape functions over each element bordering an edge. 54 rectangular elements over the surface (an array of 3 x 3 on each face) were used, giving rise to 56 unknowns with three degrees of freedom each; i.e. a 168 x 168 system of linear equations was solved. Figure 5.22 presents the results for linearly-polarized plane-wave incidence perpendicular to the center of a face at a frequency of ka = 2.0, in which 'a' denotes half the length of an edge of the cube.

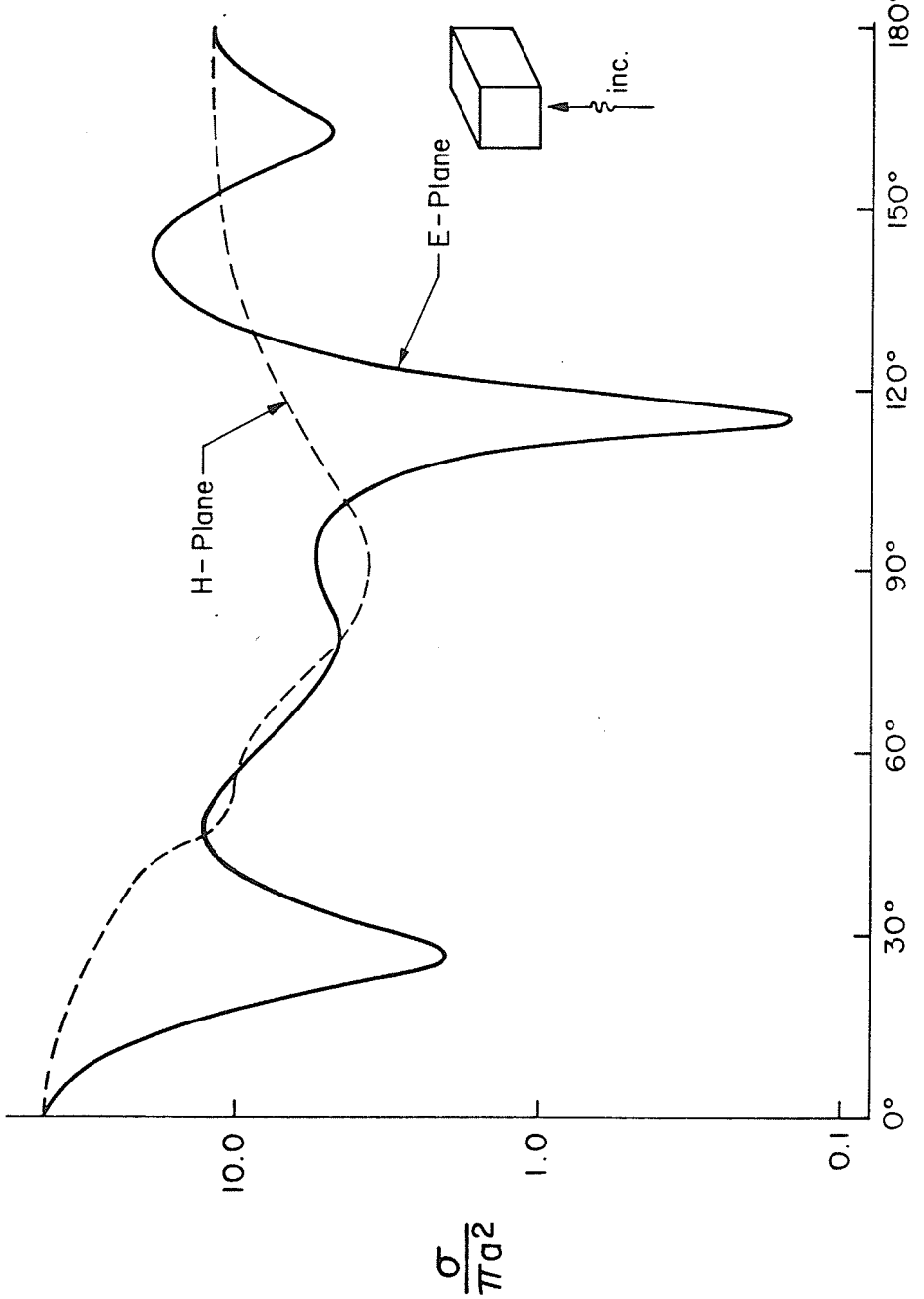

Figure 5.22. Bi-static scattering cross section of a conducting cube, k=2.0.

5.4 References.

(1) Mikhlin, S. G., Integral Equations, Second Revised Edition, Pergamon Press, 1964.

(2) Zabreyko, P. P., et. al., Integral Equations - a reference text, Noordhoff International Publishing, 1975.

(3) Jaswon, M. A. and Symm, G. T., Integral Equation Methods in Potential Theory and Elastostatics, Academic Press, 1977.

(4) Lean, M. H., Electromagnetic Field Solution with the Boundary Element Method, Ph.D. Dissertation, University of Manitoba, 1981.

(5) Bryant, T. G. and Weiss, J. A., "Parameters of microstrip transmission lines and of coupled pairs of microstrip lines", IEEE Trans. Microwave Theory and Techniques, vol. MTT-16, pp. 1021-1027, 1968.

(6) Jones, D. S., The Theory of Electromagnetism, Pergamon Press, 1964.

(7) McDonald, B., Friedman, M., and Wexler, A., "Variational Solution of Integral equations", IEEE Trans. Microwave Theory and Techniques, vol. MTT-22, pp. 237-248, 1974.

(8) Van Bladel, J., Electromagnetic Fields, McGraw-Hill, 1964.

(9) Mei, K., and Van Bladel, J., "Low-frequency Scattering by Rectangular Cylinders", IEEE Trans. Antennas and Propagation, vol. AP-11, pp. 52-56, 1963.

(10) Eyges, L., and Gianino, P., "Polarizabilities of Rectangular Dielectric Cylinders and of a Cube", IEEE Trans. Antennas and Propagation, vol. AP-27, pp. 557-560, 1979.

(11) Reitan, D. K., and Higgins, T. J., "Calculation of the Electrical Capacitance of a Cube", Journal of Applied Physics, vol. 22, pp. 223-226, 1951.

(12) Parr, W. E., "Upper and Lower Bounds for the Capacitance of Regular Solids", Journal of the Society for Industrial Applications of Mathematics, vol. 9, pp. 334-386, 1961.

(13) Daffe, J., and Olsen, R. G., "An integral equation technique for solving rotationally symmetric electrostatic problems in conducting and dielectric material", IEEE Trans Power Apparatus and Systems, vol. PAS-98, pp. 1609-1615, 1979.

(14) Wexler, A., Perspectives on the solution of Simultaneous Equations, Report TR79-2, Electrical Engineering Department, University of Manitoba, 1979.

(15) Mentzer, J. R., Scattering and Diffraction of Radio Waves, Pergamon Press, 1955.

(16) Kleinman, R. E., "The Rayleigh region", Proceedings of the IEEE, vol. 53, pp. 848-856, 1965.

(17) Stratton, J. A., Electromagnetic Theory, McGraw-Hill, 1941.

(18) Harrington, R. F., Time-Harmonic Electromagnetic Fields, McGraw-Hill, 1961.

(19) Kouyoumjian, R. G., An Introduction to Geometrical Optics and the Geometrical Theory of Diffraction, Antenna and Scattering Theory: Recent Advances, Vol. I; Short Courses at Ohio State University, 1966.

(20) Harrington, R. F., Field Computation by Moment Methods, Macmillan, 1968.

(21) Miller, E. K., and Poggio, A. J., "Moment-method techniques in electromagnetics from an applications viewpoint", in Uslenghi, P.L.E. (ed.), Electromagnetic Scattering, Academic Press, 1978.

(22) Burke, G. J., and Poggio, A. J., Numerical Electromagnetic Code (NEC) - Method of Moments, Part I, Naval Ocean Systems Center, San Diego, California, 1977.

(23) Abramowitz, M. and Stegun, I. A. (eds.), Handbook of Mathematical Functions, Dover, 1968.

(24) Mei, K. K., and Van Bladel, J. G., "Scattering by Perfectly-Conducting Rectangular Cylinders", IEEE Trans. Antennas and Propagation, vol. AP-11, pp. 185-192, 1963.

(25) Andreasen, M. G., "Scattering from Parallel Metallic Cylinders with Arbitrary Cross Sections", IEEE Trans. Antennas and Propagation, vol. AP-12, pp. 746-754, 1964.

(26) Andreasen, M. G., "Comments on Scattering by Conducting Rectangular Cylinders", IEEE Trans. Antennas and Propagation, vol. AP-12, pp. 235-236, 1964;
Mei, K. K., "Author's reply", ibid., p. 236.

(27) Shafai, L., "An improved integral equation for the numerical solution of two-dimensional diffraction problems", Canadian Journal of Physics, vol. 48, pp. 954-963, 1970.

(28) Meixner, J., "The behavior of electromagnetic fields at edges", New York University Institute of Mathematical Sciences, Division of Electromagnetic Research, Report No. EM-72, New York, 1952.

(29) Richmond, J. H., "Scattering by a dielectric cylinder of arbitrary cross section shape", IEEE Trans. Antennas and Propagation, vol. AP-13, pp. 334-341, 1965.

(30) Mei, K.K., "Unimoment method of solving antenna and scattering problems", IEEE Trans. Antennas and Propagation, vol. AP-22, pp. 760-766, 1974.

(31) McDonald, B. H., and Wexler, A., "Finite element solution of unbounded field problems", IEEE Trans. Microwave Theory and Techniques, vol. MTT-20, pp. 841-847, 1972.

(32) McDonald, B. H., and Wexler, A., "Mutually constrained partial differential, and integral equation field formulations", in Chari, M.V.K., and Silvester, P,K., (eds.), Finite Elements in Electrical and Magnetic Field Problems, John Wiley & Sons, 1980.

(33) Poggio, A. J. and Miller, E. K., "Integral Equation Solutions of Three-dimensional Scattering Problems", in Mittra, R. (ed.) Computer Techniques for Electromagnetics, Pergamon Press, 1973.

(34) Wu, T. K., and Tsai, L.L., "Numerical Analysis of Electromagnetic Fields in Biological Tissues", IEEE Proceedings Letters, pp. 1167-1168, Aug. 1974.

(35) Morita, N., "Surface Integral Representations for Electromagnetic Scattering from Dielectric Cylinders", IEEE Trans. Antennas and Propagations, vol. AP-26, pp. 261-266, 1978.

(36) Solodukhov, V. V. and Vasil'ev, E. N., "Diffraction of a plane electromagnetic wave by a dielectric cylinder of arbitrary cross section", Soviet Physics - Technical Physics, Vol. 15, pp. 32-36, 1970.

(37) Morita, N., "Resonant Solutions Involved in the Integral Equation Approach to Scattering from Conducting and Dielectric Cylinders", IEEE Trans. Antennas and Propagation, vol. AP-27, pp. 869-871, 1979.

(38) Waterman, P. C., "Numerical solution of electromagnetic scattering problems", Mittra, R. (ed.), Computer Techniques for Electromagnetics, Pergamon Press, 1973.

(39) Hurd, R. A., "On Meixner's edge condition for dielectric wedges", Canadian Journal of Physics, vol. 55, pp. 1970-71, 1977.

(40) Bowman, J. J., Senior, T.B.A., and Uslenghi, P.L.E., Electromagnetic and acoustic scattering by simple shapes, North-Holland Publishing Co., 1969.

(41) Andersen, J. B., and Solodukhov, V.V., "Field Behavior near a Dielectric Wedge", IEEE Trans. Antennas and Propagation, vol. AP-26, pp. 598-602, 1978.

(42) King, R.W.P., and Wu, T.T., The Scattering and Diffraction of Waves, Harvard University Press, 1959.

(43) S. Bilgen, M. H. Lean, A. C. Lee, F. Rahman, L. Shafai, A. Wexler, Techniques for Improving Computational Efficiency of the Numerical Electromagnetic Code (NEC), Department of Electrical Engineering Technical Report TR 80-10, University of Manitoba, 1981.

(44) Singh, J., and Adams, A. T., "A Nonrectangular Patch Model for Scattering from Surfaces", IEEE Trans. Antennas and Propagation, vol. AP-27, pp. 531-534, 1979.

(45) Glisson, A. W., and Wilton, D. R., "Simple and Efficient Numerical Methods for Problems of Electromagnetic Radiation and Scattering from Surfaces", IEEE Trans. Antennas and Propagation, vol. AP-28, pp. 593-603, 1980.

CHAPTER VI

CONCLUSION

The goal of this work was to investigate the viability of a new methodology of solving boundary value problems posed in integral equation form. It involved a novel boundary element discretization scheme with uni-variate and bi-variate elements in two- and three-dimensional space. Galerkin's technique of solution was adopted as the standard approach. The overall technique was applied to a wide spectrum of electromagnetic field problems in order to demonstrate its merits and establish the shortcomings.

The first general conclusion is one that was expected: cubic splines provide an effective tool for surface modelling - a fact that has long been established [1] in the area of computer aided design and manufacturing. Contrary to the surface design area, however, the boundary element implementation involved a representation of unknown electromagnetic surface sources and their mathematical recovery. As such, reformulation of the surface representation techniques originally geared to an "input-only" operation was necessary. In other words, surface design involves accurate representation and reproduction of user-specified information, whereas the boundary element method has to address the additional requirement of evaluating unknown functional behavior, and the ensuing algebraic symbolism has to be amenable to manipulation within the discretization and solution algorithms. The uni-variate and bi-variate cubic spline elements developed in Chapter III and summarized in the expressions (3.3) and (3.21), respectively, respond to these stipulations.

In particular, the three-dimensional cubic spline element is an effective instrument that ensures curvature continuity (unless otherwise required), and high-fidelity modelling with a minimum of support information. The most striking illustration of these features is provided for the case of a sphere modelled with only 12 unknowns to achieve highly acceptable results in the electrostatic Dirichlet and electromagnetic plane-wave scattering problems (subsections 5.2.5 and 5.3.5). As the problem size is reduced and geometry simplified, the advantage of splines over earlier tools such as pulse or Lagrangian-polynomial approximation diminishes. In most two-dimensional problems, while a definite advantage over the classical pulse expansion technique is enjoyed in terms of the size of the discrete equation system and precision of results, comparable accuracy has been achieved with Lagrangian elements. The results and comparisons presented for the parallel plate and coaxial capacitors and infinite dielectric cylinders reinforce this observation.

The fundamental improvement that the spline methodology procures, in comparison to the Lagrangian interpolation scheme, relates to the fact that as interpolation order is increased in the latter approach, some of the added nodes are associated only with one element, whereas with the cubic spline element methodology devised in this work, all unknowns (or vertices) are shared by a large number of not even necessarily adjacent elements (*). This fact accounts for the notable savings demonstrated in the three-dimensional problems - a justification of the preference for the communal over the private!

(*) See Appendix.

A second conclusion relates to the use of a "modified spline" basis to approximate functions which manifest singular behavior. This implementation involved algorithmic modification of the expansion functions used for source approximation to reflect the expected form of singularity. As much as it is a generally applicable scheme, this is still an ad hoc approach and there is much room for further work on the subject. The following issues have to be addressed: What should be done when the form of the singularity is not known a priori? How does the utilization of a "modified" i.e. non-polynomic basis affect the convergence and general validity of the Galerkin scheme, originally proven [2] for non-singular basis functions only? Furthermore, the algorithmic problem of dealing with the Green's function and expansion function singularities concurrently in terms of quadrature integration can be studied in depth. Our approach to this latter issue involved utilizing a quadrature scheme that catered for the Green's function singularity explicitly and rigorously, while the expansion function singularity was relegated to an ordinary Gauss-Legendre quadrature formula, noting that increased quadrature orders were necessitated.

Our observation has been (cf. the problem of the three-dimensional conducting cube) that even when the exact form of the singularity of sources was not known, use of expansion functions that contained some singularity helped to achieve physically plausible results. Hitherto unexplored subject of singular field behavior in three-dimensional wedges and tips can be probed with this tool. Note, also, that the variational functional, related to minimized energy content of the system, was significantly less in the case with singular expansion functions in

comparison to that computed with a polynomic basis alone, in the problem of the conducting square cylinder - demonstrating better approximation of the phenomena. When the form of the singularity was known, (e.g. the parallel plate capacitor) solution accuracy was very high. Thus, despite the unanswered questions raised above, the technique of basis modification was shown to be viable. The particular scheme (expressions (4.48), (4.49) and (4.50)) of adding a singular term to one end of the element while preserving spline behavior elsewhere can be said to have been generally successful.

An important area of relevant future research has to do with the structure of the system of linear equations that the BEM gives rise to. It is well known that the Finite Element Method of partial differential equation solution yields sparse matrices, and a banded matrix can be obtained if special care is taken in numbering the elements and the nodes [3]. The BEM, on the other hand, usually produces a dense matrix. Especially if the simple- or double-layer distribution formulations (cf. sec. 5.1) are followed, an ordinary factorization scheme seems to be the only relatively efficient way to solve the linear equation system that is produced. The Green's Theorem formulation, restricting each integral to one closed (may be bounded by the "surface at infinity") region only, seems to be an exception. The equations per region will be dense, but the system matrix in the case of a multiregion problem will be block-sparse. The equations will be coupled only at common interfaces. Wexler [3] has indicated the applicability of the method of Diakoptics to such field problems. But a BEM program that incorporates this feature is still a goal of the future, whose realization will

possibly be rewarding not only to its proponents in the area of electromagnetic fields, but also in a broad spectrum of engineering disciplines that are concerned with the analysis of large systems.

The Progressive Numerical Method [4] is another candidate for efficient solution of large-scale block-structured systems with a properly designed essentially iterative algorithm.

To sum up, the cubic spline methodology has been shown to be a reliable approach in the implementation of the BEM. In many real-life cases two-dimensional or symmetric models involve a degree of simplification, and the capability of tackling the three-dimensional actual problem itself is invaluable. The cubic spline technique, cutting down computational overhead by reducing the necessary information support, and ensuring high-fidelity geometrical modelling, is seen as a key feature in the solution of many real engineering problems.

6.1 References

(1) Barsky, B. A., "Computer-Aided Geometric Design", IEEE Trans. Computer Graphics and Applications, July 1981, pp. 67-108.

(2) Mikhlin, S. G., Variational Methods in Mathematical Physics, Pergamon Press, 1964.

(3) Wexler, A., Perspectives on the solution of Simultaneous Equations, Report TR79-2, Electrical Engineering Department, University of Manitoba, 1979.

(4) Shoamanesh, A. and Shafai, L., "An approximate method for investigation of large circular loop arrays," in Large Engineering Systems, Proc. Int. Symp., Wexler, A. (ed.), Pergamon Press, pp. 120-138, 1976.

BIBLIOGRAPHY

Abramowitz, M. and Stegun, I. A. (eds.), Handbook of Mathematical Functions, Dover, 1968.

Acton, F. S., Numerical Methods that Work, Harper & Row, 1970.

Ahlberg, J. H., Nilson, E. N. and Walsh, J. L., The Theory of Splines and Their Applications, Academic Press, 1967.

Andersen, J. B. and Solodukhov, V. V., "Field Behavior near a Dielectric Wedge", IEEE Trans. on Antennas and Propagation, vol. AP-26, no. 4, pp. 598-602, 1978.

Andreasen, M. G., "Comments on Scattering by Conducting Rectangular Cylinders", IEEE Trans. Antennas and Propagation, vol. AP-12, pp. 235-236, 1964.

Andreasen, M. G., "Scattering from Parallel Metallic Cylinders with Arbitrary Cross Sections", IEEE Trans. Antennas and Propagation, vol. AP-12, pp. 746-754, 1964.

Barsky, B. A., "Computer-Aided Geometric Design", IEEE Trans. Computer Graphics and Applications, July 1981, pp. 67-108.

S. Bilgen, M. H. Lean, A. C. Lee, F. Rahman, L. Shafai, A. Wexler, Techniques for Improving Computational Efficiency of the Numerical Electromagnetic Code (NEC), Department of Electrical Engineering Technical Report TR80-10, University of Manitoba, 1981.

Birkhoff, G. and DeBoor, C. R., "Piecewise Polynomial Interpolation and Approximation", Approximation of Functions, H.L. Garabedian (ed.) Elsevier, 1965.

Birkhoff, G., "Angular Singularities of Elliptic Problems", Journal of Approximation Theory, vol. 6, pp. 215-230, 1972.

Birkhoff, G. and Fix, G. J., "Higher-order Linear Finite Element Methods" , Report to the U.S. Atomic Energy Commission and the Office of Naval Research, 1974.

Bouwkamp, C. J., "A note on singularities occurring at sharp edges in electromagnetic diffraction theory", Physica XII no. 7, pp. 467-474, 1946.

Bowman, J. J., Senior, T.B.A., and Uslenghi, P.L.E., Electromagnetic and acoustic scattering by simple shapes, North-Holland Publishing Co., 1969.

Braunbek, W., "On the diffraction field near a plane-screen corner", IRE Trans. Antennas and Propagation, Vol. AP.4, pp. 219-223. 1956.

Bryant, T. G. and Weiss, J. A., "Parameters of microstrip transmission lines and of coupled pairs of microstrip lines", IEEE Trans. Microwave Theory and Techniques, vol. MTT-16, pp. 1021-1027, 1968.

Burke, G. J., and Poggio, A. J., Numerical Electromagnetic Code (NEC) - Method of Moments, Part I, Naval Ocean Systems Center, San Diego, California, 1977.

Coons, S. A., "Surface Patches and B -Spline Curves", in Computer Aided Geometric Design, Barnhill and Riesenfeld (eds.), Academic Press, 1974.

Coons, S. A., "Surface Patches and B-Spline Curves", Computer Aided Geometric Design, Barnhill and Riesenfeld (ed.s.), Academic Press, 1974.

Daffe, J. and Olsen, R. G., "An integral equation technique for solving rotationally symmetric electrostatic problems in conducting and dielectric material", IEEE Trans. Power Apparatus and Systems, vol. PAS-98, pp. 1609-1615, 1979.

De Boor, C., "On Calculating with B-Splines", Journal of Approximation Theory, vol. 6, pp. 50-60, 1972.

Decreton, M. C., Treatment of Singularities in the Finite Element Method, M.Sc. Thesis, University of Manitoba, 1972.

Eyges, L., and Gianino, P., "Polarizabilities of Rectangular Dielectric Cylinders and of a Cube", IEEE Trans. Antennas and Propagation, vol. AP-27, pp. 557-560, 1979.

Fix, G. J., et. al, "On the Use of Singular Functions with Finite Element Approximations", Journal of Computational Physics, vol. 13, pp. 209-228, 1973.

Glisson, A.W. and Wilton, D.R., "Simple and Efficient Numerical Methods for Problems of Electromagnetic Radiation and Scattering from Surfaces", IEEE Trans. Antennas and Propagation, vol. AP-28, pp. 593-603, 1980.

Gordon, W. J., "Distributive Lattices and the Approximation of Multivariate Functions", Approximations with Special Emphasis on Spline Functions, Schoenberg (ed.), Academic Press, 1969.

Gordon, W. J. and Hall, C. A. "Construction of curvilinear co-ordinate systems and applications to mesh generation", International Journal for Numerical Methods in Engineering, vol. 7, pp. 461-477, 1973.

Greville, T.N.E., Theory and Applications of Spline Functions, Academic Press, 1969.

Han Hou-de and Ying Lang-an, "An Iterative Method in the Infinite Element", Department of Mathematics and Mechanics, Peking University, 1980.

Harrington, R. F., Time-Harmonic Electromagnetic Fields, McGraw-Hill, 1961.

Harrington, R. F., Field Computation by Moment Methods, Macmillan, 1968.

Hughes, T.J.R. and Akin, J.E., "Techniques for developing special finite element shape functions with particular reference to singularities", International Journal for Numerical Methods in Engineering, vol. 15, pp. 733-751, 1980.

Hurd, R. A., "The Edge Condition in Electromagnetics", IEEE Trans. on Antennas and Propagation, Succinct Papers, January 1976, pp. 70-73.

Hurd, R. A., "On Meixner's edge condition for dielectric wedges", Canadian Journal of Physics, vol. 55, no. 22, pp. 1970-1971, 1977.

Jaswon, M. A., "Integral equation methods in potential theory-I", Proceedings of the Royal Society of London, A275, pp. 23-32, 1963.

Jaswon, M. A. and Symm, G. T., Integral Equation Methods in Potential Theory and Elastostatics, Academic Press, 1977.

Jeng, G., Isoparametric Finite-Element Boundary Integral Solution of Three-Dimensional Fields, Ph.D. Dissertation, University of Manitoba, 1977.

Jeng, G. and Wexler, A., "Isoparametric Finite Element Variations Solution of Integral Equations for Three-Dimensional Fields", International Journal of Numerical Methods in Engineering, vol. 11, pp. 1455-1471, 1977.

Jeng, G. and Wexler, A., "Self-adjoint Variational Formulation of Problems Having Non-Self-Adjoint Operators", IEEE Trans. on Microwave Theory and Techniques, vol. MTT-26, pp. 91-94, 1978.

Jones, D. S., "Diffraction by an edge and by a corner", Quarterly Journal of Mechanics and Applied Mathematics, vol. V, pp. 363-378, 1952.

Jones, D. S., The Theory of Electromagnetism, Pergamon Press, 1964.

Kellogg, O. D., Foundations of Potential Theory, Dover Publications, 1953.

King, R.W.P., and Wu, T.T., The Scattering and Diffraction of Waves, Harvard University Press, 1959.

Kleinman, R. E., "The Rayleigh region", Proceedings of the IEEE, vol. 53, pp. 848-856, 1965.

Kondrat'ev, V. A., "Boundary problems for elliptic equations with conical or angular points", Transactions of the Moscow Mathematical Society, vol. 17, pp. 105-128, 1968.

Kouyoumjian, R. G. An Introduction to Geometrical Optics and the Geometrical Theory of Diffraction, Antenna and Scattering Theory: Recent Advances, Vol. I; Short Courses at Ohio State University, 1966.

Lachat, J. C. and Watson, J. O., "Effective numerical treatment of boundary integral equations", International Journal of Numerical Methods in Engineering, vol. 10, pp. 991-1005, 1976.

Lean, M. H., Friedman, M., and Wexler, A., "Application of the Boundary Element Method in Electrical Engineering Problems in Developments in Boundary Element Methods -1,Banerjee and Butterfield (ed.s), Applied Science Publishers Ltd., London, 1977.

Lean, M. H. and Wexler, A., "Accurate field computation with the Boundary Element Method, IEEE Trans. Magnetics, vol. MAG-18, March 1982, pp.331-335.

Lean, M. H., Electromagnetic Field Solution with the Boundary Element Method, Ph.D. Dissertation, University of Manitoba, 1981.

Lehman, R. S., "Developments at an Analytic Corner of Solutions of Elliptic Differential Equations", Journal of Mathematic and Mechanics, vol. 8, no. 5, pp. 727-760, 1959.

Lord Rayleigh, Scientific Papers, vol. IV, p. 288, 1903.

McDonald, B. H., Constrained Variational Solution of Field Problems, Ph.D. Dissertation, University of Manitoba, 1975.

McDonald, B. H., and Wexler, A., "Finite element solution of unbounded field problems", IEEE Trans. Microwave Theory and Techniques, vol. MTT-20, pp. 841-847, 1972.

McDonald, B., Friedman, M., and Wexler, A., "Variational Solution of Integral equations", IEEE Trans. Microwave Theory and Techniques, vol. MTT-22, pp. 237-248, 1974.

McDonald, B.H., and Wexler, A., "Mutually constrained partial differential and integral equation field formulations", in Chari, M.V.K., and Silvester, P. K., (eds.), Finite Elements in Electrical and Magnetic Field Problems, John Wiley & Sons, 1980.

Mei, K.K., "Unimoment method of solving antenna and scattering problems", IEEE Trans. Antennas and Propagation, vol. AP-22, pp. 760-766, 1974.

Mei, K.K., and Van Bladel, J. G., "Scattering by Perfectly-Conducting Rectangular Cylinders", IEEE Trans. Antennas and Propagations, vol. AP-11, pp. 185-192, 1963.

Meixner, J., "Die Kantenbedingung in der Theorie der Beugung electromagnetischer Wellen an vollkommen leitenden ebenen Schirmen", Annalen der Physik, vol. 6, no. 6, pp. 1-9, 1949.

Meixner, J., "The behaviour of electromagnetic fields at edges", New York University Institute of Mathematical Sciences, Division of Electromagnetic Research, Report No. EM-72, New York, 1952.

Mentzer, J. R., Scattering and Diffraction of Radio Waves, Pergamon Press, 1955.

Mikhlin, S. G., Integral Equations, Second Revised Edition, Pergamon Press, 1964.

Miller, E. K., and Poggio, A. J., "Moment-method techniques in electromagnetics from an applications viewpoint", in Uslenghi, P.L.E. (ed.), Electromagnetic Scattering Academic Press, 1978.

Morita, N. "Surface Integral Representations for Electromagnetic Scattering from Dielectric Cylinders", IEEE Trans. Antennas and Propagation, vol. AP-26, pp. 261-266, 1978.

Morita, N., "Resonant Solutions Involved in the Integral Equation Approach to Scattering from Conducting and Dielectric Cylinders", IEEE Trans. Antennas and Propagation, vol. AP-27, pp. 869-871, 1979.

Motz, H., "The treatment of singularities in relaxation methods", Quarterly of Applied Mathematics, vol. 4, pp. 371-377, 1946.

Oshiro, F. K. and Su, C. S., A Source Distribution Technique for the Solution of General Electromagnetic Scattering Problems - Phase 1 Report, Northrop, Norair, NOR 65-271, 1965.

Parr, W. E., "Upper and Lower Bounds for the Capacitance of Regular Solids", Journal of the Society for Industrial Applications of Mathematics, vol. 9, pp. 334-386, 1961.

Poggio, A. J. and Miller, E. K., "Integral Equation Solutions of Three-dimensional Scattering Problems", in Mittra, R. (ed.), Computer Techniques for Electromagnetics, Pergamon Press, 1973.

Prentner, P. M., Splines and Variational Methods, John Wiley & Son, 1975.

Reitan, D. K., and Higgins, T. J., "Calculation of the Electrical Capacitance of a Cube", Journal of Applied Physics, vol. 22, pp. 223-226, 1951.

Richmond, J. H., "Scattering by a dielectric cylinder of arbitrary cross section shape", IEEE Trans. Antennas and Propagation, vol. AP-13, pp. 334-341, 1965.

Riesenfeld, R. F., Applications of B-Spline Approximation to Geometric Problems of Computer Aided Design, Ph.D. Dissertation, Syracuse University, New York, 1973.

Schoenberg, I. J., "Contribution to the problem of approximation of equidistant data by analytic functions", Parts A and B, Quarterly of Applied Mathematics, vol. 4, pp 45-99, 112-141, 1946.

Schultz, M. H., Spline Analysis, Prentice-Hall, 1973.

Shafai, L., "An improved integral equation for the numerical solution of two-dimensional diffraction problems", Canadian Journal of Physics, vol. 48, pp. 954-963, 1970.

Shoamanesh, A. and Shafai, L., "An approximate method for investigation of large circular loop arrays," in Large Engineering Systems, Proc. Int. Symp., Wexler, A., (ed.), Pergamon Press, pp. 120-138, 1976.

Singh, J., and Adams, A. T., "A Nonrectangular Patch Model for Scattering from Surfaces", IEEE Trans. Antennas and Propagation, vol. AP-27, pp. 531-534, 1979.

Solodukhov, V. V. and Vasil' ev, E. N., "Diffraction of a plane electromagnetic wave by a dielectric cylinder of arbitrary cross section", Soviet Physics - Technical Physics, Vol. 15, pp. 32-36, 1970.

Stratton, J. A., Electromagnetic Theory, McGraw-Hill, 1941.

Stroud, A. H. and Secrest, D., Gaussian Quadrature Formulas, Prentice-Hall Inc., 1966.

Thatcher, R. W., "The Use of Infinite Grid Refinements at Singularities in the Solution of Laplace's Equation", Numerical Mathematics, vol. 25, pp. 163-190, 1976.

Van Bladel, J., Electromagnetic Fields, McGraw-Hill, 1964.

Wait, R., and Mitchell, A. R., "Corner Singularities in Elliptic Problems by Finite Element Methods", Journal of Computational Physics, vol. 8, pp. 45-52, 1971.

Waterman, P. C., "Numerical solution of electromagnetic scattering problems", Mittra, R. (ed.), Computer Techniques for Electromagnetics, Pergamon Press, 1973.

Watson, J. O., "Hermitian Cubic Boundary Elements for Elastostatics", Innovative Numerical Analysis for the Engineering Sciences, Proc. 2nd Int. Symposium on Innovative Num. Anal. in App. Eng. Sci., University Press of Virginia, pp. 403-412, 1980.

Wexler, A., Finite Elements for Technologists, Electrical Engineering Department Technical Report, TR80-4, University of Manitoba, 1980.

Wexler, A., Perspectives on the solution of Simultaneous Equations, Report TR79-2, Electrical Engineering Department Report, University of Manitoba, 1980.

Wu, T. K., and Tsai, L. L., "Numerical Analysis of Electromagnetic Fields in Biological Tissues", IEEE Proceedings Letters, pp. 1167-1168, Aug. 1974.

Ying Lung-an, "The Infinite Similar Element Method for Calculating Stress Intensity Factors", Scientia Sinica, Vol. 21, no. 1, pp. 19-43, 1979.

Zabreyko, P. O. et. al., Integral Equations - a reference text, Noordhoff International Publishing, 1975.

Zienkiewicz, O. C., The Finite Element Method in Engineering Science, McGraw-Hill, 1971.

Appendix A

EXAMPLES OF CUBIC SPLINE ELEMENTS

A.1 TWO-DIMENSIONAL (UNI-VARIATE) ELEMENTS.

Definition: $P(\xi) = \sum_{j=1}^{4} V_j \alpha_j(\xi)$.

Ends of element: $P_1 = P(0)$,

$P_2 = P(1)$.

A.1.1 A straight-line element.

$V_1 = (2,1)$

$V_2 = (1,1)$

$V_3 = (0,1)$

$V_4 = (-1,1)$

$P_1 = V_1 + 4V_2 + V_3 = (1,1)$

$P_2 = V_2 + 4V_3 + V_4 = (0,1)$

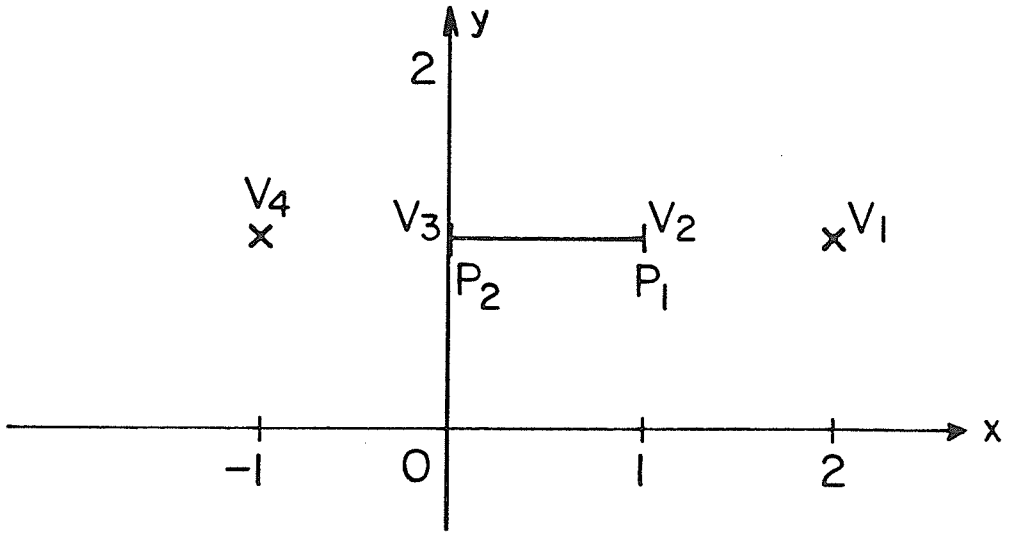

Figure A.1. A straight-line element.

A.1.2 A curved two-dimensional element.

$V_1 = (1.5,0)$

$V_2 = (0,1.5)$

$V_3 = (-1.5,0)$

$V_4 = (0,-1.5)$

$P_1 = V_1 + 4V_2 + V_3 = (0,1)$

$P_2 = V_2 + 4V_3 + V_4 = (-1,0)$

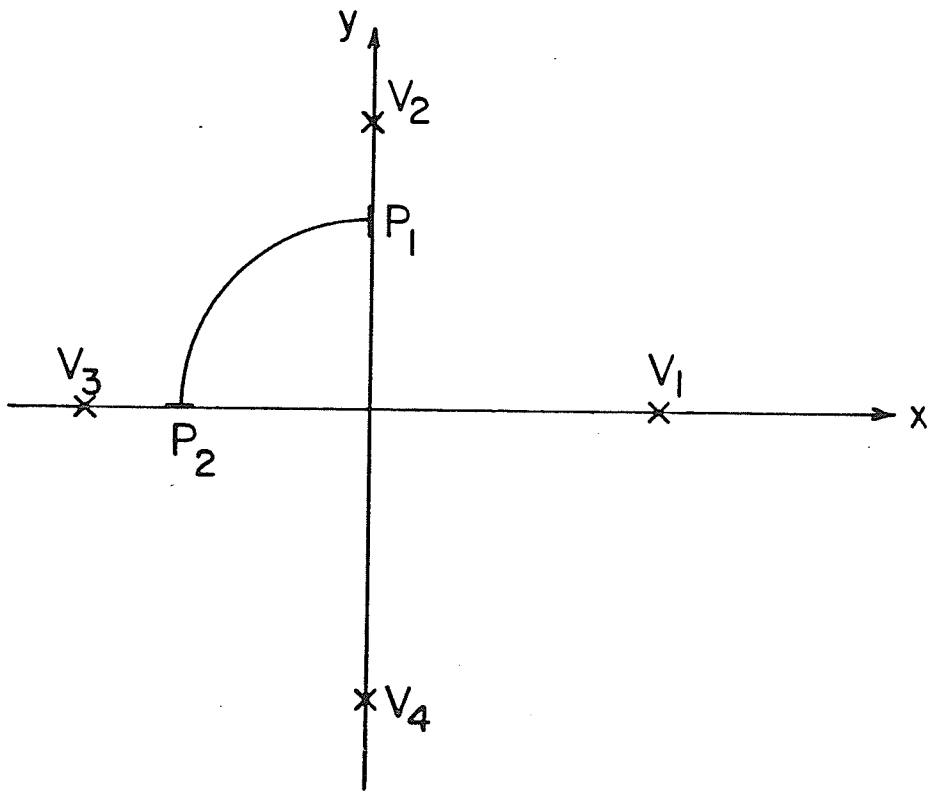

Figure A.2. A curved two-dimensional element : approximate circular quadrant.

A.1.3 The simplest circle model.

$V_1 = (1.5,0)$

$V_2 = (0,1.5)$

$V_3 = (-1.5,0)$

$V_4 = (0,-1.5)$

Vertices of elements:

element	vertices	P_1	P_2
1	$V_4\ V_1\ V_2\ V_3$	(1,0)	(0,1)
2	$V_1\ V_2\ V_3\ V_4$	(0,1)	(-1,0)
3	$V_2\ V_3\ V_4\ V_1$	(-1,0)	(0,-1)
4	$V_3\ V_4\ V_1\ V_2$	(0,-1)	(1,0)

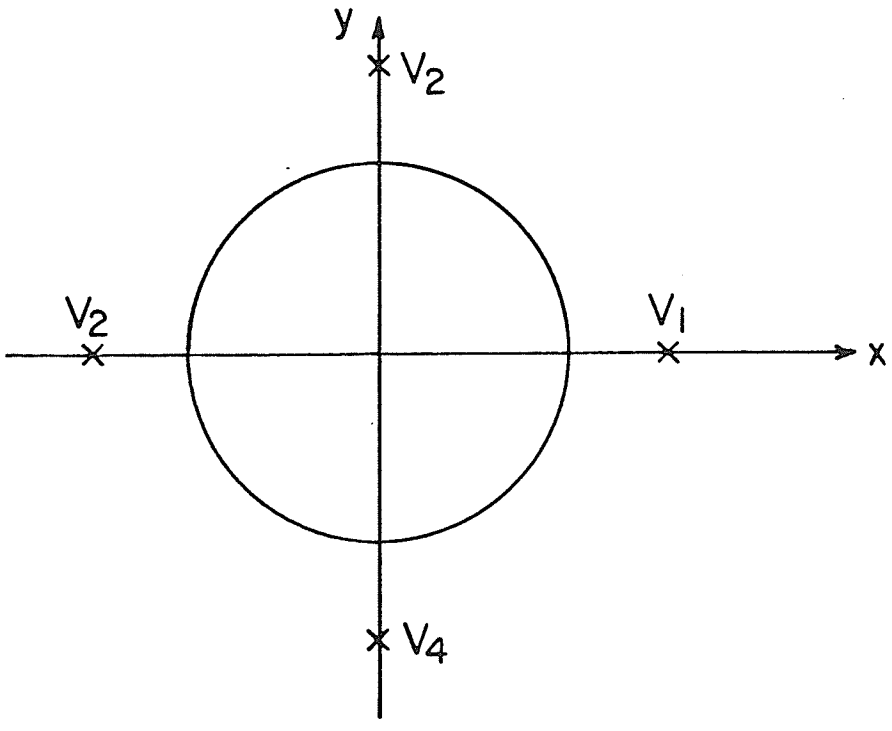

Figure A.3. A circle model.

A.1.4 A square model.

$V_1 = V_2 = V_3 = (1,1)$

$V_4 = V_5 = V_6 = (-1,1)$

$V_7 = V_8 = V_9 = (-1,-1)$

$V_{10} = V_{11} = V_{12} = (1,-1)$

Elements are defined similar to the circular example, in a cyclical fashion, i.e. (V_1 , V_2 , V_3 , V_4) for element #1, $(V_{11} , V_{12} , V_1 , V_2)$ for element #11, etc.

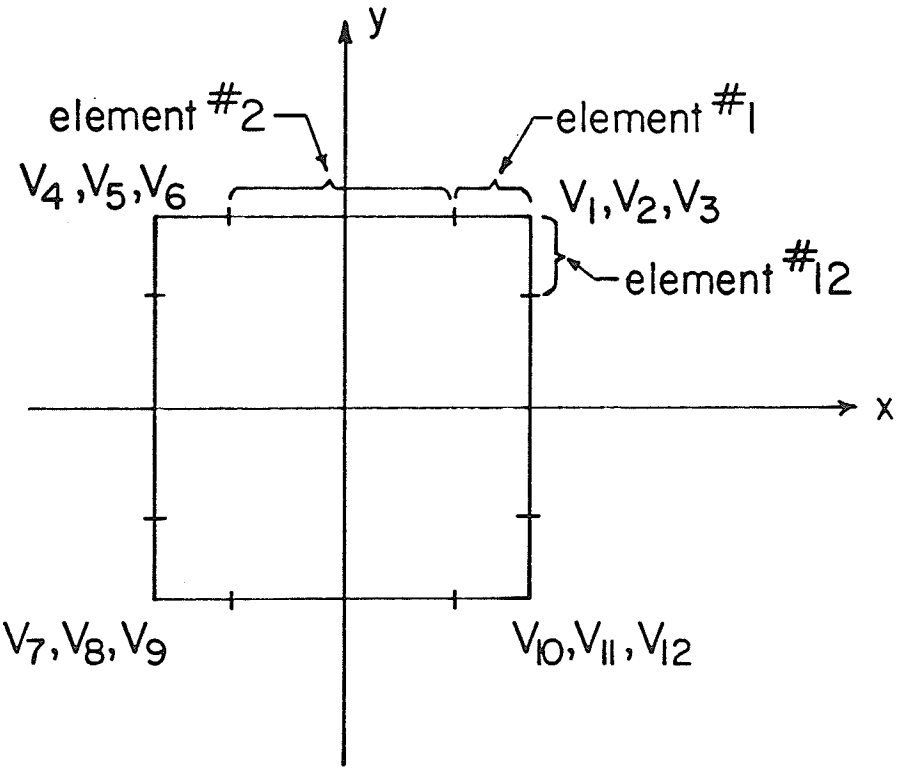

Figure A.4. Boundary elements for a square cylinder.

A.2 THREE-DIMENSIONAL (BI-VARIATE) ELEMENTS

Definition: $P(\xi,\eta) = \sum_{j=1}^{12} V_j \, A_j(\xi,\eta)$.

Corners of element: $P00 = P(0,0) = V_9$, $P01 = P(0,1) = V_{10}$

$P10 = P(1,0) = V_{11}$, $P11 = P(1,1) = V_{12}$

A.2.1 A planar square surface

$V_1 = (-1,0,1)$

$V_2 = (2,0,1)$

$V_3 = (-1,1,1)$

$V_4 = (2,1,1)$

$V_5 = (0,-1,1)$

$V_6 = (0,2,1)$

$V_7 = (1,-1,1)$

$V_8 = (1,2,1)$

$V_9 = (0,0,1) = P00$

$V_{10} = (0,1,1) = P01$

$V_{11} = (1,0,1) = P10$

$V_{12} = (1,1,1) = P11$

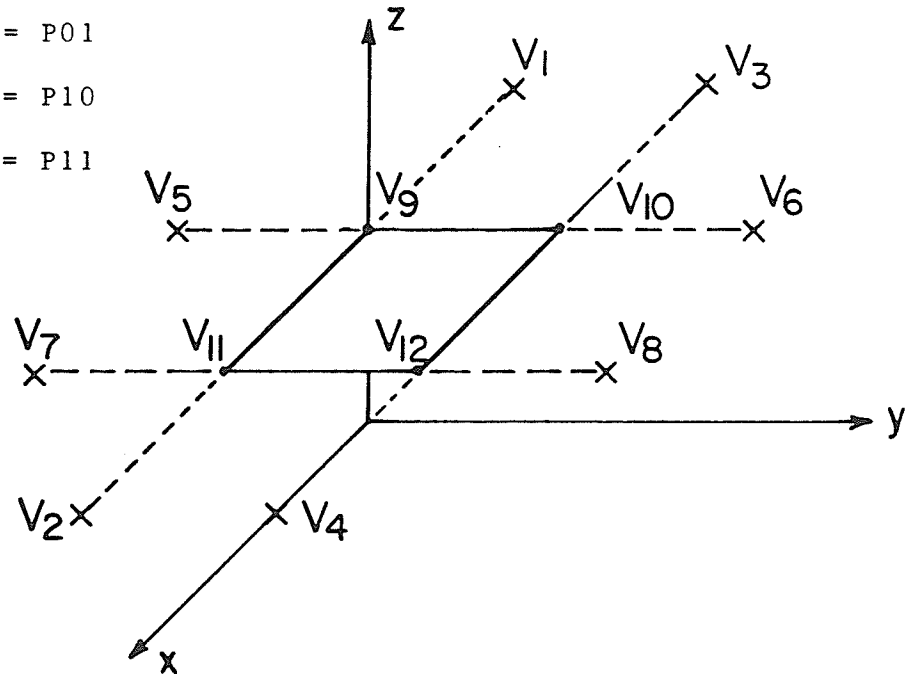

Figure A.5. A planar square boundary element.

A.2.2 The 12-vertex sphere model.

$V_1 = (0,0,1.5)$

$V_2 = (0,0,-1.5)$

$V_3 = (1.5,0,0)$

$V_4 = (0,1.5,0)$

$V_5 = (-1.5,0,0)$

$V_6 = (0,-1.5,0)$

$V_7 = (0,0,1)$

$V_8 = (0,0,-1)$

$V_9 = (1,0,0)$

$V_{10} = (0,1,0)$

$V_{11} = (-1,0,0)$

$V_{12} = (0,-1,0)$

element	defining vertex numbers											
1	5	2	6	2	7	7	6	5	7	7	9	10
2	6	2	3	2	7	7	3	6	7	7	10	11
3	3	2	4	2	7	7	4	3	7	7	11	12
4	4	2	5	2	7	7	5	4	7	7	12	9
5	1	5	1	6	6	5	8	8	9	10	8	8
6	1	6	1	3	3	6	8	8	10	11	8	8
7	1	3	1	4	4	3	8	8	11	12	8	8
8	1	4	1	5	5	4	8	8	12	9	8	8

The sphere model is presented in Figure A.6.

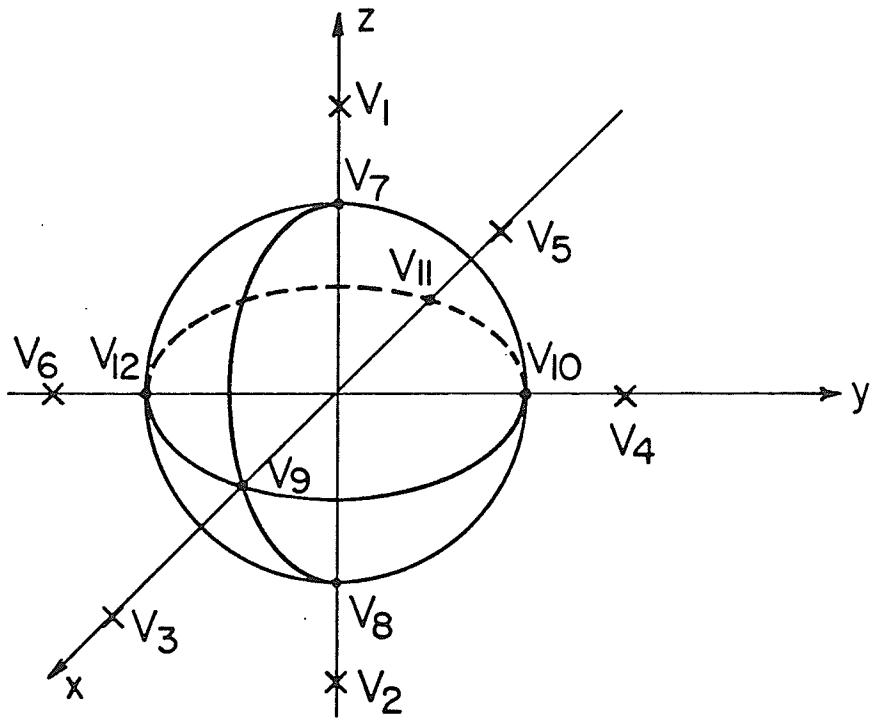

Figure A.6. The 12-vertex, 8-element cubic spline model of a sphere.